ADDIS ABABA UNIVERSITY

COLLEGE OF NATURAL SCIENCES

SCHOOL OF EARTH SCIENCES

SEISMIC HAZARD ANALYSIS FOR THE DEBREZEIT AREA

BY

KASAHUN DANDER AMARE

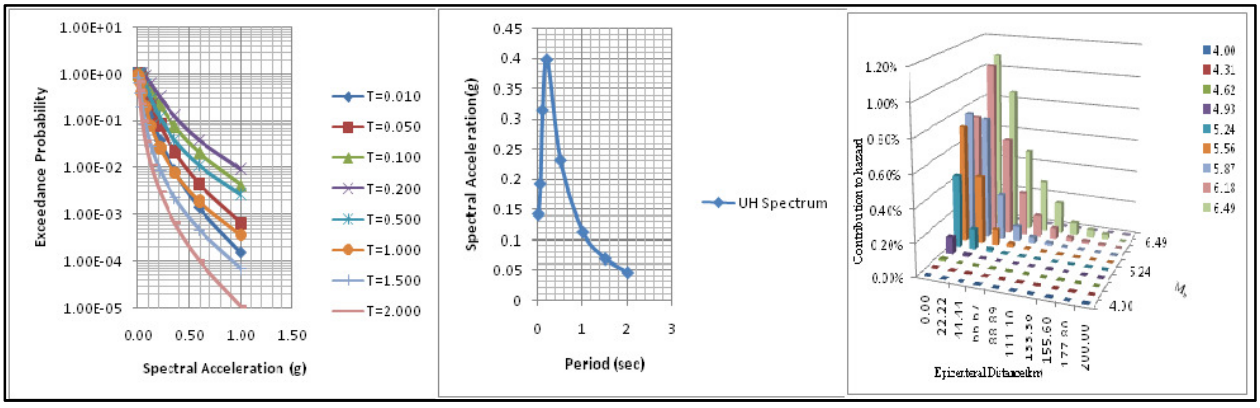

A THESIS SUBMITTED TO THE SCHOOL OF GRADUATE STUDIES OF ADDIS ABABA UNIVERSITY IN PARTIAL FULFILLMENT OF THE REQUIREMENTS FOR THE DEGREE OF MASTER OF SCIENCE IN EXPLORATION GEOPHYSICS

Addis Ababa

May, 2015

ADDIS ABABA UNIVERSITY

COLLEGE OF NATURAL SCIENCES

SCHOOL OF EARTH SCIENCES

SEISMIC HAZARD ANALYSIS FOR THE DEBREZEIT AREA

BY

KASAHUN DANDER AMARE

SCHOOL OF EARTH SCIENCES

Approved by Board of Examiners:	Signature	Date
Prof. Tilahun Mammo	_____	_____
Chairperson		
Prof. Tilahun Mammo	_____	_____
Advisor		
Dr. Mulugeta Alene	_____	_____
Co-Advisor		
Dr. Abera Alemu	_____	_____
Internal Examiner		
Dr. Bekele Abebe	_____	_____
External Eximiner		

Acknowledgments

First of all, I would like to thank the almighty God for the countless blessings.

I have no words to thank my advisor Prof. Tilahun Mammo for his pivotal assistance all the way through this thesis work. The productive suggestions he gave me were vital to accomplish the work and this final manuscript. Furthermore, I would like to thank him for organizing the fieldwork and, computational facilities like providing different software for processing geophysical data. Your support in suggesting valuable reading materials and in sharing your field and research experiences contributed greatly.

I would like to express my profound thanks to my co-advisor, Dr. Mulugeta Alene for his support and comment for the success of this thesis.

I want to acknowledge Dr. Abera Alemu and Prof. Tigestu Haile for their help in providing some valuable comments and sharing their research experiences.

I extend my acknowledgement to all my friends for their aid in learning the geophysical data processing software and for suggesting other supportive ideas.

Finally yet prominently, my sincere thank goes to my family who helped me a lot in finalizing this thesis work within the limited time frame.

Table of Contents

List of Figures

List of Tables

List of Appendices

Acronyms

AAE	Addis Ababa Seismic Station
CDP	Common Depth Point
CMP	Common Mid Point
EBCS	Ethiopian Building Code of Standards
EM-DAT	Emergency Events Database
GEM	Global Earthquake Model
GMPE	Ground Motion Prediction Equation
IBC	International Building Code
ISC	International Seismological Center
MASW	Multi-Channel Analysis of Surface Waves
MEC	Maximum Credible Earthquake
MER	Main Ethiopian Rift
MMI	Modified Mercalli Intensity Scale
NEHRP	National Earthquake Hazard Reduction Program
NGA	Next Generation Attenuation Models
PEER	Pacific Earthquake Engineering Research Center
PGA	Peak Ground Acceleration
PGD	Peak Ground Displacement
PGV	Peak Ground Velocity
PSA	Pseudo Spectral Acceleration
PSHA	Probabilistic Seismic Hazard Analysis
RADIUS	Risk Assessment tools for Diagnosis of Urban Areas against Seismic Disaster
UHS	Uniform Hazard Spectrum

Abstract

In this thesis work we have presented a seismic hazard investigation conducted at Debrezite area, central Ethiopia. In this work we carried out a probabilistic seismic hazard analysis with an emphasis on the local site conditions. The analyses were carried out using the ISC-GEM (International Seismological Center and Global Earthquake Model) earthquake catalogue available over a radius of 200 km around Debrezeit city considering destructive earthquakes from 1906 to 2011. The analysis was also carried out by considering known seismogenic sources that are identified on the basis of seismicity and tectonics. Earthquake data from ISC-GEM (International Seismological Center and Global Earthquake Model) catalogue were analyzed statistically and Gutenburg-Richter recurrence relation is used to obtain the b-value of 0.67, 1.03 and 1.11 for the three seismic zones: Main Ethiopian Rift, Afar and Escarpment respectively that are considered to generate earthquakes that affect the Debrezeit area.

Seismic refraction data was collected at Kuriftu site, Debrezeit using McSEIS-SX24 seismogram. Multi-Channel Analysis of Surface Waves method is used to analyze the surface waves and determine the shear wave velocity at the depth of 30m. SeisImager/ SW software were used to produce a 2-D shear-wave velocity section. The shear wave velocity observed at Kuriftu site has the mean Vs30 value of 360m/s. Therefore, according to the National Earthquake Hazard Reduction Program classification the site can be classified under soil class C. Based on the site classification value, we can conclude that the main part of the study area is under substantial risk of soil amplification.

After the implementation of a seismic hazard analysis by using CRISIS2012 software, the probabilistic seismic hazard curves: Exceedance probability and Uniform Hazard Spectrum curves were developed based on the selected attenuation relationship, with a probability of exceedance of 10% in 50, 100, 250 and 500 years to a return period of 475 years for bed rock condition and considering local site effects. On the other hand the highest hazard levels were determined at soil site for Debrezeit, the peak ground acceleration and spectral acceleration values calculated based on attenuation relationship by (Campbell and Bozorgnia 2008) were found to be applicable for 10% probability of exceedance in 50, 100, 250 and 500 years, taking into consideration the fact that a considerable portion of the city is founded over alluviums.

Key words: Debrezeit, Earthquake, b-value, hazard curve, attenuation relationship, peak ground acceleration.

CHAPTER ONE

1 INTRODUCTION

1.1 BACKGROUND

Ethiopia is, amongst the developing countries, the most vulnerable to natural and man-made disasters. Among others, drought induced famine, flood, landslide, crop-pests, infrequent earthquake and wars are the major triggering events that have, over the past many years, been causing incalculable suffering to communities and millions of dollar worth of property destructions. Drought induced famine has, for many years, been the worst disaster event from which millions of Ethiopians, mostly rural residents, experienced immense anguish and it still remains a national policy agenda and problem. Over the last three decades, Ethiopia learned the hardest way to transform its disaster management from a mere apparatus of response and recovery to preparedness, mitigation, and development. Resources and technical (technological) capacities aside, Ethiopia now possesses a wealth of drought disaster management experiences. Disaster management activities in Ethiopia have tended to focus most on drought disaster management. Less attention has been paid to other types of disasters, like earthquakes and volcanic eruptions.

Hazards (natural or man-made) are potentially damaging/destructive events with a potential to cause loss of life and/or injury to human beings as well as damage or destruction to property. The definition attests to the fact that a hazard can turn to disaster only when communities and property are susceptible/vulnerable to losses, due mainly to administrative and structural fallacies. For instance, the terrible recent earthquake that occurred in Sichuan province in China 2008 and the subsequent building collapses said to have stemmed from poor building structures, thereby resulting immense agony to the people. The 1973/74 and 1983/84 famines in Ethiopia that left millions of deaths, sufferings, and dislocation to the poor farmers in the country was mainly attributed to deficiencies in the systems of government administration that failed to put an early warning system in place. More generally, administrative malaise, such as poor building structures in seismic zones, archaic land use, and relentless aforestation in drought and flood prone areas, and low risk perception and/or absence of alert, informed, and resilient public, will lead to inherent hazards to disasters.

Vulnerability is, therefore, the extent to which a community, structure, service, or region is likely to be damaged or destroyed by the impact of a particular disaster. There are many factors, physical and socioeconomic in nature, which determines the susceptibility of community to threats of disasters. Physical vulnerability arises from location in relation to the hazard under consideration. Community living near flood plains or river areas is as much vulnerable to flood disaster as people in drought regions are to famine. The same holds true to communities in Iran, Japan, Los Angeles, Turkey, and some parts of China who live in and around earthquake prone zones. The largest part of coastal areas of the US, the Caribbean, and South Asia are also vulnerable to hurricanes and cyclones, respectively. In terms of overall seismic risk, the presence of part of the East African Rift, which runs through the centre of the country, means that Ethiopia is prone to seismic activity and related natural disasters: earthquakes and volcanic eruptions, and Ethiopia is also a landlocked country, it is not at risk from tsunamis.

The centre of Ethiopia faces a medium risk of earthquake hazard – more so than its neighboring countries. The country has experienced a number of earthquakes and these have caused some deaths, and damage to buildings. According to the EM-DAT database, from 1900 to 2013 earthquakes in Ethiopia have caused a total of 93 deaths, 165 injured, 420 homeless, and affected 11,000 people, and a total estimated economic cost of more than US$7 million. Debrezeit is located close to the western edge of the Ethiopian Rift Valley. Despite only facing high seismicity, the urban public there is more vulnerable to disasters due to weak infrastructure and lack of preparedness.

In terms of vulnerability, data suggests that in Ethiopia:

- 46 per cent of the population has a “medium” exposure to seismic hazard;
- 20 per cent of the population has a “low” exposure; and
- 26 per cent has a “very low” exposure. No people are identified as facing a “high” or “very high” exposure.
- Most vulnerability analyses do not cite seismic hazards and so not identify specific vulnerable communities. Urban areas are also identified as facing seismic vulnerability.

1.1.1 Seismic hazard in Ethiopia

The active Great Rift Valley makes Ethiopia susceptible to two types of seismic hazard: earthquakes and volcanic eruptions. Table 1.1 shows that from 1900 to 2013 there were a total of ten earthquakes and eruptions leading to a total of 93 deaths, 165 injured, 420 homeless and affecting 11,000 people. It is important to note that data in these areas is often limited and is expected to be highly underreported. Other sources of data and literature report different figures, for example (Kinde 2006) explains that Gouin estimates 15,000 tremors occurred in Ethiopia and the Horn of Africa in the 20th century, while another study by Fikadu Kebede identified a total of 16 recorded earthquakes of magnitude 6.5 and higher in Ethiopia in the same period.

Table 1. 1 Number and impact (human and economic) of earthquakes and volcanoes in Ethiopia (1900-2013) Source: Data downloaded from EM-DAT database on 17 January 2013.

Disaster type	Number of disaster	Number of people killed	Number of people injured	Number of people affected	Number of homeless	Total number of people affected	Total economic damage (US$'000)
Earthquake	7	24	165	0	420	585	7070
Volcano	3	69	0	11000	0	11000	0
Total	10	93	165	11000	420	11585	7070

Mount Erta Ale has caused frequent lava flows in recent years, and is Ethiopia's most active volcano. In 2001 the Nabro volcano (located in Eritrea) erupted following a series of earthquakes (including two at magnitude 5.7), with spill-over affects in Ethiopia. Eight villages in the Biddu district of Ethiopia were affected by volcanic ash, affecting at least 5,000 people and polluting water sources. Mount Dabbahu became active in 2005, causing evacuations. Other historically active volcanoes include Alayta, Dalaffilla, Dallol, Dama Ali, Fentale, Kone, Manda Hararo, and Manda-Inakir.

Table 1. 2 Number and impact (human and economic) of earthquakes and volcanoes in Ethiopia and neighbor (1900-2013) Source: EM-DAT database.

Country	Disaster type	Number of disaster	Number of people killed	Number of people injured	Number of people affected	Number of homeless	Total number of people affected	Total economic damage (US$'000)
Ethiopia	Earthquake	7	24	165	0	420	585	7070
Kenya	Earthquake	2	1	0	0	0	0	100000
Somalia	Earthquake	1	298	283	104800	0	105083	100000
Sudan	Earthquake	2	3	15	8000	0	8015	0

Table 1. 3 Seismic hazard intensity levels and number and percentage of people exposed, in Ethiopia Source: World health Organization, 2011.

Hazard	Hazard intensity levels and number and percentage of people exposed					
	Very high No.exposed (%)	High No.exposed (%)	Medium No.exposed (%)	Low No.exposed (%)	Very low No.exposed (%)	No data No.exposed (%)
Seismic	0 (0.00 %)	0 (0.00 %)	39,035,265 (45.94 %)	20,409,928 (24.02 %)	25,530,413 (30.04 %)	0 (0.00 %)

1.1.2 Earthquake hazard in Ethiopia

According to the EM-DAT database from 1900 to 2013 there were a total of seven earthquakes, killing a total of 24 people, affecting 585 people and causing more than US$7 million in economic damage (see Table 1.1). Earthquakes occur along the Ethiopian rift system Figure 1.1 depicts the seismicity of the Horn of Africa region by mapping the earthquakes that have occurred in the region from 1900 to 2010 (Atalay Ayele, private correspondence). The size of the red dots represents the magnitude of earthquakes ranging from 3.5 to 7.2. The yellow stars are the major towns in Ethiopia revealing that the seismic areas are often inhabited areas.

Figure 1.1 shows Ethiopia's major cities in relation to seismic hazard, notably the three most populous cities: Addis Ababa, Dire Dawa, and Mek'ele. Sixteen recorded earthquakes, are found in the most seismically hazardous areas, marked in yellow in the centre of the country and categorized as having a "medium" risk of seismic hazard. The cities Addis Ababa, Debrezeit, Nazret, Dire Dawa and Awassa are very near main fault lines (e.g. the Wonji fault, Nazret fault, Addis-Ambo-Ghedo fault, and Fil Woha fault) where many earthquakes have previously occurred (Kinde, 2006).

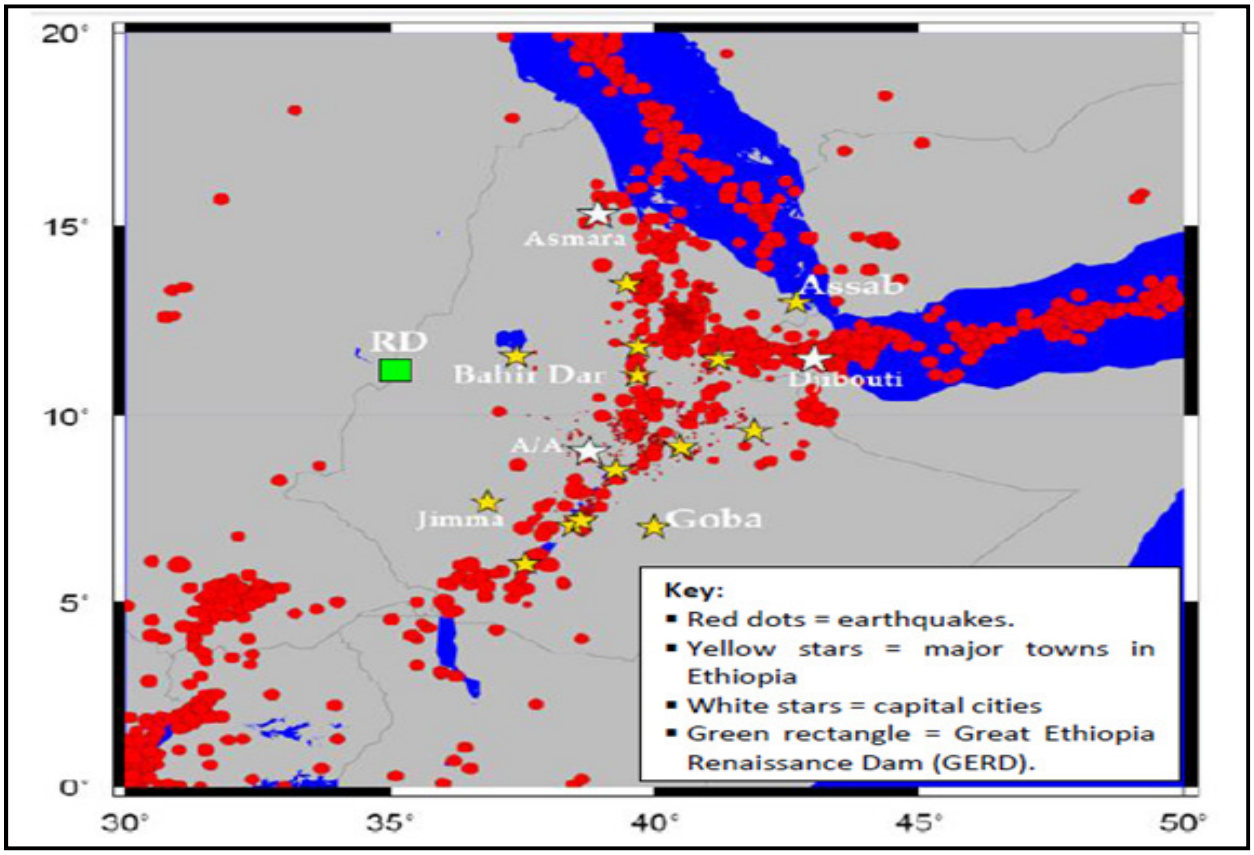

Figure 1. 1 Earthquake recorded in the Horn Africa region from 1900 to 2010.

Source: Atalay Ayele (Addis Ababa University), via private correspondence on 15 January 2014, based on data from: Institute of Geophysics Space Science and Astronomy of Addis Ababa University; United States Geological Survey; and International Center of Seismology in UK.

1.2 LOCATION OF THE STUDY AREA

The study area, Debrezeit is located about 50km from Addis Ababa and found in the western margin of the seismically active Main Ethiopian Rift (MER) system and upper part of Awash River Basin. It is specifically situated in Central Ethiopia, in Oromia Regional State, and bounded approximately, between geographic coordinates of $38^0$53'E – 39°14'E and $8^0$41'N - $8^0$50'N latitude and longitude respectively. The area topographically varies between 1600 and 1900m above the mean sea level. The mean annual rainfall of the study area is about 902 mm, and, the mean monthly temperature varies from 16 to 22°C.

The area comprises the major industrial zone of the country includes towns of Debrezeit and Dukem that are expanding tremendously in industry and other infrastructures built in the area. This growth which form a significant portion of the national economy occurs at the junction of the transportation system from the most resourceful southern and eastern parts of the country that contribute the largest share of national economic output. Moreover, the area also contains the access route of railway and road to the Djibouti Port. This adds increased importance to seismic hazard study in the area. On account of all ongoing development programs and the large settlement, the study of vulnerability of the region to earthquakes is of tremendous interest to a variety of organization. Especially designers and decision makers must be alerted to the fact that Debrezeit area has been shaken several times by earthquakes since their foundation in the late 19th century. The area is also one of the major producers of agricultural outputs such as teff, cereals and well known in livestock production. A site of military establishments, tourism and recreation sites of the nation consisting of lakes like Hora, Babogaya and Bishoftu and many picnic centers that attract very large number of tourists and vacationers each year. In addition, the population of the study area amounts to 100,000 and growing annually at a very rapid rate (Population and Housing Census, 2007).

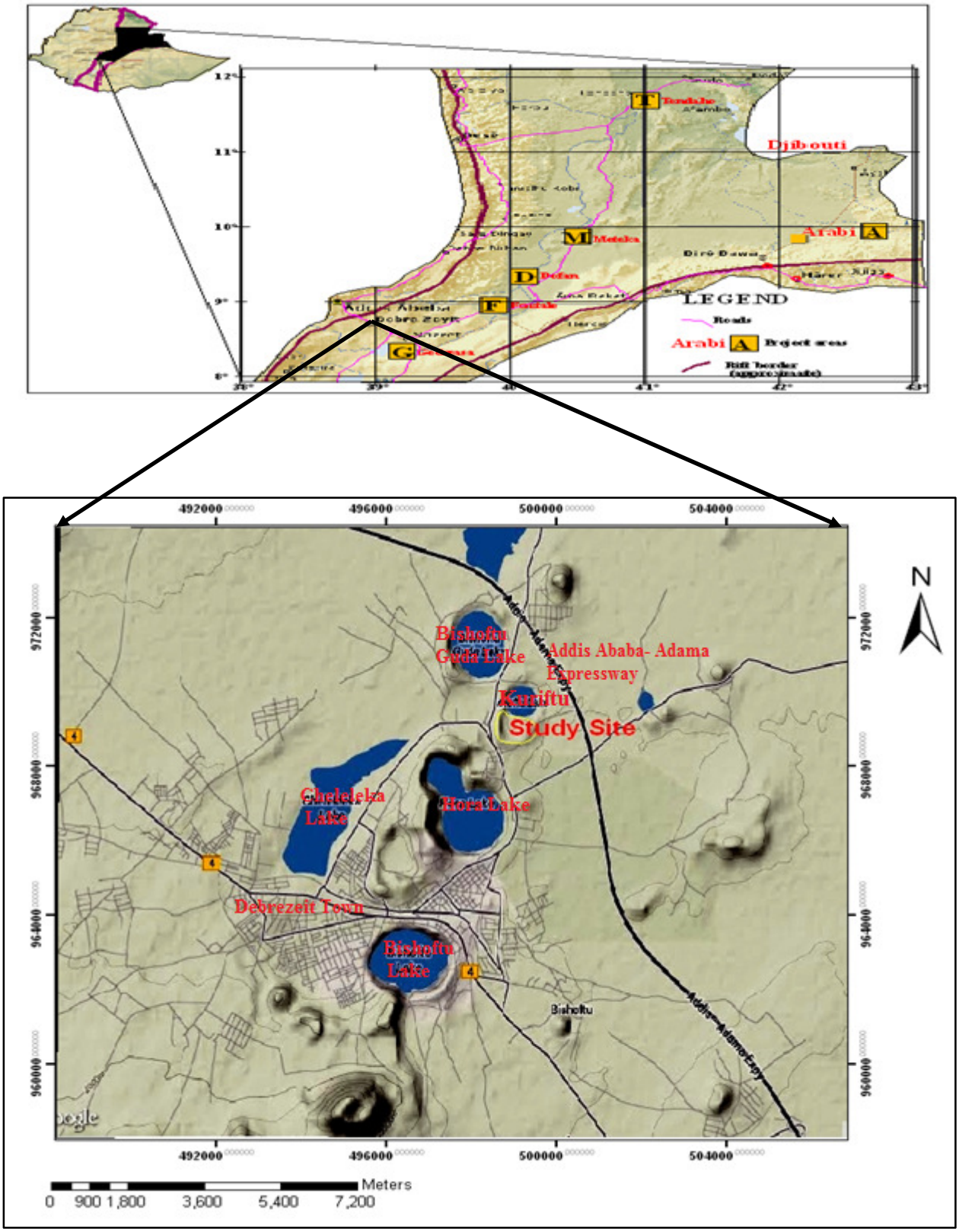

Figure 1. 2 Location map of Debrezeit area.

1.3 Objectives

1.3.1 General Objective

The main objective of the study is to provide seismic hazard analysis for the Debrezeit area, with the emphasis at Kuriftu site.

1.3.2 Specific Objectives

Probabilistic Seismic Hazard Analysis including the local soil site condition was intended to conduct in the selected area with the aim of:

- To identify appropriate seismic source zones that affects the area of interest.
- To determine the b-value for the seismic source zones identified on the bases of seismicity and tectonics.
- To select appropriate ground motion attenuation relation for the Debrezeit area.
- To determine seismic hazard curves including site effect for the Debrezeit area.

In order to achieve this Objective: Literature on global and regional seismicity and tectonics, regional earthquake catalogue and b-values, strong ground motion attenuation relations, global and regional earthquake hazards and methods of seismic hazard evaluation are reviewed.

- The earthquake catalogue of the study area is compiled from the revised and updated catalogues of various sources and agencies in such a way that by merging and editing their databases and considering destructive earthquakes from 1906 to 2011 that originated within 200km from the grid (Appendix I).
- The seismicity data were checked for completeness with respect to time and magnitude using the least-squares regression and the threshold magnitude is obtained in least-square fitting from the Gutenberg-Richter power low distribution in the time interval of completeness chosen to be considered as the best representative sample of the current trend of seismicity of the area; on the basis of accuracy, completeness and the minimum time span for the sampling period to cover enough fluctuations in seismic region to represent the actual long term trend for the seismic activity.
- The heterogeneous and fragmented data obtained from different agencies that use different magnitude scales are homogenized into a single unifying magnitude.

- Using the Geological map and section, topographic map, Seismicity and tectonic maps of the region the seismo-tectonic source zones are identified.
- The b-value was computed using Gutenberg-Richter method for the seismic source zones identified on the basis of seismicity and tectonics.
- A Strong ground motion attenuation relation that best represent the study area is selected.
- Based on the information of the seismic sources: the dynamic parameters, the catalogue compiled and the strong ground motion attenuation relation adopted the parameters used to evaluate seismic hazard of the study area are computed.
- Using a method that closely agrees with that recently recommended by Global Seismic Hazard Assessment Program and computer program CRISIS2012 the seismic hazard for the grid at 08.50°N and 39.00°E at a bed rock and soil site is evaluated for the computed seismic hazard parameters.

1.4 Methodology

Probabilistic seismic hazard analysis (PSHA) is the most widely used approach for the determination of seismic design loads for engineering structures. The use of probabilistic concept has allowed uncertainties in the size, location, and rate of recurrence of earthquakes and in the variation of ground motion characteristics with earthquake size and location to be explicitly considered for the evaluation of seismic hazard. In addition, PSHA provides a frame work in which these uncertainties can be identified, quantified and combined in a rational manner to provide a more complete picture of the seismic hazard. In general, PSHA involves 4 basic steps: identification of sources; establishment of recurrence relationships, magnitude distribution and average rate of occurrence for each source; selection of attenuation relationship; and finally, the computation of the site hazard curve.

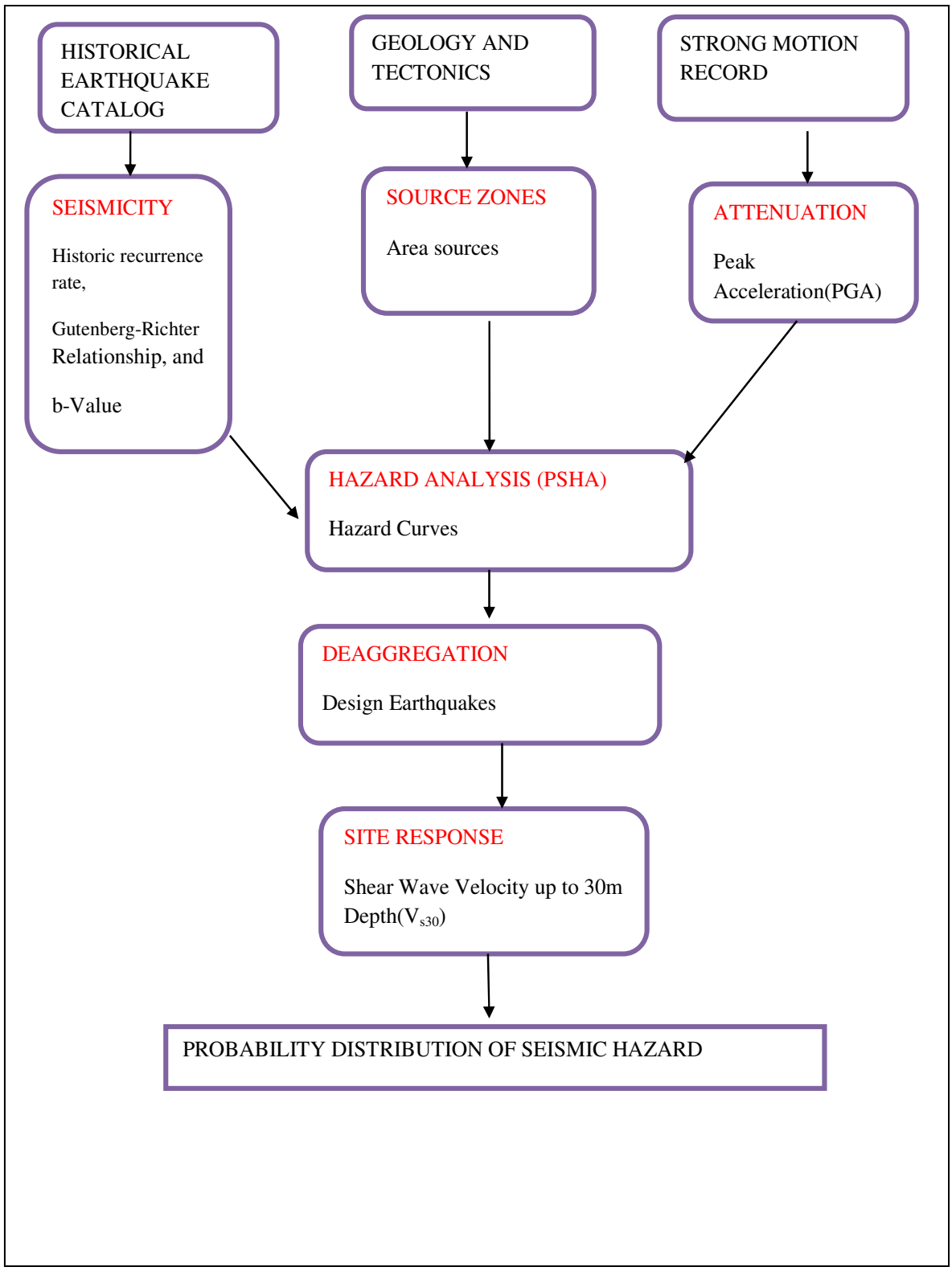

Figure 1. 3 Flowchart showing the elements of the probabilistic hazard analysis methodology.

1.5 Significance of the Study

The aim of engineering seismology is to ensure engineering structures safety by using techniques like anti-seismic, shock isolation and shock-absorbing. The ways of earthquake disasters prevention include project site and planning, earthquake resistant design and earthquake emergency response.

Although earthquakes cause deaths and destruction from secondary effects such as landslides, tsunamis, fires and fault rupture, their principal hazard is the effect of shaking on structures built on or in the ground. The study of recent seismicity in the study area is relevant for understanding the active tectonics of the region. With these rationales, the main purpose of this study is to provide seismic hazard evaluation important for development and settlement in the Debrezeit area. The result of this study could:

- Contribute scientific idea in the area for further research
- Be used to take a measure of earthquake disaster prevention
- Help geotechnical engineer to design a sound earthquake resistant structures in the area
- Assist a Seismologist to understand strong ground motion prediction in the area
- Be relevant for understanding of tectonics of the area.
- Assists designers, town planners and decision makers in, what and where to build, land use categorization and optimum way of ensuring high-rise structures are adequately protected from earthquakes
- Can be used as an input of regional seismic microzoning and for the appropriate revision of the current Code of Building standards of the country
- Helps to estimate possible damage in an eventuality and to formulate the appropriate hazard mitigating measures
- Can assist in identifying the most vulnerable localities in the area

1.6 Layout of the thesis

This thesis is organized in eight chapters. The first chapter is introduction to the thesis expressing background and justifications of the study, location of the study area, methodologies and materials needed to conduct the study, the objective, significance and scope of the study. The second chapter reviews regional seismicity and tectonic, geological setting, theories and findings that form the basis of this study. Chapter three deals with PSHA methodology and chapter four is about selecting and constructing the geometry of seismogenic sources that are responsible for earthquakes in the area of study. The fifth chapter discusses source seismicity and b-value. The sixth chapter deal about strong-ground motion and selection of attenuation relation for study area. Chapter seven deals with computing hazard curves and presents the results of seismic hazard evaluation at a bed rock and soil site in the area of study. The last chapter deals with discussion, conclusion and recommendations.

CHAPTER TWO

2 Seismicity, Tectonics and Geological Review

2.1 Seismicity and Tectonics of the East African Rift System (EARS)

According to geological evidence regarding the overall geodynamics, the EARS region was under sea in the Mesozoic era. The regression of the sea due to the up warping of the region resulted in a single landmass consisting of Africa and Arabia, known as Afro-Arabian dome (Gass, 1975) that represents an uplifted region of the earth's crust. It is believed that about 15 million years ago, a plume that rose beneath what is now the Afar Triangle heated and stretched the overlying continental crust (Afro-Arabian dome) until it fractured in three directions.

The great mass of pre-rift volcanic in the region is perceived by (Almond,1986) as directly related to the initial phase of rapid extension across the Red Sea and Gulf of Aden axes at a time when the Afar triple junction was first being formed. He concluded that before early Miocene there was no recognizable Afro- Arabian dome. The wide-spread late Eocene uplift in the Ethio-Arabian region indicated by rapid marine regression which is considered the formation of the Eastern rift system uplift and axial down wrapping. The process of rifting was always preceded by a long period of uplift; in the case of younger rifts the uplift is related to the rise of hot, low-density material from the mantle and formation of a transitional layer at the base of the crust.

The Afro Arabian dome is then dissected into three parts consisting of the Arabian**,** the Nubian (African) and the Somalian plates. The continents (Africa and Arabia) separated along two of the fractures, and the basaltic magma welled up from the mantle between the continental blocks forming denser oceanic crust. Eventually, the Indian Ocean flooded these canyons to create what are now the Red Sea and the Gulf of Aden as shown in Figure 2.1. Today, these narrow seaways are volcanically active spreading center and continue to widen with the passage of time as the result of the drifting apart of the Nubian plate with the Arabian plate and the Arabian plate with the Somalian plate in the Red sea and the Gulf of Aden, respectively.

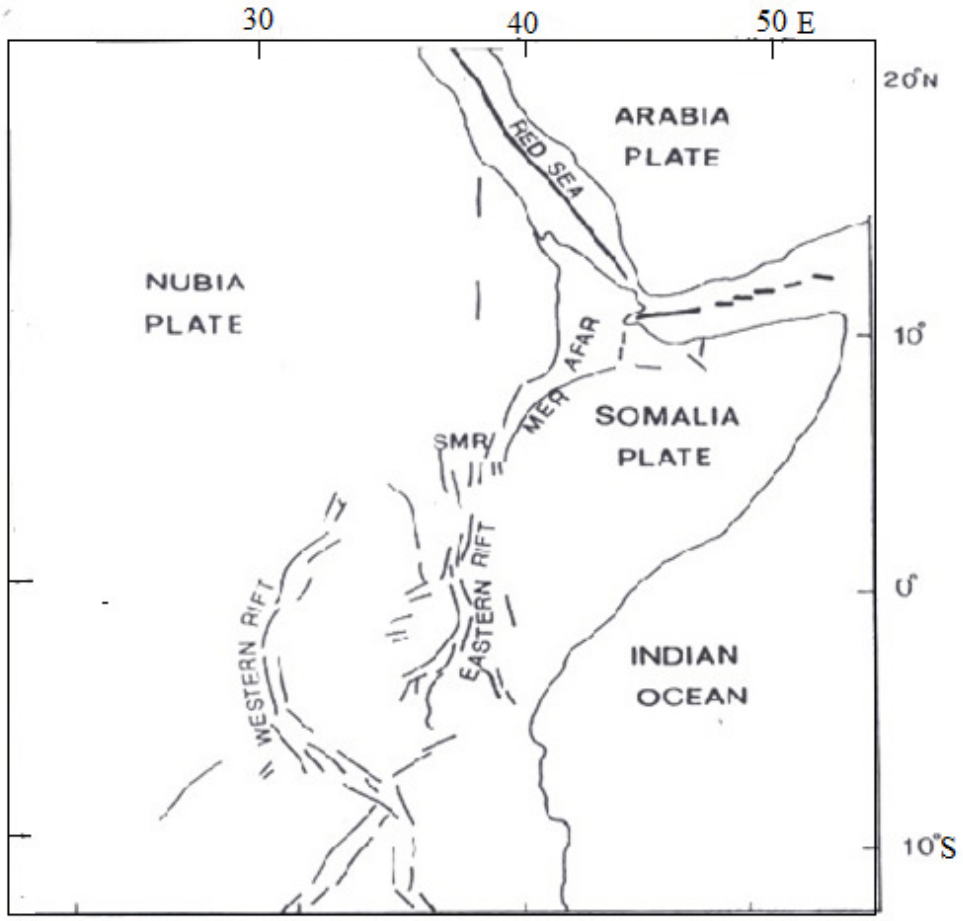

Figure 2. 1 Structural elements and regions in the East African Rift system and southern Red Sea, where: SMR: Southern Main Rift, MER: Main Ethiopian Rift (After Kebede, 1989).

The East African Rift System (EARS) is one of the most fascinating geologic features observed on the surface of the earth. Like the Red sea and Gulf of Aden rifts, East African rift system marks the locus of divergence between continental plates. It is an incipient boundary between the Nubian and Somalian plates as shown in Figure 2.2. The East African rift system is part of the Afro-Arabian Rift system also called Great Rift Valley that extends for about 7200 km from Turkey in southern Asia to Mozambique southeastern Africa (Mohr, 1968). On regional basis, the East African rift system follows broad, NNE-SSW direction from the Red sea in the North to the Mozambique belt in south and offers a unique opportunity to observe the initiation of plate divergence in a continental environment and is considered to be the best example of continental rifting. It represents the most extensive currently active zone of continental rifting on the earth. Thus, it has been the focus of many research works aimed at understanding both the status of

rifting in East Africa and the process involved in continental rifting in general (Shudofsky, 1985).

The three rift systems: the Red Sea trough, the Gulf of Aden ridge and the East African rift meet at the Afar triple junction, which together with Iceland, is a unique geological and geophysical provinces in the world of observing young ocean floor created on land; that is, it is one of the two areas where crustal spreading, dike injections and the formation of new lithospheric plate material may be observed. Different geophysical methods have confirmed that the drifting apart of the Arabian plate is still going on in the direction consistent with that found from the records of the geological past (Gass, 1975; Bohannon et al, 1989; Bonatti, 1987). In contrast, the general northward motion of the African plate (Shudofsky, 1985; Hempton, 1987) resulted into a collision with the Eurasian plate while the whole continent is under a compressive stress environment due to the diverging oceanic ridges from the Atlantic and Indian oceans.

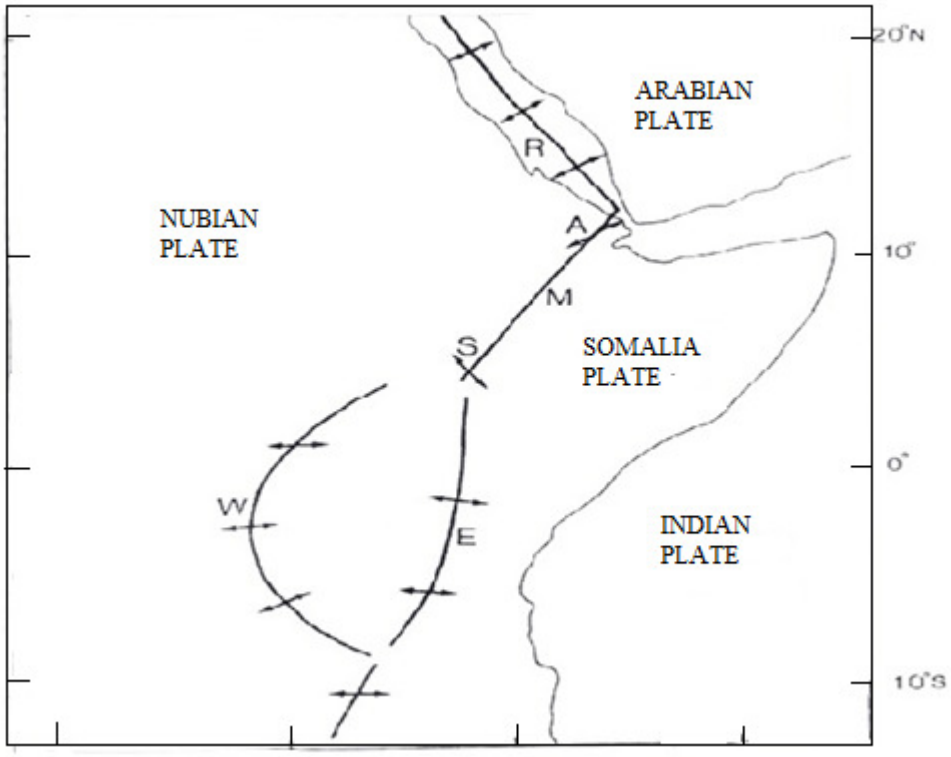

Figure 2. 2 Position of the East African Rift System and Southern Red sea, Schematic map (after kebede 1989).

Development of rifts joined at a triple junction was not simultaneous but arose from differential rift movements initiated at different times; the Gulf of Aden in the early Miocene, the Red Sea in the late Cretaceous, the Afar in the lower Miocene or Oligocene, and the Main Ethiopia Rift in the Pliocene or late Miocene. The East African rift system in turn comprises several discrete rift segments; among which the prominent ones are the Afar depression**,** the Main Ethiopian Rift (MER) and the Southern rifts which constitute the Ethiopian Rift System and the Eastern and Western branches of the East African Rift system.

The East African rift system has a clear structural link with the worldwide oceanic rift system via the triple junction where Afar depression and the Gulf of Aden and the Red sea rift segments converge. Seismicity and focal mechanism studies of the East African rift system show that the constructive boundary of East African rift system is complex and forms a series of inter-connecting rifts through eastern and southern African. This rift display fault patterns that cannot be simply explained by geometric lines with extension perpendicular to the rift. This could be due to either one or both of the following reasons as proposed by (Sykes, 1970):

- The pattern of failure is more in continental areas than in oceanic areas, perhaps because continents are older and contain many zones of weakness;
- The breakup of Africa is in an early stage and this pattern of breakup is complex and multi-branched.

One of the long-standing controversies about East African rift system is the extent to which pre-existing Precambrian structural trends control the location and strike of the rift (e.g., Boccaletti et al., 1994). The East African rift system parallels pre-existing Precambrian structural trends in some places and it is independent of this trend in others. As clearly seen in Figure 2.3, due to its geographical location in the vicinity of two recognized seismically active tectonic features, namely the major tectonic plate boundary that divides continental Africa from the Arabian Peninsula and the major break in the earth's crust due to the East African rift systems, the region has experienced the effects of earthquakes and volcanic activity throughout its history. The overall distribution of epicenters in East Africa differs, however, from the narrow linear pattern of activity usually associated with mid-ocean ridges.

Seismicity studies of the East African rift system by many scholars have helped to recognize that the seismcity associated with the East African rift system continues in to the Indian Ocean and joins with Mid-Atlantic rift (Fairhead and Stuarte, 1982). The Red Sea and Gulf of Aden have subsequently been recognized as parts of the world rift system. In general, both the structural and seismic features suggest a connection of the East African rift system to the world rift system.

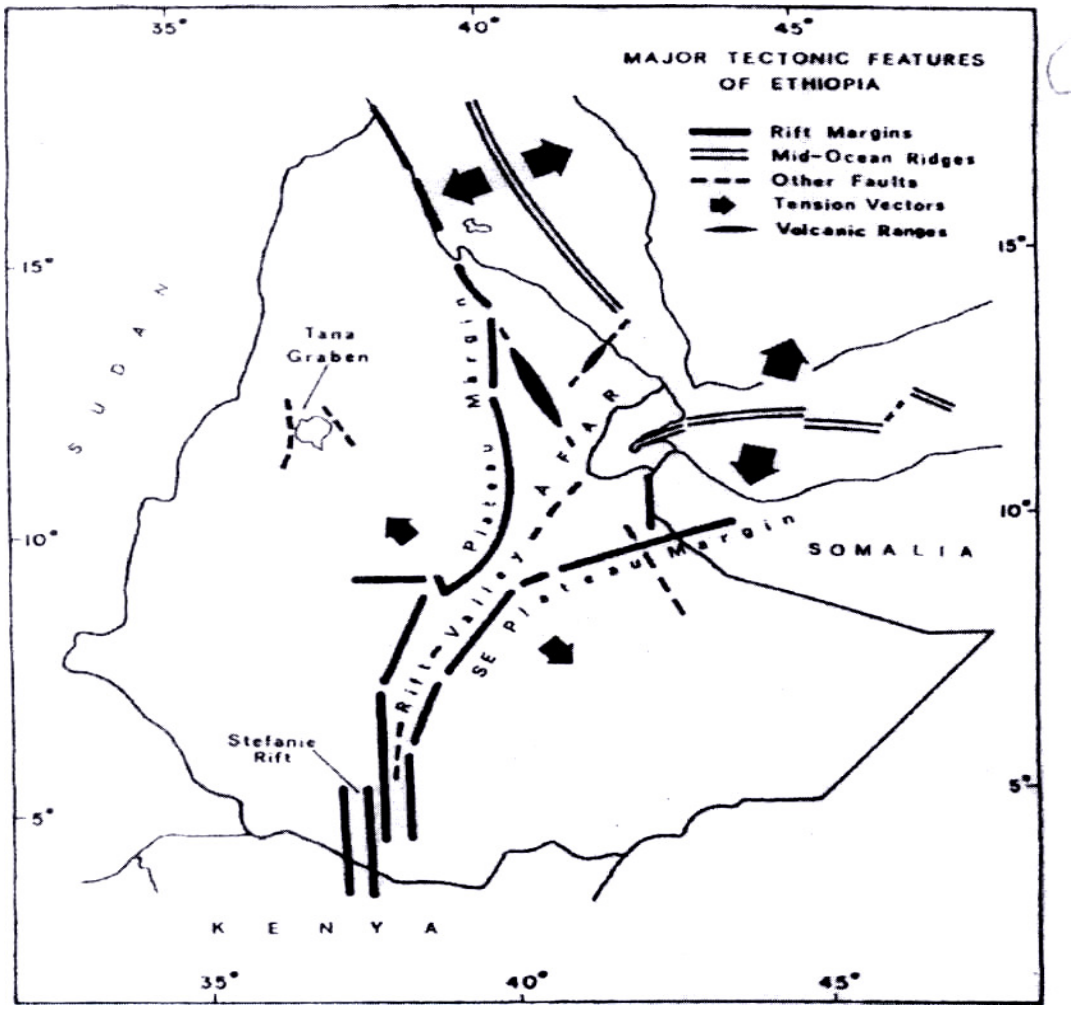

Figure 2. 3 Major earthquake-causative tectonic features of the region; diagrammatic map (after Gouin, 1979)

2.2 Seismicity and Tectonics of the Ethiopian Rift System

Written history of earthquakes in the region, as presently known, started in 1400 A.D with eruption of the Dabbi volcano, some 120km north of Asseb, at the present day Eritrea. The earth tremors, which accompanied this volcano, were felt up to the coast of Yemen (Gouin, 1976).

Since seismic instrumental recording started, a number of destructive earthquakes have been recorded in the region. The list of major earthquakes occurred in the region is provided in Table 2.1. These instrumental records, both by local and international stations show that the Ethiopian rift system, the Gulf of Aden and the Red Sea are seismically active regions and are characterized by several intermediate-size (5.5<M<6.5) and major (6.5<M<7.5) earthquakes (Asfaw, 1996). For example, the one that occurred in Awasa with M_b= 6.3 in 1960 (Gouin, 1979), in Serdo, central Afar, with Ms=6.3 in 1969, the Yemen earthquake of 1982 with Ms=6.0, and the 1987 southern most rifts earthquake in Ethiopia with Ms=6.2 and the 1989 Dobbi graben, central Afar, earthquake with Ms=6.3 are intermediate size earthquakes that occurred in the region. While the Langano earthquake of 1906 with Ms=6.8 (Gouin, 1979), the Kara kore earthquake of 1961 with Ms=6.6, the Southern Red Sea event in 1977 with Ms= 6.6 and the Juba earthquake, Southern Sudan, in 1990 with Ms=7.1 are the major earthquakes in the region. These events indicate that the whole segment of the East African rift within Ethiopia and the neighboring region is characterized by damaging earthquakes and the seismicity of the region from 1960 to 1993 is shown in Figure 2.4.

Table 2. 1 List of Major earthquakes (M > 6.5) that occurred in the region, (after Kebede and Asfaw, 1996)

Year	M	D	h	Min	Lat.	Lon.	depth	M_b	M_s	M,	Mp
1986	05	13	00	00	3.70	36.30	00	0.0	6.8	0.0	0.0
1906	08	25	11	54	8.00	38.50	00	0.0	6.6	0.0	6.5
1906	08	25	13	49	8.00	38.50	00	0.0	6.8	0.0	0.0
1912	07	09	08	18	3.00	33.00	00	0.0	0.0	0.0	6.8
1915	03	18	21	00	14.00	42.00	N	6.5	5.7	0.0	0.0
1915	05	21	04	18	06.00	31.00	00	0.0	0.0	0.0	6.6
1915	09	23	08	14	16.00	39.00	00	0.0	0.0	0.0	6.8
1928	01	06	19	32	00.40	36.10	00	0.0	6.9	0.0	0.0
1941	01	11	08	32	16.40	43.50	N	6.5	5.9	0.0	0.0
1961	06	01	23	29	10.40	39.90	00	0.0	0.0	0.0	6.6
1966	03	20	01	42	00.81	29.90	34	0.0	7.0	0.0	0.0
1967	03	28	02	41	19.86	38.71	27	6.7	0.0	0.0	0.0
1977	12	28	02	45	16.65	40.27	33	5.9	6.6	0.0	6.8
1990	05	20	02	22	5.07	32.15	14	0.0	7.1	0.0	0.0
1990	05	24	19	34	5.32	31.84	36	0.0	6.6	0.0	0.0
1990	05	24	20	00	5.35	31.86	16	0.0	7.0	0.0	0.0

m=month d=date h=hour M_P=magnitude made by personal judgment

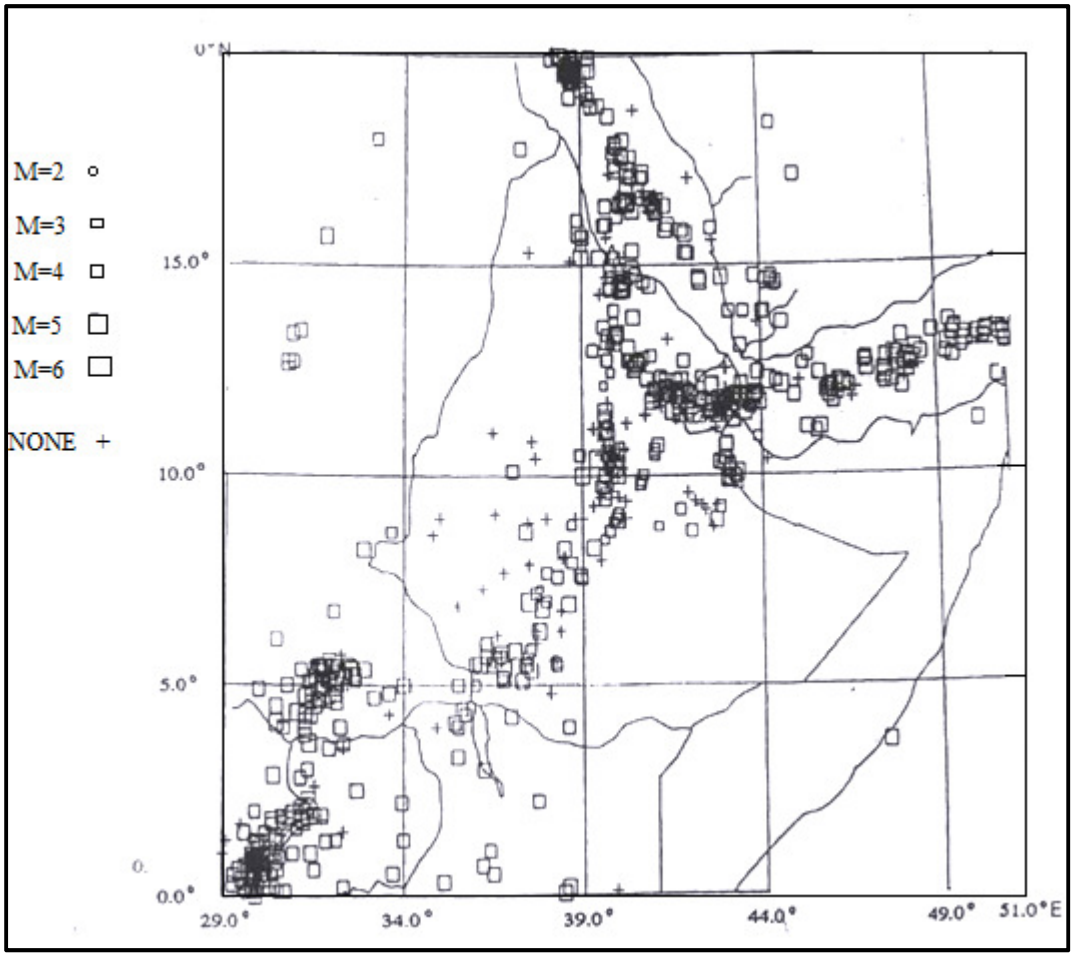

Figure 2. 4 Seismicity of the region for the period 1960-1993. Magnitude is proportional to the size of the square and the '+' symbol is used for earthquakes without magnitude (Ayele 1995).

To have a further insight in to the Main Ethiopian rift system and the Afar depression, as the two segments ultimately affect the seismotectonics of the study area, it is better to have a close look into of the seismicity and tectonics of these segments. The Afar depression is a huge depressed region of about 110,000 sq. km. area, triangular, for which reason it is often referred to as Afar triangle**.** The Afar triangle and its surrounding region are areas of active tectonics. Plate separation is known to accommodate diffuse crustal extension and abundant in volcanism all over the rift floor in Afar. Recent studies indicate, however, that although fault scarps and fissures are distributed over the whole width of Afar triangle active rifting is currently localized in some narrow zones of principal rifts, especially along the westward propagating Gulf of Aden rift (Sigmundsson, 1992; Leipine and Him, 1992 and Tapponnier et al, 1990).

As argued by Acton and Stein (1991) the extensions concentrated on a set of rifts are transferred into a single rift that eventually emerges as a sea floor spreading. The central part of the Afar depression tends to be a featureless and monotonous flat plain. The recent developments in the understanding of the tectonics of the region suggest two types of plate boundaries, namely, spreading and transform faults are present in Afar. As can be seen in Figure 2.5 below, the central part of the Afar Depression is dominated by WNW-ESE to NW-SE trending faults. In the south two differently oriented fault systems are dominant - the NNE-SSE to N-E striking faults, which are the extension of the Ethiopian rift system and the E-W to ENE-WSW trending faults. The seismic activity in the Afar Depression is high, characterized by small and intermediate size earthquakes. The Western escarpment of Afar depression is characterized by almost N-S running faults and it is one of the most seismically active zones in the whole region. Several destructive earthquakes occurred in the region that includes the earthquake of 1969 in Serdo, the 1989 earthquake and the 1961 Kara Kore earthquake.

As far as the evolution of tectonics is concerned, initiation of the MER was in late Tertiary times by the Pliocene there was a shallow trough with a deep infilling of silicic volcanics, dominated by ignimbrites originated from a center close to the rift margins. The term rift margins can be defined in terms of physiographic as the strip between the flat rift floor and the escarpment of the high (eastern and western) plateau.

A major episode of uplift and graben faulting early in the Pleistocene created the lofty escarpments of the rift margin. Subsequent tectonic fragmentation of the rift floor formed a persistent belt of intense, fresh faulting which has been termed the Wonji Fault Belt that marked the floor of MER as shown in Figure 2.5. The faults are short and of normal type and are notably associated with tensional features. Thus, the Wonji Fault Belt that extends further north across Afar dominates the tectonics of the floor of the Main Ethiopian Rift. The Wonji Fault Belt is frequently, but not always, axial to the rift and is dextrally, displaced along the same cross-rift lineaments, which displaces the rift margins.

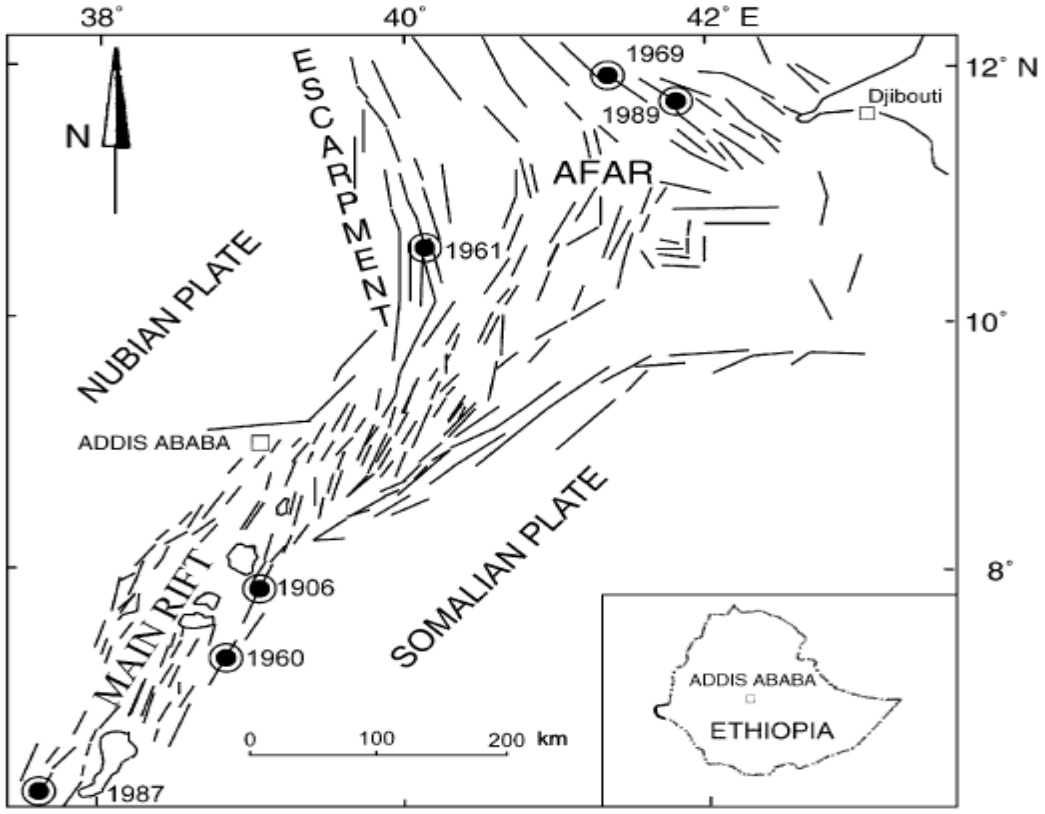

Figure 2. 5 Structural pattern of the Main Ethiopian and Afar Rift region (after Mammo, 2005).

Two main fault systems have been recognized in this region; a NE-SW trending fault system which characterizes mainly the rift margins and a NNE-SSW to N-S striking fault system (the Wonji Fault Belt), oblique to the rift margins, which constitute sigmoidal fault pattern marked by a right stepping en-echelon faults. The latter fault system affects both the rift floor and margins (Mohr, 1970a). The seismic activity is usually represented as small to intermediate size earthquakes. However, large size of magnitude 6.8 occurred in 1906 at Langano, the 1960 Awasa earthquake of magnitude 6.3 and the 1989 Afar, Dobi graben earthquake of magnitude 6.3 are the prominent ones.

Concomitant volcanism broke on the rift floor-giving rise to volcanic centers such as Wechecha, Yerer and Zequala (Cuqqaala) younging riftwords (Morton W.H et el, 1978). The region in the MER lying on the extension of the alignment of earthquake epicenters exhibits a change of direction in the volcano-tectonic alignment. The Dimtu-Moye- Gadamsa alignment changes to the Boset-Kone alignment (Berhe, 1987).

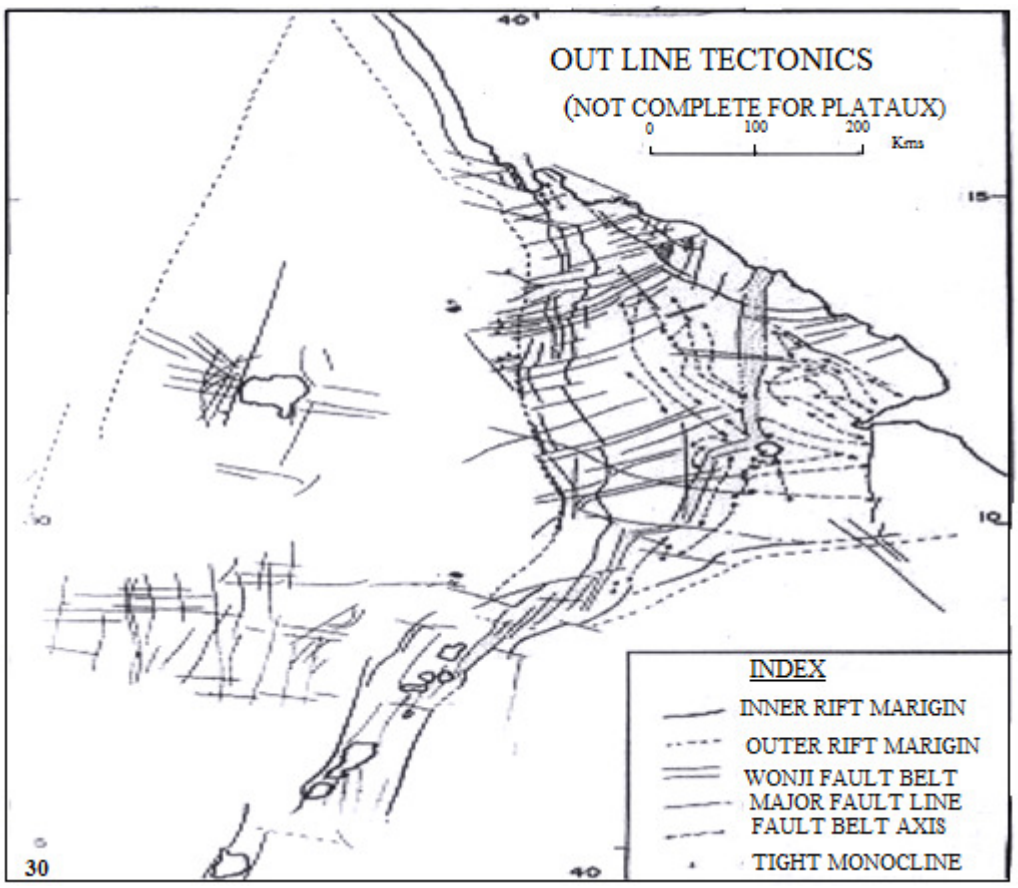

Figure 2. 6 Outline tectonics of the region (after Mohr, 1967).

2.3 Regional Geology

The regional geology of the area is characterized by a series of formation and events from early Tertiary to Quaternary Period. The grand Afro-Arabian swell was formed in upper Eocene. Following uplift of horn of Africa, immense quantities of lavas, the Trap series, extruded from fissures and eruption centers (Mohr, 1961). The trap series lavas, which are mostly basaltic in composition (with some acidic flows in the upper parts), cover large areas of Mesozoic sediments and in some places; they rest directly on the Basement complex. Such uplifts, together with the extrusion of thick and extensive Trappean lava, account for the formation of the present highland region of Ethiopia.

In the upper Pliocene to recent, a succession of pantelleritic Rhyololites, Trachytes and Ignimbrites with subordinate intermediate and basic rocks, were erupted chiefly at the rift margins and along the seismically active Wonji fault. This trachyte-pantelleritic ignimbrite

covered most of the southern Ethiopian plateau and filled the Main Ethiopian Rift. Its thickness ranges from about 300m to 500m, probably even greater on the rift floor (Mohr 1968, Baker et al. 1972).

2.4 Geologic structures and Tectonics of the study area

Brittle deformation consisting of fractures, joints and faults are dominant in the area. Structures are extensional and affect chiefly the rocks of the Intra Rift Complex and partially those of the Western Rift Margin Complex. These structures are grouped into four main fracture systems consisting mainly of joint sets and some faults (Abebe et al., 1999). These are:

1. The N-S/NNE-SSW fracture system which is analogous to Wonji Fault Belt, constitutes normal faults with steeply dipping joints with dip amount of $>85^{o}$.

2. The NE-SW fracture system that parallels the regional trend of the MER, and has normal fault of about 1m thrown and dip amount $>85^{o}$. It is widespread especially in the Nazret unit where the most important physiographic features are NE trending ridges and escarpments.

3. The E-W fracture system mainly concentrated in zones close to the Yerer Volcano to the east of Addis Ababa. It parallels the trend of the Yerer-Tullu Wellel Volcanic Lineament (YTVL) structure. It consists of sub vertical to vertical joints with an estimated dip amount $>85^{0}$.

4. The NW-SE fracture system. Few high angle normal faults have been documented with high morphologic evidence (escarpments). This system affects mainly the oldest units of western Rift margin.

The structural geometry of the area is controlled by the left-lateral oblique rifting of the MER (Boccalitti et al., 1999) and right lateral transtensional Yerer-Tullu Wellel Volcanic Lineament structure (Abebe et al., 1998). Thus, the interference between the MER and YTVL structures would be the first order cause of features like gradual transition between the rift floor and the West Rift shoulder.

High *P*-wave velocities and *Vp*/*Vs* ratios are imaged beneath the Debre Zeit chain of Quaternary eruptive centres. This region marks the intersection of the MER border faults and the reactivated Precambrian Ambo fault to the west of the main rift axis. Xenoliths derived from crustal depths exhibit evidence of melt beneath the Debre Zeit volcanic chain (Rooney *et al.* 2005). High *P*-

wave velocities and *Vp*/*Vs* ratios beneath Debre Zeit suggest that a small portion of the melt intrudes the crust directly above the low velocity mantle anomaly. Geochemical data also suggests that the source of the melt creating our high velocity and *Vp*/*Vs* anomaly is at a greater depth than that of the magmatic segments along the rift axis. However the Debre Zeit region lacks the closely spaced, morphologically young fault scarps, and active seismicity of the rift axis (Wolfenden *et al.* 2005; Casey *et al.* 2006; Keir *et al.* 2006a). It also lacks the large relative positive Bouguer anomalies observed over the magmatic segments (e.g. Mahatsente *et al.* 1999; Mickus *et al.* 2004). Therefore, this chain of Quaternary volcanoes may represent either a failed or underdeveloped (i.e. incipient) zone of strain.

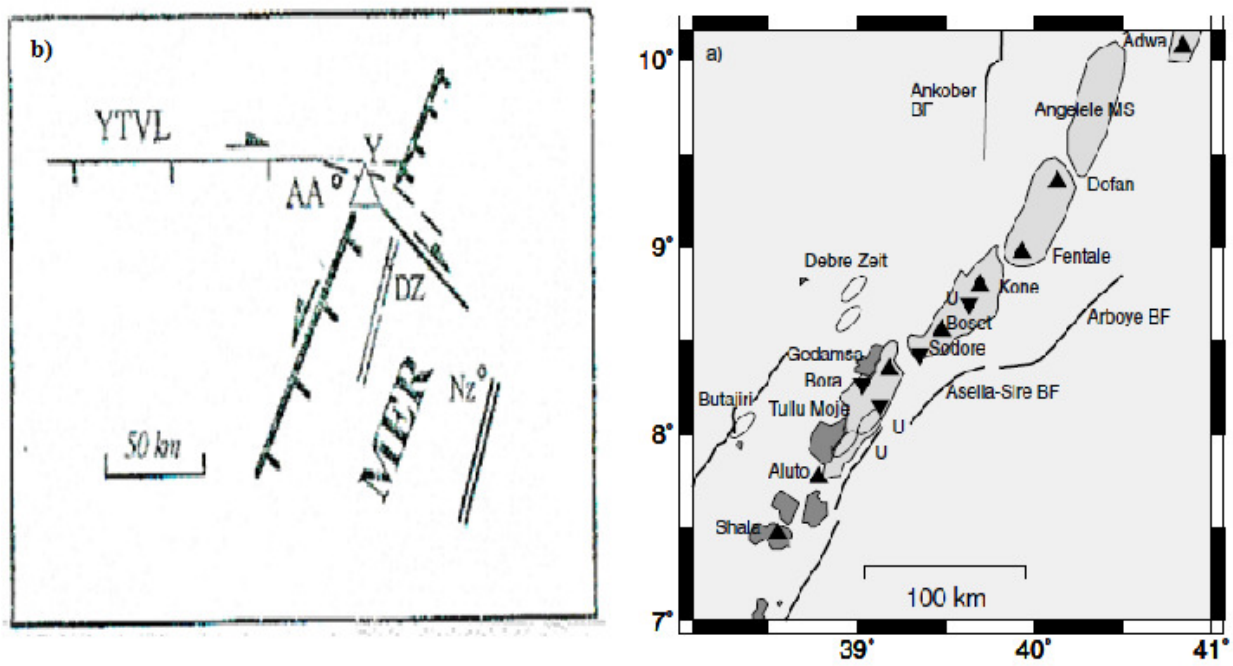

Figure 2. 7 (a) Geological map of the Ethiopian Rift, including border faults (thick black lines), magmatic segments (light grey polygons), Quaternary volcanoes (black triangle), Butajira and Debre Zeit volcanic chains (ellipses). (b) Sketch of the present tectonic setting in the Debrezeit area.

AA:Addis Ababa ; DZ:Debrezeit ; NZ:Nazret ; MER: Main Ethiopian Rift ; YTVL: Yerer-Tulu Wellel Volcano-Tectonic Lineament. Arrows indicate strike slip movements; Barbs; Down throw block. Heavy parallel lines: Main Ethiopian Rift; Thin parallel lines: secondary expansion axis of Debrezeit.

Thus, the interference between the MER and YTVL structure would be the first order cause of the two main features of the area, that are:

a. The gradual transition between the rift floor and the west rift shoulder;

b. The onset of the local expansion axis of Debrezeit.

In particular, the Debrezeit area is interpreted as the place where the opposite movement along YTVL and MER accommodate since Quaternary (Fig 2.7), with the consequent formation of a localized zone of extension where volcanic activity concentrates. This evolution is in agreement with the change from NW-SW to E-W between 2-1.7 Ma observed by Boccaletti et al. (1999) in the adjacent rift sector near Debrezeit area.

2.5 Geologic Setting of Debrzeit

The geologic setting of Debreziet area had been studied by different authors such as (Mohr, 1961; Justine- Visentin et al., 1994; Kazmin, 1995; Wolde, 1996; Chernet et el., 1998). According to Mohr (1964), the oldest exposed lavas near Debrezeit are peralkaline rhyolites and trachytes, and equivalent welded tuff of the volcanic center forming hills southwest of the town. Contemporaneously with the emplacement of peralkaline rhyolites and trachytes, lavas and igmbrites, there were wide spread basaltic cinder cones eruptions as well as restricted local flows of olivine basalt and olivine trachy basalt. This was later followed by the formation of explosion craters.

The area around Debrezeit, is mainly covered by volcanic and sedimentary rocks. The sedimentary rocks consist of alluvial cover and lacustrine sequences. Volcanic activity in the area resulted in central composite volcanoes and monogenic apparatea as domes, spatter cones and maars. Ignimbrites, consisting of several units, appear as wide subhorizontal covers, while basaltic lavas are generally tabular.

The detailed (1:100,000) geological map of Debrezeit (Mazzarini, 1999) recognize ten volcanic units that were grouped into four volcanic complexes. These were defined on the basis of field data and morpho-structural features, further they define three main structural sectors; the western rift margin, the main rift floor and an intra-rift depression. Since upper Miocene, the Debrezeit area was the site of the interaction between the Main Ethiopian Rift and an E-W traverse structure (Yerer- Tullu Wellel Volcanic Lineament, YTVL) (Figure 2.7) that produced the smoothing of the morphological expression of the rift margin and the onset of a secondary rift axis associated with the most recent volcanic activity (Mazzarini, 1999).

The geologic mapping and the morpho-structural analysis lead to the identification of two volcanic sequences belonging to the floor of the rift and to its margin, respectively. Furthermore, a third local sequence has been recognized along a secondary expansion axis parallel but shifted west ward in respect to the axis of MER. Accordingly three informal complexes has been distinguished, characterized by distinct evolution of the volcanic products. The complex defining the western limit of the rift consists of tabular basalts, large composite volcanoes, ignimbrites and scoria cones with associated basaltic lava flows, and ranges in age from 7.5 and 2 Ma (Mohr, 1961). The floor complex is chiefly formed by a sequence of ignimbrites, considered as part of Nazareth group which displays a widespread regional distribution. The ignimbrites are covered by tabular basalt and pyroclastics, mainly of rhyolitic composition. The volcanic activity shows ages comprised between 5.4 and 1.8 Ma (Boccaletti et al., 1999). Finally the axial sequence developed since 1.2 Ma up to Holocene; it is constituted by composite volcanoes, scoria cones and maars grown along a relatively narrow NNE trending depressed area. The youngest volcanic are interbeded with lacustrine deposits. The geology of the area is strongly conditioned by the interaction between the left lateral oblique rifting of the MER (Bonini et al., 1997; Boccaletti etal., 1998) and right lateral transitional YTVL structure (Abebe et al., 1998). A simplified geological map of Debrezeit by (Abebe, et al., 1999) is shown on figure 2.8.

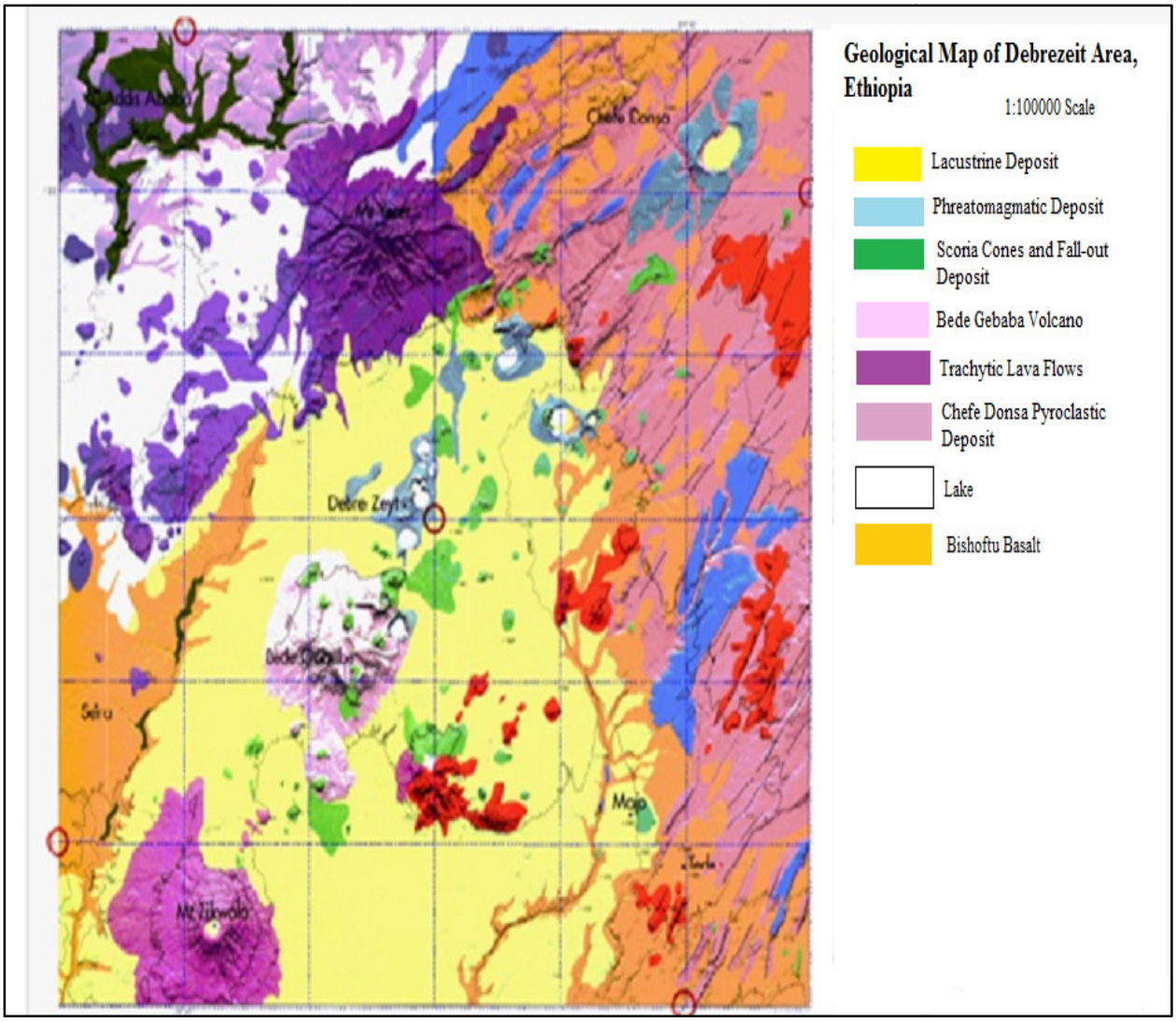

Figure 2. 8 Geological map of Debrezeit area. *Source*: Abebe, et al., 1999.

Bishoftu Volcanics (BV)

In the Bishoftu Volcanics there are two groups represented by spatter and cinder cones with associated tabular lavas and phreatomagmatic deposits, respectively. The second, consisting mainly of pyroclastic surges and highly fragmented deposits associated with maars are chiefly concentrated in the central part of the study area and the highest thickness of the lacustrine sediments frequently intercalated with the phreatomagmatic products. The composition of lavas and juvenile glass ranges from alkali basalts to olivine basalts and trachyandesites (Abebe, 1999). This unit is found extensively in the central part of the study area forming a NNE trending

belt in the rift axis complex. Bishoftu volcanics represent the most recent basic lava flow of the Debrezeit area (Tsegaye Abebe. et al., 1999), which was also reported as the younger volcanics by (Grasparon et al., 1993).

Vesicular basalt is found associated with and/or sandwiched between pyroclastic and lacustrine deposit and covering the volcanic tuff in some parts of the area. It is dark gray in color, vesicular, massive and sometimes scoracious and at places secondary minerals, dominantly zeolites and calcite fill the vesicles. According to Adane (1999), this unit has high porosity and permeability due to secondary structures and the interconnection of the pore spaces.

Lacustrine Deposits

Lacustrine environment started after the Bede Gebabe volcano unit and continued during the eruptive activity of Bishoftu (Abebe, 1999). The lacustrine sedimentations are the results of deposition in this large ancestral lake (Mohr, 1967 and Abebe, et al., 1999) and they are inter-bedded with Pliocene-Pleistocene ignimbrite in lakes region and on the rift shoulders in general, and within Debrezeit and the surrounding areas in particular (Mohr, 1966). These fine-grained deposits are generally brown-yellowish, thinly stratified and often contain abundant volcanic matrix. Their thickness ranges from less than 5 m up to 8 m. In these successions, volcanic layers are frequent and become predominant and coarse grained in the neighboring of the maars. Due to their fine-grained composition and compactness, these deposits have low porosity and permeability (Adane, 1999).

Alluvial Cover

Due to their loose nature, alluvial sediments are porous and permeable. Moreover, their grain size constitution varies from coarse to silty and clayey, giving rise to the occurrence of highly yielded unconfined, confined and semi-confined aquifer together with local perched ones (Tamiru, 1992). The pair-wise comparison of geologic unit was done in terms of their importance with respect to groundwater occurrences by considering their characteristic such as rock type and thickness, fracture density, compactness, the type and degree of cementation etc. The high weight was calculated for Bishoftu volcano unit due to high porosity and permeability.

Addis Ababa Ignimbrite (AAI)

This unit is exposed in north western part of the study area and make up the minor portion of the volcanic rocks. It occurs along the foot of eastern escarpment of the Main Ethiopian Rift (MER). It is found resting on Addis Ababa basalt. This unit comprises different flow units, consisting of pale green to pale-yellow welded and crystal rich ignimbrite. K-Ar age dating conducted on samples from this unit has given an age ranging from 5 to 3.3Ma (Cherenet et al., 1999). This unit is moderately to strongly welded, characterized by well developed vertical joins and fractures which provide for high to moderate permeability (Adane, 1999).

Central volcano

Central volcano unit is represented by Yerer volcanic unit within the western rift margin complex and found in the northern part of the study area. It occurs occupying a series of NE-SW aligned ridges and domes within the largest Yerer volcanic edifies with relief of 1000m difference from the plain. This volcanic edifies is 14km wide along E-W direction. Rock samples taken from this unit were dated by K-Ar method and gave an age of 3.9 to 3.3Ma (Cherenet et al., 1999). The Yerer volcanic unit mainly comprises lava flow with subordinate pyroclastic deposit in the central and eastern sectors. Porhritic trachyte is the main lava flow constituting this unit. It is composed of plagioclase, anorthoclase, oliven and clino-pyroxene phenocryst set in ground mass made up of alkali-feldspars, pyroxene and Fe- and Ti- oxides. The ground mass exhibits trachytic texture. To the top it consists recent spatter cones and associated basaltic lava. Due to their massive nature they have low permeability (Adane, 1999).

CHAPTER THREE

3 Seismic Hazard Analysis Methodology

3.1 Deterministic Versus Probabilistic Seismic Hazard Analysis

Prior to PSHA, most hazard assessments were completed using a deterministic approach, considering individual scenarios of magnitude and location for each source, often with the "worst-case" scenario, or largest magnitude/closest source-to-site distance used to evaluate the design ground motion (Abrahamson, 2006). PSHA can be viewed as the assessment of an infinite number of deterministic hazard analyses, with the hazard being integrated over all potential earthquake sources for all possible scenarios of magnitude and distance. Further, by assigning probability distributions to source and ground motion characteristics, a reasonable ground motion, at some accepted level of probability of occurrence, can be chosen for design. This allows for a more intelligent and economic design in comparison with the often overly conservative, deterministic, "worst-case" scenario approach.

3.2 Deterministic Method

Time is not a factor in the deterministic method, instead, the worst-case scenario is considered regardless of when, if ever, the earthquake is expected to occur. If the design is based on the worst scenario, then the safety will be guaranteed (Dolgoff, 1998). The deterministic method is useful especially where tectonic features are reasonably active and well defined. The focus is generally on determining the maximum credible earthquake (MCE) motion at the site (Kebede and Van Eck, 1997).

To carry out the deterministic method of seismic hazard analysis, the steps to be followed are:

1. Identify the active fault or faults that is likely to cause an earthquake and study the activities of the fault or faults
2. Assume the largest earthquake that happens at the closest position to the site of consideration and determine the focal mechanism and the characteristics of the assumed earthquake.
3. Calculating the ground motion using the proper attenuation relationship and also incorporating other factors.

Some of the advantages of the deterministic method include (kebede and Van Eck 1997):

- It is relatively easier to carry out than probabilistic method;
- It is based on the genetic mechanism of earthquake there will be less exaggeration or diminishment caused by statistical results based on limited earthquake records;
- With the improvement in the study of active tectonics, the deterministic method can do fairly well with better understanding of earthquake.
- The deterministic method is based on tectonic feature; it tends to be conservative, since the maximum earthquake the fault is "capable" of generating is assumed to occur at the location on the fault closest to the site. This conservative answer is especially useful for the important structures like nuclear power plant, large dams and storage for hazardous chemicals etc

And some of its drawbacks are (kebede, Van Eck, 1997):

- It is not always the case that the seismogenic tectonics is well known or identified. It is still hard to determine precisely the seismogenic mechanism for many areas in the world. A perfect relationship between earthquake and active tectonics is seldom available.
- The grossly over-conservative values of the largest earthquake possible on the fault may be unpractical for many of the civil structures which last only for decades. It is not an option for seismic design to treat such large event for both technical and economic reasons. So the application of the results obtained from the deterministic method is still a problem to be discussed.
- The deterministic method does not treat uncertainties well. Rudimentary statistics can be incorporated into the procedure by taking one standard deviation above median at each step (magnitude, PAG, etc.), which give a very big, very conservative estimate. However, the deterministic method does not account for the probability of an earthquake occurring on a fault.

3.3 Probabilistic Method

In general, PSHA involves four basic steps: identification of sources; establishment of recurrence relationships, magnitude distribution and average rate of occurrence for each source; selection of attenuation relationship; and finally, the computation of the site hazard curve. Probabilistic seismic hazard assessment (PSHA) is the most favored approach today. The goal of PSHA is to quantify the probability of certain level of ground motion being exceeded at a given site (or sites) given all possible earthquakes. Thus, the probabilistic method provides a clear picture of the intensity of ground motion and its probability within certain period. This approach, especially the one developed by (Cornell, 1968) allows the use of multi-valued or continuous events and models. This implies that it incorporates the effects of all earthquakes believed to be capable of affecting the site in question. In other word, it is flexible, and takes into account as much data as one can have (kebede and Asfaw, 1996). The main input parameters for this approach are *b*-value, activity rate, minimum and maximum threshold magnitudes, attenuation relation and areal and/ or line seismic source zones. Probabilistic method rectifies several problems inherent in its deterministic predecessor the lack of quantification of uncertainty and probability of earthquake occurrence.

The basic theory of probabilistic method is (kebede and van Eck, 1997):

- ✓ The site of interest at a particular area has source zone nearly, and earthquake in the source zone could affect the site of interest. The source zone can be divided into one or several seismic sources according to tectonics or other seismogenic evidence. Each seismic source has certain characteristics. A simple assumption is that earthquake has an equal probability of occurring at any spot in the source. At an advanced level, the source can have a more complicated model so that the information such as the strike of fault, the statistical results of spatial distribution of earthquake occurrence, and the difference of earthquake magnitude and earthquake mechanism may be identified spatially etc.
- ✓ There is a catalogue of earthquake that occurred in the source zone available, so the probability of an earthquake of a given magnitude occurring in the zone in a period in the future can be worked out. In case that such information is not good enough due to lacking of records or scarce study has been done, further data must be derived from the seismogenic or

active tectonics study or comparison between similar situations. The frequency distribution of earthquakes is well described by the Gutenberg and Richter equation (1966).

- ✓ Considering a certain period for seismic hazard level calculating, for example next 50 years. The selection of the period of exceedance probability will mainly depend on what is the hazard level to be considered. If the levels of seismic hazard to be considered are very high such as for the nuclear power plant, then the period should be much longer usually 500 or even 1000 years should be selected. Otherwise, for ordinary civil buildings the period considered should be shorter, usually 50 years.
- ✓ The exceedance probability of ground motion at certain level is the probability that the ground motion will exceed such a level in certain period in the future. So this indicates what level of risk has to be faced if the design of a structure can resist ground motion up to this level of ground motion. We can get valuable information on the safety and risk we shall mostly like to have.
- ✓ The attenuation relationship, which is based on the statistical results of observation, is anything, but absolute due to condition variation such as site condition, direction to the focal mechanism, etc. and also the anisotropic nature of earth crust. The uncertainty of ground motion predicted by the attenuation relationship can be substantial and must be taken into consideration to reflect the reality.

Thus, the result from the probabilistic method is far more useful for seismic hazard prevention and civil design. With both the level of seismic hazard and its risk, it would be possible for the engineers and other professional to choose for the seismic hazard level that should be well endured by their structure while the corresponding risk level is acceptable for their structures. Thus, the high cost incurred by the conservative safe value or the unexpected high risk as a result of reduced cost without deliberation are both avoided given that the PSHA are applied in the proper way (Dolgoff, 1998). The probabilistic method now covers wide range of seismic hazard assessment including the compiling of seismic zoning map, micro zoning and seismic hazard assessment for engineering structures (Dolgoff, 1998). Although probabilistic method is well accepted, it is not without critics.

Some of the flaws and problems are (kebede and Van Eck. 1997):

- The definition of seismic source model is a difficult thing, sometimes. The earthquake catalogue one has to work with is often too short to show all the information on earthquake that might happen in the future. It is therefore necessary to make a number of interpretative decisions based on both geological and seismological studies in order to build up the proper seismic source model used for calculation. Since, sometimes, a small difference in the model can cause quite large effects on the ground motion at a site, it is important to take great care over the details of the seismic sources model. This does mean that probabilistic method is a much more major undertaking than in the methodologies described previously. But on the hand, the large amounts of data that can be used to justify the model do increase the power of the method.
- A dilemma is that the actual earthquake can be larger than the hazard analysis predicts but will likely be smaller than a deterministic estimate. Then, the question of what is to be used to design for becomes difficult. The main purpose of the characterization carried out using probabilistic method is to determine the earthquake ground motion, which will be used in the design of the structure. While values of peak ground acceleration, velocity and displacement are interesting and important parameters, they provide little useful design information by themselves. Ground motion time histories and response spectra are needed for the design and analysis of the structure in a more reliable fashion. But still there is a long way to go find this kind of solution.
- The calculation and theories are very complex, and different individuals use a varying amount of restriction. Also, many assumptions are involved due to the limited amount of data available.
- Another objection to PSHA is the degree of subjectivity and personal judgment that have to be used in probabilistic method. Some seismologists are looking for ways round this by using a smoothed version of the original seismicity in place of source zones.
- Probabilistic method makes use of a principle known as stationary. This maintains that the seismic hazard at a place is constant in the same length of time, that is the expected intensity in 50 years is the same whether the 50 years in question starts in 1990 or 2000. Common sense suggests that this is probably not true: in the case of an area where there has recently been a big earthquake, seismic energy has been dissipated and there should now be a long

period before it builds up again; conversely there are other areas where a big earthquake appears to be due or even overdue. In this case, the seismic hazard risk should be much higher.

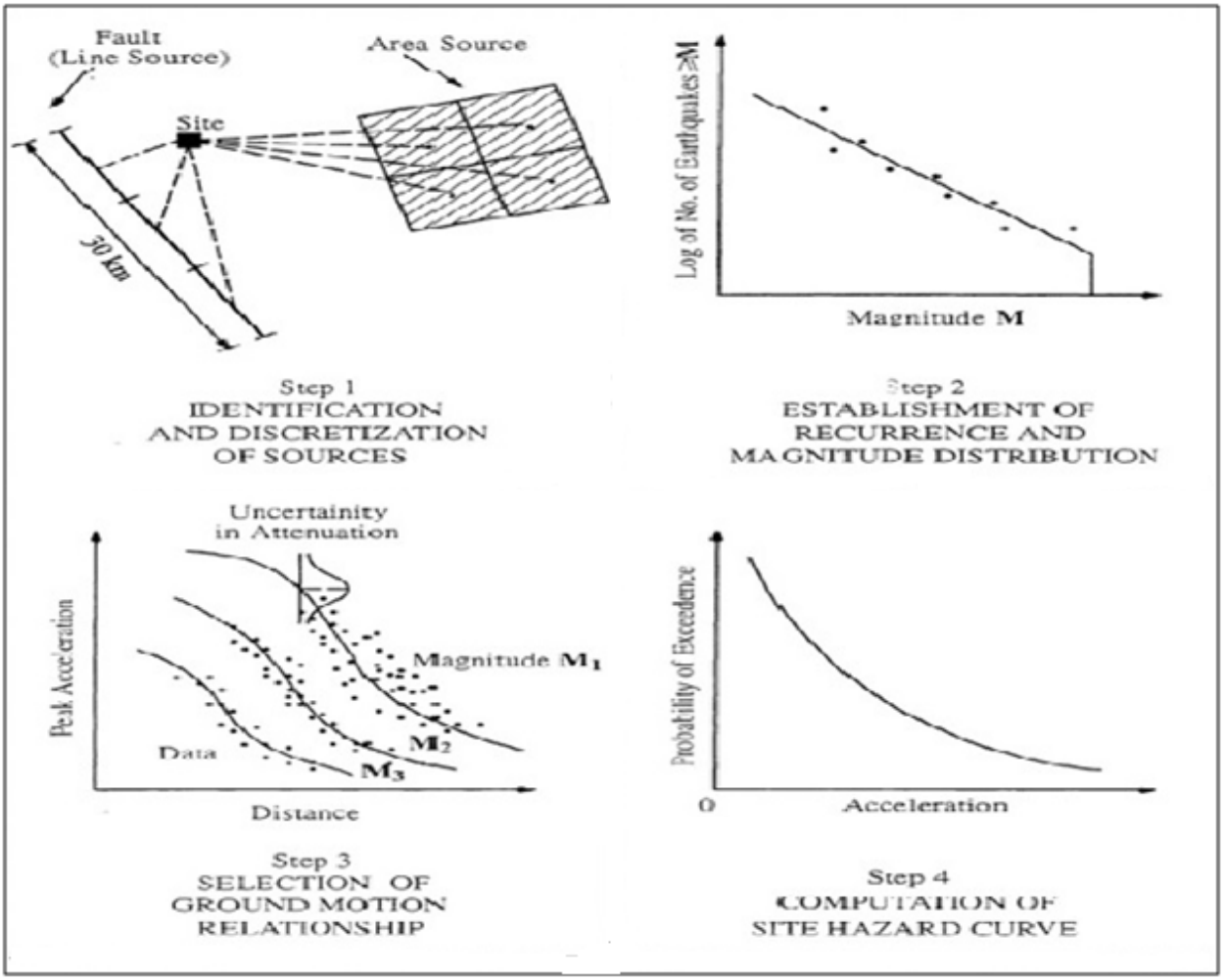

Figure 3. 1 Basic steps of probabilistic seismic hazard analysis (after Reiter, 1990).

(Figure 3.1) shows Step 1 is "the definition of earthquake sources". Sources are nearby active faults, each defined as being of uniform earthquake potential. Step 2 is "the definition of seismicity recurrence characteristics", or in other words the frequency-magnitude distribution. A maximum credible earthquake is chosen for each source. The third step is estimation of the earthquake effect, taking attenuation, peak acceleration and distance to the source into account. The final step determines the hazard at the site, quantifying the probability of exceeding different levels of ground motion at the site during a specified period of time.

CHAPTER FOUR

4 Source Geometry

The characterization of seismic sources describes the rate at which earthquakes of given magnitude and dimensions occur at a given location. The first step of the source characterization involves identifying potential sources and modeling their geometric parameters. This includes defining the source type, estimating the source dimensions, and finally assigning a distribution to the uncertainty in earthquake location within the source.

4.1 Seismic Zoning for Ethiopia

Gouin (1976) who used probabilistic approach is credited for the initial attempts in producing the first seismic hazard map of Ethiopia as shown in Figure 4.1 Gouin's work served as a basis for the seismic zoning adopted by the ESCP-1:1983 building code of Ethiopia (see Figure 4.1(c)). Since the production of Gouin's map, quite a large number of destructive earthquakes have occurred in the country causing damages both to property and human life. Further, destructive earthquakes that occurred in the neighboring countries were not included in the production of the first map in 1976. Subsequently, Kebede (1996, 1997), Panza *et al* (1996) and Kebede and Vaccari (1996) produced a new seismic hazard map of Ethiopia and its northern neighboring countries to account for these additional earthquake records. Unlike previous works, the seismic zoning of Ethiopia and the Horn of Africa reported by Kebede (1996), Kebede and Asfaw (1996) also account for ground motion attenuation in addition to newer data obtained from such sources as the US National Earthquake Information Service (NEIS). The works of Kebede (1996, 1997), Kebede and Asfaw (1996) along with the works of Lake Mariyam Asfaw (Asfaw 1994) served as a basis for the seismic zoning adopted by the current Ethiopian building code - EBCS-8:1995 as shown in Figure 4.1(b). Further, there have been other attempts on seismic zoning of some of the country's important economic regions such as the city of Addis Ababa. The work of the RADIUS project (1999) is a notable example. And the present work can also be a good outcome for seismic zoning of more other major cities of the country.

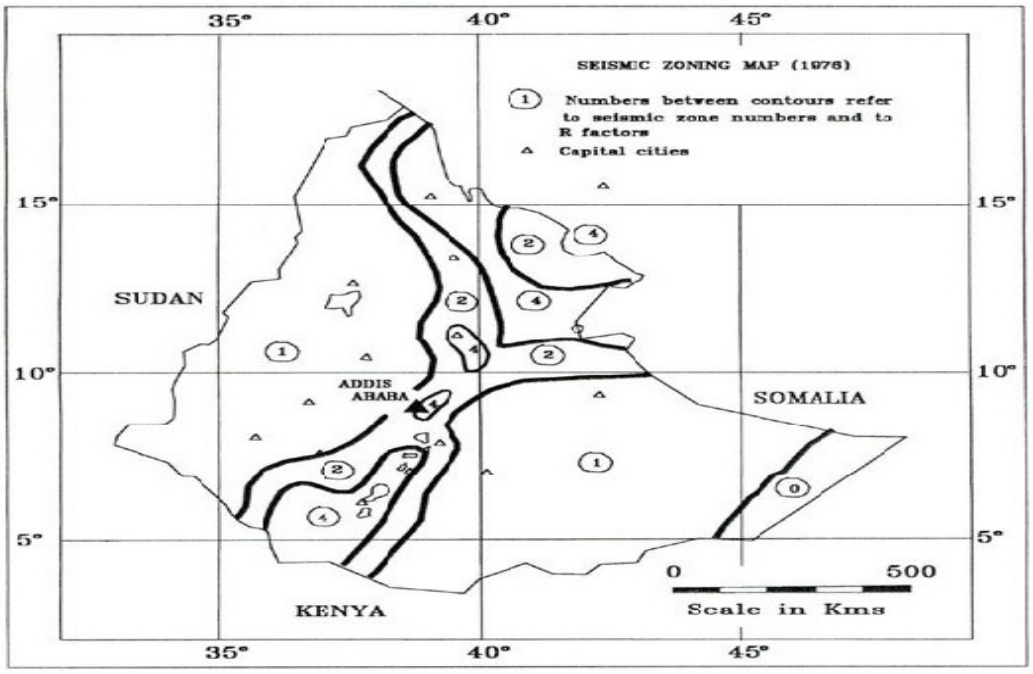

a) Seismic zoning of Ethiopia as per Gouin (1976).

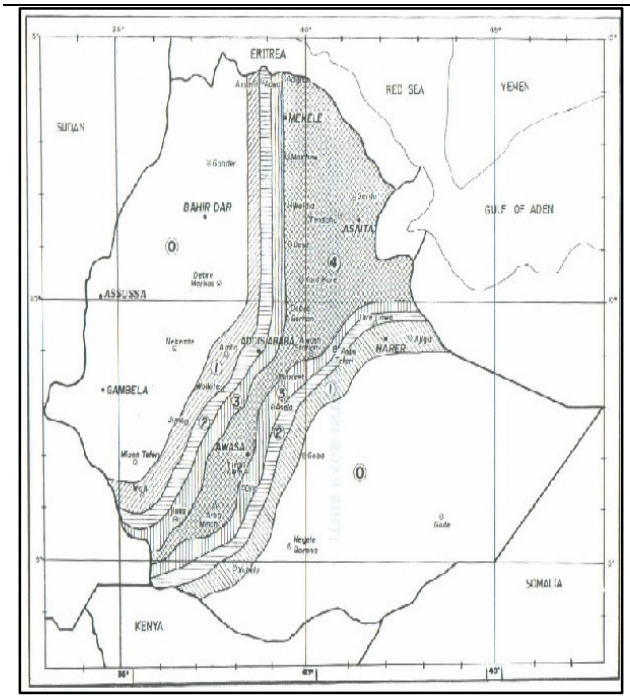

b) Seismic zoning of Ethiopia as per EBCS-8:1995.

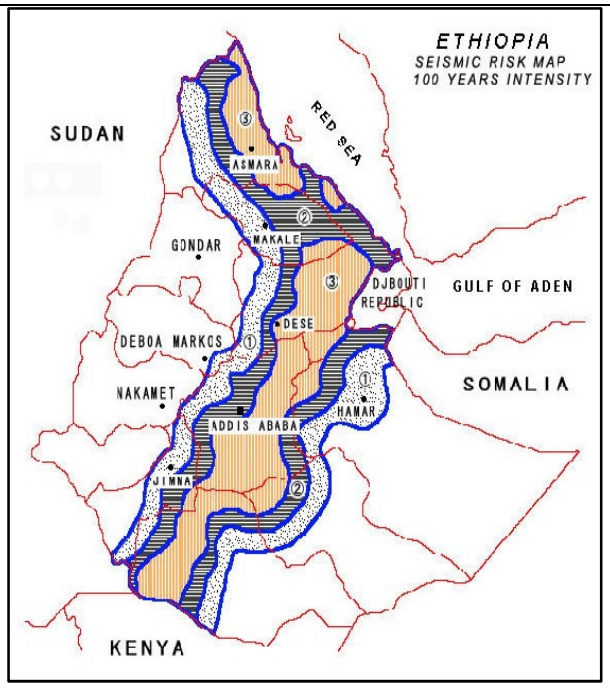

c) Seismic zoning of Ethiopia as per ESCP-1:1983.

Figure 4. 1 Seismic zoning for Ethiopia

4.2 Seismic Source Zones of the Study Area

The first step of probabilistic seismic hazard analyses is the definition of the earthquake sources that could most probably affect the site of interest at which the seismic hazard that going to be calculated. So it will be useful to understand the meaning and the real concept of a seismic source zone. A seismic source is usually called a seismotectonic source which is activated by tectonic forces and whose concept is a relatively modern one. In fact, the characterization of seismic source zones depends on the interpretation of the geological, geophysical and seismological data obtained by many tools such as tectonic theory, seismicity, surface geological investigations and subsurface geophysical techniques (Reiter, 1990).

In the region of these study detailed quaternary fault maps at a desirable scale indicating active faults are lacking. As a result, faults, which could be characterized in terms of geometry, direction of slip, segmentation and rapture length with reasonable accuracy, are virtually non-existent. This implies that alternative scenarios for seismic hazard analysis could not be made.

Based on the seismicity and the knowledge of the geology and tectonics the region can broadly be divided into three seismogenic provinces or seismic source zones. These are the Afar Depression, the Escarpment and the Ethiopian Rift System seismic source zones (Figure 4.2). Each zone is, therefore, distinguished by its own specific tectonic, geologic and seismic characteristics. In each zone earthquakes are assumed to occur randomly, that is, every point in the zone has the same probability of being an epicentre.

a) The Afar Depression Seismic Source Zone

This zone constitutes an area of interaction of three rift structures, namely the Red sea, Gulf of Aden and the Ethiopian Rift System. It represents a triple point junction. Complicated fault systems exist in the Depression. The northern and central part of the Depression is dominated by WNW–ESE to NW–SE trending faults. In the south two differently oriented fault systems are dominant—the NNE–SSW to N–E striking faults which are the extension of the Ethiopian Rift System and the E–W to ENE–WSW trending faults. The seismic activity in the Afar Depression is high, characterized by small and intermediate size earthquakes. Several destructive earthquakes occurred in the zone. The two most significant earthquakes are the ones that occurred in 1969 and in 1989. The 1969 Serdo earthquake had magnitude 6.1 and it completely

destroyed the nearby town of Serdo. Out of its population of 420, some 40 people lost their lives while 160 persons were injured (Gouin, 1979). This is about 50% casuality. In connection with this earthquake over 250 foreshocks and aftershocks of magnitude greater than 3 were recorded at AAE, the Addis Ababa seismic station. The 1989 Dobi graben earthquake had a magnitude of 6.3 and destroyed several bridges (Mammo, 2005).

b) The Western Escarpment Seismic Zone

This zone is characterized by almost N–S running faults and it is one of the most seismically active zones in the whole region. The 1961 Kara Kore earthquake of magnitude 6.7 seriously damaged the nearby Kara Kore town and completely destroyed the village of Majete. Over 3500 foreshocks and aftershocks of magnitude greater than 3.5 were recorded in connection with this earthquake. The effect of the Kara kore earthquake was felt as far as Addis Ababa some 200 km away. In the same region two intermediate size earthquakes of magnitude 5.3 and 5.1 occurred in 1971 inflicting damage to Kombolcha town (Mammo, 2005).

c) The Ethiopian Rift System Seismic Zone

This Rift System links the Red sea and Gulf of Aden rifts to the East African Rift System through the Afar Depression. Two main fault systems have been recognized in this zone—a NE–SW trending fault system which characterizes mainly the rift margins and a NNE–SSW to N–S striking fault system (the Wonji Fault Belt), oblique to the rift margins, which constitute a sigmoidal fault pattern marked by a right stepping en-echelon faults. This latter fault system affects both the rift floor and the margins. The seismic activity is usually represented by small to intermediate size earthquakes. However, large size earthquake of magnitude 6.8 occurred in this zone in 1906 at an epicentral distance of about 120 km south of Addis Ababa. This was the largest earthquake ever that was recorded in Ethiopia. Its effect was widely felt in Addis Ababa. Other prominent earthquakes in this zone are the 1960 earthquake of magnitude 6.3 and the 1987 earthquake of magnitude 6.2 (Mammo, 2005).

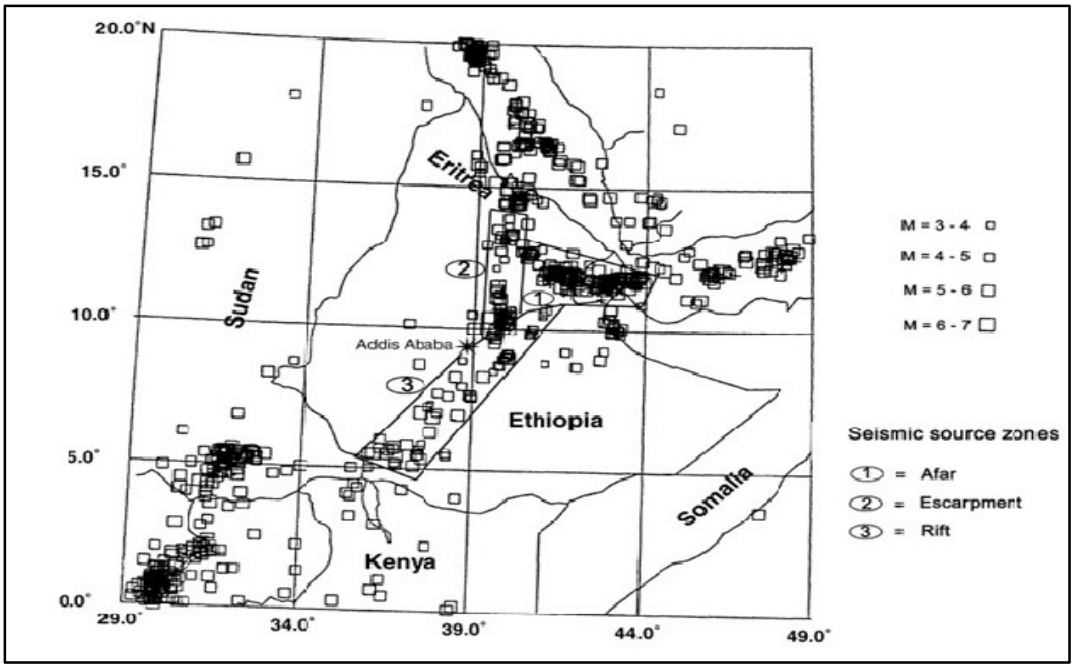

Figure 4. 2 Seismicity of the region with the seismic source zones (after Mammo, 2005).

4.3 Types of Sources

4.3.1 Areal Sources

Due to insufficient geological data of known faults, seismic sources were initially modeled as areal source zones based on historical seismicity data. Generally, these seismic zones were assumed to have uniform source properties in both time and space. Although today most hazard analyses are completed using a fault source characterization, areal sources are still used to model seismicity in regions with unknown fault locations. In addition, areal sources can be used to model background zones of seismic regions to account for any earthquakes that may occur off identified faults (Abrahamson, 2006). Nevertheless**,** existing scale of tectonic maps and the level of precision of the earthquake catalogue imply that the location of earthquakes must be designed in terms of areal sources within which earthquake characteristics will be taken to be uniform.

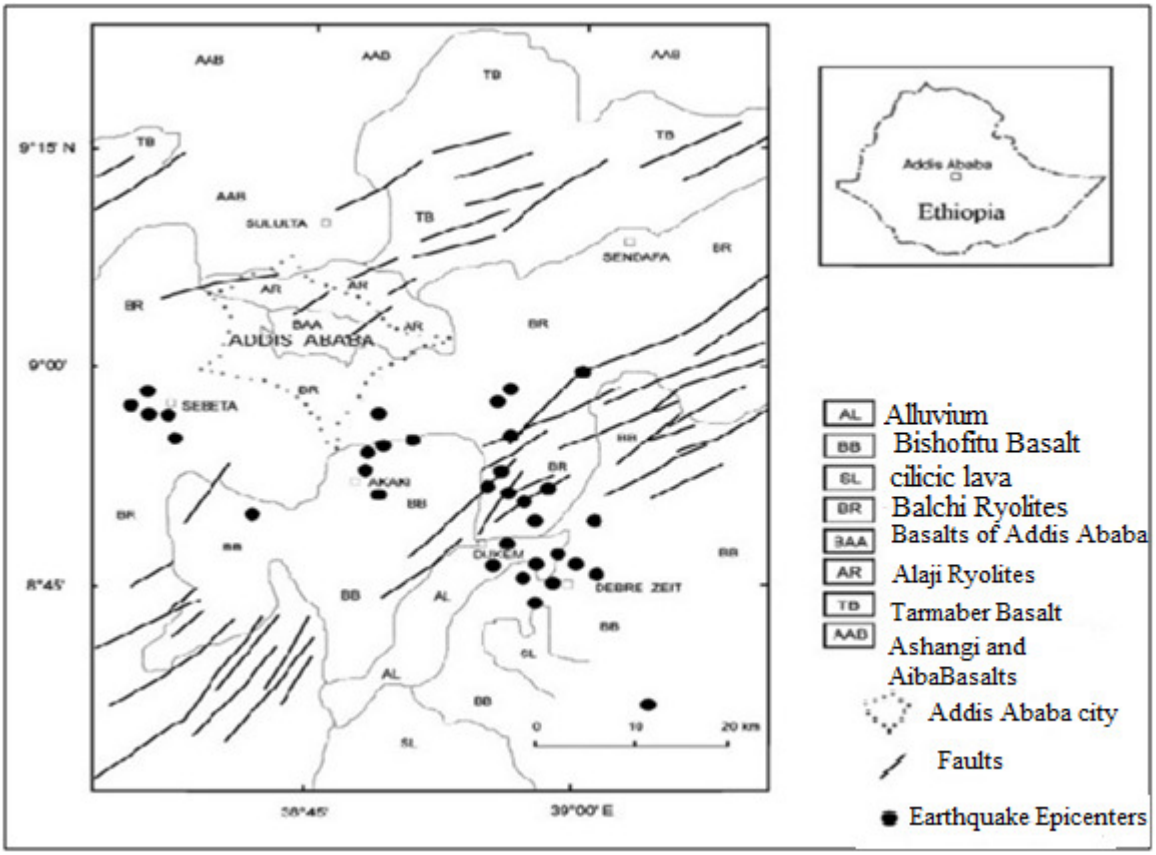

Figure 4. 3 The geology, tectonic structures and seismicity of Debrezeit area (after Mammo, 2005).

4.3.2 Fault Sources

As more geological data became available, locations of faults were able to be identified and more accurately defined. Although originally only modeled as linear sources, most fault source models now have multi-planar features and ruptures are assumed to be distributed over the entire fault plane (Abrahamson, 2006).

The study of geology, tectonics and seismicity in the study area shows a genetic relationship between faults and earthquake epicenters. Swarms of NE-SW trending faults cut the Bishoftu basalts, the orientation of faults in the MER system. The epicenters are seen to follow the same strike as the faults and generally fall on the causative faults or on the extension of these faults. Most of the faults in the area have dimensions greater than 10km; one of such faults is the Dukem fault. As shown on the Figure 4.3 the geology of the study area is characterized by volcanic rocks. In Debrezeit, the Olivine basalts (Bishoftu basalts, 2.8M_a) dominated the area.

CRISIS2012 (Seismic Hazard Analysis Program) assumes that, within a source, seismicity is evenly distributed by unit area (area sources) or by unit length (line sources). For point sources, of course, all seismicity is assumed to be concentrated at the points. In order to correctly account for this modeling assumption, CRISIS performs a spatial integration by subdividing the original sources. Once subdivided into sub-sources, CRISIS assigns to a single point all the seismicity associated to a sub-source, and then the spatial integration adopts a summation form. These sources are originally given by the user as 3D polygons; the user gives the coordinates (longitude, latitude and depth) of the N vertex defining the area source. First, the area source is subdivided into N-2 triangles. These triangles will be further subdivided until one of the following two conditions are met:

1) The size of the triangle is smaller than the value "Minimum triangle size" given by the user. That is, the triangle is subdivided if it is still big.

2) The ratio between the site-to-source distance and the triangle size is larger than the value "Minimum Distance/Triangle Size ratio" given by the user. In other words, the triangle is subdivided if the site is still not far enough. The sub-sub divisions are performed by means of a recursive function.

The site-to-source distance is measured from the computation site to the centroid of the triangle whose possible subdivision is being examined. The size of the triangle is simply the square root of its area. The seismicity associated to each centroid is proportional to the triangle's area. If CRISIS decides that a triangle has to be subdivided, this is done dividing the triangle into four new ones, whose vertexes are the mid-points of the three sides of the original triangle. CRISIS uses the following as default parameters: Minimum triangle size=11km; Minimum Distance/Triangle Size ratio = 7. The following graph shows the resulting subdivision of a squared source of size 1°x1° when the computation site is located at the center of the source, using the default integration parameters (CRISIS2012 Manual).

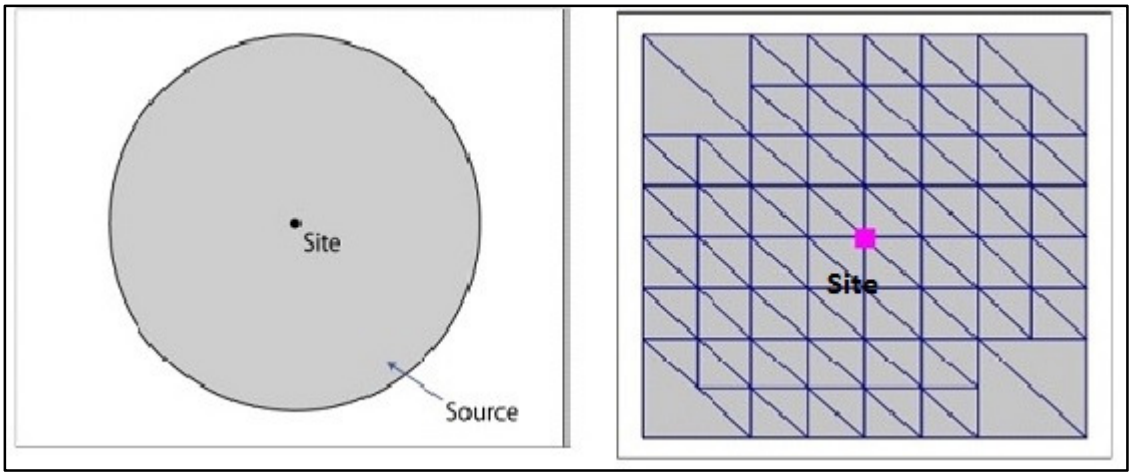

Figure 4. 4 (a)Representation of area-source geometry and (b) Source subdivision with minimum Distance/Triangle ratio=3.

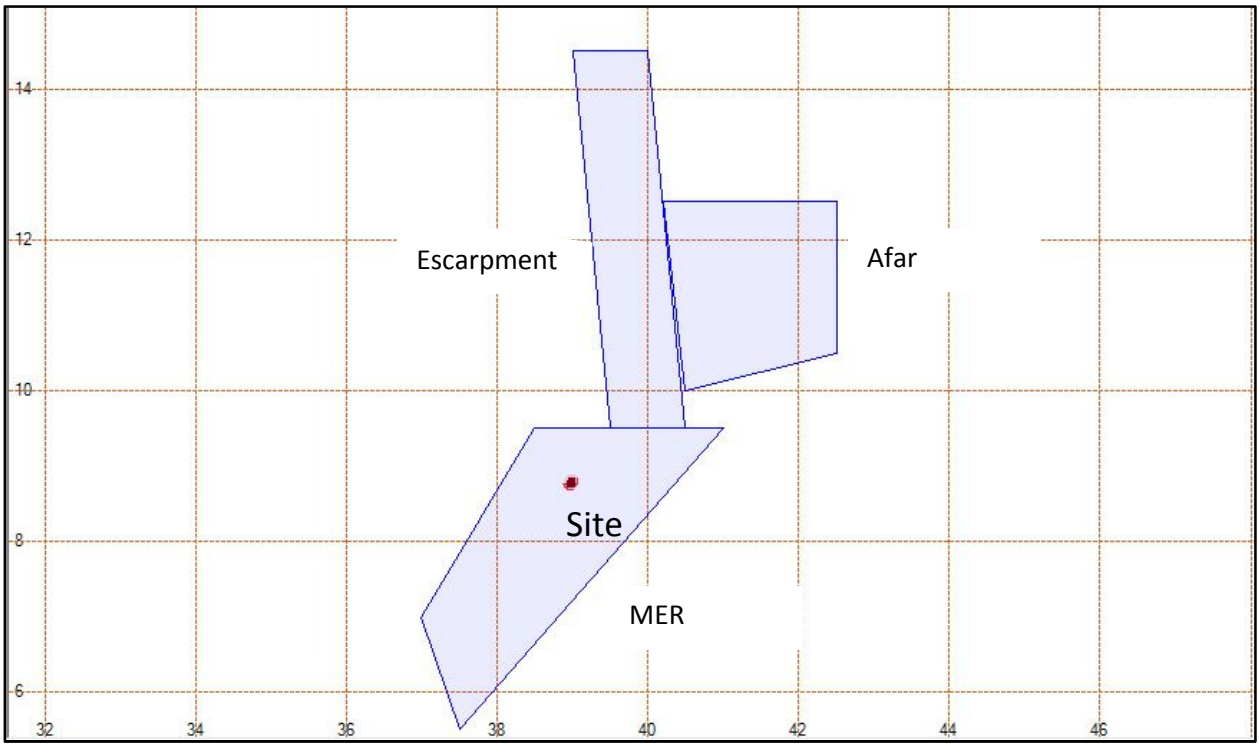

Figure 4. 5 Representation of area source geomety of MER, Afar and Escarpment seismic zones that are considered for the Debrezeit area, done by CRISIS2012 program.

CHAPTER FIVE

5 SOURCE SEISMICITY

Once the geometry of a seismic source is defined the next step is to estimate the distribution of all possible size earthquakes that can occur within the source dimensions. This involves defining a consistent measure of magnitude scale and representing the source seismicity through a magnitude recurrence relation as defined by (equation 5.6) a magnitude distribution function and activity rate.

5.1 Historical Seismicity

The records of the pre-instrumental (historical) seismicity may be used to identify the earthquake sources by means of the historical accounts of the ground shaking effects which could confirm the occurrence of the past earthquakes and sometimes estimate their geographic distributions of the intensity. Although the maximum intensity may be used to assess the epicentral location and the magnitude of a specific earthquake event, the accuracy of this location found by this method depends strongly upon the population density and the rate of the earthquake recurrence. However, the geographic distribution of the historic epicenters still provides a good evidence for the existence of the earthquake source zones, at least it can be used to evaluate the rate of recurrence of the earthquakes or simply the 'seismicity' in some areas (Kramer, 1996).

5.1.1 Instrumental Seismicity

Although the instrumental records of the large earthquakes have been available since about 1900 (lots of them before 1960 are incomplete or of uneven quality), they represent the best, the most significant information for the evaluation of the earthquake sources. The most important disadvantage of using these records is the short period of time when compared with the average time interval between the large earthquakes. But, still the alignment of the instrumentally located epicenters or even hypocenters together with the analysis of the aftershocks can help in the subjects of the detection and the delineation of the earthquake source zones.

After the interpretation of the geological, geophysical and seismological data obtained by many tools, the characterization of an earthquake source first demands the consideration of the spatial characteristics of this source, the distribution of the earthquakes within that source, the

distribution of the earthquake sizes for each source then the distribution of these earthquakes with time. It is evident that these characteristics should involve specified, required uncertainties (Kramer, 1996).

5.2 Magnitude Scales

When dealing with the definition of seismicity it is important to pay attention to the terminology and parameters used. For instance, there are several different ways to express the magnitude of an earthquake, the most common using surface, body, local and moment magnitude scales. The greater the energy released during earthquake, the larger the amplitude recorded on the seismogram. Therefore, wave amplitude can serve as an objective measure of an earthquakes size or magnitude, a measure of earthquake strength as interpreted from the maximum wave amplitude recorded by a seismograph.

With the knowledge of the amplitude variation curve, the magnitude scale for the corresponding seismic phase can be defined, if two further conditions are specified: When to consider two earthquakes with the same focal depth to have magnitudes 0 and 1 respectively, and when to consider two earthquakes with different focal depths to have identical magnitudes. As in any analogous definition of a physical quantity the answer can only be arbitrary.

According to the intention of (Gutenberg and Richter 1956), two events are assigned the same body-wave magnitude, if the seismic energies released in the events are identical. The seismic energy is thus intended to link with each other events having different focal depths. This implies that a unique relation exists between the body-wave magnitude and the seismic energy released. It also implies that it is possible to determine the seismic energy independently and with sufficient accuracy, so as to make it applicable as standard quantity entering the definition of the magnitude. In 1935, in California Institute of Technology Seismologist Charles F.Richter, developed a practical application of this concept, which has since become known as the Richter magnitude scale.

A Richter magnitude is a measurement of amplitude of the highest wave recorded on a standard seismograph divided by its period, which is the time required for that wave to complete the vibration. Because wave amplitudes diminish with distance from the epicenter, Richter realized that a seismograph could not distinguish between a weak quake nearby and a strong one far

away. Therefore, he added a factor that corrects the measurement for distancing effects and adjusts it to the amplitude the seismograph would record if it were located 100 kms from the epicenter. Thus, an earthquake should register the same magnitude at close and distant station. The Richter scale is logarithmic, which means that adjacent number on the scale signifies wave amplitude that differs by a factor of 10. For example, the amplitude of magnitude 5 earthquakes is 10 times that of a magnitude 4 earthquake. A number of other logarithmic magnitude scales for earthquakes exist, all of which are based on measurement of amplitude of the seismic waves. All the magnitude scales are of the form;

$$M = \log\left(A / T\right) + q\left(\Delta, h\right) + a \qquad 5.1$$

Where: M the magnitude, A is the maximum amplitude of the wave (in micro's), T is the period of the wave (in sec), q is function correcting for decrease of amplitude of the wave with distance from the epicenter, h is the focal depth, Δ is the angular distance from the seismometer to epicenter of the earthquake, and a, an empirical constant. It is important in all magnitude work to use the period ranges for which the particular equation has been determined; waves of different frequencies have different amplitude behavior. Many determinations of the constant a, and the function q have been determined; wave of different frequencies have different amplitude behavior mode, for various frequency bands, focal depths, geographical locations and so on.

5.2.1 Surface, Body and Local Magnitude Scales

In the past, many earthquake magnitudes were determined using scales based on the measurement of seismic wave amplitudes at a selected period. Surface wave magnitude, M_S, is measured using the amplitude of surface Raleigh waves at a period of 20 sec (Gutenberg & Richter, 1936). Body wave magnitude, m_b, often used for deep earthquakes in which the surface waves are too small to measure, is related to the amplitude of the first few cycles of P-waves and is measured at a period of 1sec (Gutenberg, 1945). The local magnitude, M_L developed by Richter to measure shallow, local earthquakes in Southern California is also measured at a period of around 1sec. Magnitude scales that are measured in this period range are more frequently used and are often regarded as better measures of seismic damage. This is because most common structures have a natural period which lies in the neighborhood of 1sec. The scales described above are not directly related to physical parameters of the earthquake source itself but rather are related to its associated ground shaking characteristics. Because ground shaking characteristics

do not increase at the same rate as that of the total energy released during an earthquake, saturation of the scales occurs for large sized earthquakes. This is indicated by the magnitude scale becoming less sensitive to the size of the earthquake as the size of the earthquake increases (around 6-7 for body and local magnitude scales and 8 for surface) (Kramer, 1996).

5.2.2 Moment Magnitude

An alternative to the scales mentioned above, and the most widely used scale today, is the moment magnitude, M_W. The moment magnitude, as defined by (Hanks and Kanamor 1979), is related to the total amount of energy released during an earthquake, as expressed through the seismic moment, M_0 (Aki, 1966) which is the most fundamental physical parameter of a seismic source that expresses the size of an earthquake.

$$M = \frac{2}{3}\log(M_o) - 10.7 \qquad 5.2$$

The seismic moment, being the product of the rigidity μ of the earth, the area A of the surface that slips and the average slip u can be related to the elastic strain energy that is released by the earthquake source / fault. Specifically,

$$M_o = \mu A \bar{u} \qquad 5.3$$

Where μ = Shear modulus of crust (3×10^{11} dyne / cm)

A = Area of fault rupture

u = Average displacement (slip) over rupture surface

By using relations (5.2) and (5.3) above, the moment magnitude can be expressed directly as a function of the source's physical parameters (Hanks & Kanamori, 1979):

$$M_W = \frac{2}{3}\log(A) + \frac{2}{3}\log(\bar{u}) + \frac{2}{3}\log(\mu) - 10.7 \qquad 5.4$$

5.3 Earthquake Intensity

The effects of the earthquake at near epicenter distances need to be quantified, primarily for engineering purposes. While the number of instruments in earthquake prone areas capable of recording strong motions during the event is increasing, an adequately dense distribution of instruments proves to be too costly. For this, and other reasons, no instrumental observations continue to play an important role in assessing the intensity of shaking during an event, as well as in predicting the intensities to be expected in future earthquakes. The non instrumental intensity scale

eventually links with each other places in which the ground acceleration, velocity displacement, and the duration of shaking are instrumentally determined. Thereby it must be borne in mind that the frequency content of the signal recorded changes with epicentral distance, and the relation between the intensity and the respective element of ground motion needs to take into account the period of the signal (Hurting and Stiller, 1984).

If the earthquakes would occur at only one, say shallow, focal depth, the maximum seismic intensity at the surface could serve as a rating of the strength of the given earthquake, provided the ground conditions were similar at all observations. The maximum intensity shows generally only a weak correlation with the strength of the earthquake as expressed by the magnitude (Duda, 1981). However, the acceleration and velocity values for the wave motion are for firm ground only. They vary greatly depending on surface conditions and on the type of earthquake source.

The parameter "intensity" expresses the visual appraisal of the amplitude or force of earth shaking at different sites within the perceptive area of an earthquake. It is a complex non instrumental parameter combining psychological and geological observations and engineering practices. Many intensity scales have been proposed since the first one by Gastaldi in 1564. Even today, not all countries utilize the same scale (Bullen and Bolt, 1985).

In the older Ethiopian documents, the amplitude of damage or strength of earth shaking was expressed either in Mercalli, Cancani, or Sieberg intensity grades. Even at present, the intensities reported by the Meteorological Office in Djibouti are quoted in Rossi Forel grades (Gouin, 1979).The seismic intensity reflects the integral effect of all elements of ground motion. The intensity scales presently in use have 12 degrees. They differ from each other slightly, due to the variation of building standards in different parts of the world. As shown below in the Table 5.1, the intensity expressed, usually in Modified Mercalli intensity scale measures, the severity of an earthquake in terms of the level of destruction and panic it causes. Values in the form of Roman numerals I-XII are assigned to objective measures, such as the extent of damage to buildings constructed of brick, mortar, or steel, and to subjective measures, such as the degree of social disruption (hardly felt, awakened during sleep, general panic) caused by earthquake (Dolgoff, 1998).

Table 5. 1 Modified Mercalli Intensity (MMI) Scale.

Value	Description of sanction to human beings and damage to objects
I	Not felt except by a very few under especially favorable circumstances.
II	Felt only by a few persons at rest, especially on upper floors of buildings. Delicately suspended objects may swing.
III	Felt quite noticeably indoors, especially on upper floors of buildings, but many people do not recognize it as an earthquake. Standing motorcars may rock slightly. Vibration like passing of truck. Duration estimated.
IV	During the day felt indoors by many, outdoors by few. At night some awakened. Dishes, windows, doors disturbed; walls make creaking sound. Sensation like heavy truck striking building. Standing motorcars rocked noticeably
V	Felt by nearly everyone, many awakened. Some dishes, windows, and so on broken; cracked plaster in a few places; unstable objects overturned. Disturbances of trees, poles, and other tall objects sometimes noticed. Pendulum clocks may stop.
VI	Felt by all, many frightened and run outdoors. Some heavy furniture moved; a few instances of fallen plaster and damaged chimneys. Damage slight.
VII	Everybody runs outdoors. Damage negligible in buildings of good design and construction; slight to moderate in well built ordinary structures; considerable in poorly built or badly designed structures; some chimneys broken. Noticed by persons driving cars.
VIII	Damage slight in specially designed structures; considerable in ordinary substantial buildings with partial collapse; great in poorly built structures. Panel walls thrown out of frame structures. Fall of chimneys, factory stacks, columns, monuments, walls. Heavy furniture overturned. Sand and mud ejected in small amounts. Changes in well water. Persons driving cars disturbed.
IX	Damage considerable in specially designed structures; well designed frame structures thrown out of plumb; great in substantial buildings, with partial collapse. Buildings shifted off foundations. Ground cracked conspicuously. Underground pipes broken.

X	Some well built wooden structures destroyed; most masonry and frame structures destroyed with foundations; ground badly cracked. Rails bent. Landslides considerable from river banks and steep slopes. Shifted sand and mud. Water splashed, slopped over bands.
XI	Few, if any, (masonry) structures remain standing. Bridges destroyed. Broad fissures in ground. Underground pipelines completely out of service. Earth slumps and land slips in soft ground. Rails bent greatly.
XII	Damage total. Waves seen on ground surface. Lines of sight and level distorted. Objects thrown into the air.

Numerous efforts have been exerted to find whether seismic intensities do correlate with instrumentally measurable quantities like PGA occurring in course of the earthquake. (Bath, 1973) gives a relation between the ground acceleration a (cm/s^2), and the maximum intensity I_0 expressed in M.M. Scale as:[see appendix VII]

$$I_o = 3\log(a_o) + 1.5 \qquad 5.4$$

And the relationship between the surface wave magnitude and maximum intensity as:[see appendix VIII]

$$M_o = 1 + \frac{2}{3} I_o \qquad 5.5$$

The value gets significance however, if only incomplete information on the earthquake is available, as an example for historical earthquake. Here, the description of damage inflicted, as eventually found in historical records at large, may lead to .an estimate of the maximum intensity of shaking, and subsequently to at least a rough estimate of the magnitude of the earthquake.

5.4 Magnitude Recurrence Relations

Once the geometry of the source is defined and an appropriate magnitude scale chosen, the seismicity of a source can be expressed through a magnitude recurrence relation. Describing the average rate at which earthquakes with magnitudes greater than or equal to a specified magnitude, *M*, occur on a source, magnitude recurrence relations are characterized by a source's activity rate and magnitude distribution function. As shown below, a recurrence relation is

computed by integrating the magnitude distribution density function and scaling by the activity rate:

$$\lambda_M = \upsilon_{M_{\min}} \int_{m=M}^{M_{\max}} f_m(m)dm \qquad 5.6$$

Two types of models are typically used to represent magnitude distributions, the truncated exponential model & characteristic earthquake model. Although the exponential model works well for large regions in which the hazard is not controlled by one particular fault, studies have shown that the characteristic model is more appropriate for characterizing individual fault sources (Youngs and Coppersmith, 2000). Some models take advantage of a combined magnitude distribution, using the truncated exponential model for the distribution of small-to-moderate earthquakes and the characteristic model for large magnitude events. Differences in resulting hazard between these two models is a function of fault-to-site distance and acceleration level and therefore is specific to each analysis (Youngs and Coppersmith, 2000).

5.4.1 Truncated Exponential Model

The truncated exponential model is based on Gutenberg-Richter magnitude recurrence relation (Gutenberg-Richter, 1956). The Gutenberg-Richter recurrence relation is expressed as:

$$\log \lambda_m = a - bM \qquad 5.7$$

The a-value represents the activity rate of the source which represents the absolute rate of earthquake occurrence with magnitudes greater than zero. Based on empirical estimates, the b-value is related to the relative likelihood of earthquakes with different magnitudes and typically takes a value between 0.8-1.0. The truncated exponential model is often rewritten in the following form of a standard recurrence relation:

$$\lambda_m = \nu_o \cdot \exp(-\beta m) \qquad 5.8$$

Where $\nu_o = 10^a$ and $\beta = b\ln(10) \cong 2.3b$

As can be seen (Eqn.5.8), the earthquake magnitudes are exponentially distributed. This implies that the mean recurrence rate for small magnitude earthquakes is greater than that of large magnitude earthquakes.

$$f_m(m) = \frac{\beta \cdot e^{-\beta(m - M_{min})}}{1 - e^{-\beta(M_{max} - M_{min})}} \qquad 5.9$$

Although the standard Gutenberg-Richter recurrence relation can be applied to an infinite range of magnitudes, it is common to apply bounds at minimum and maximum magnitude values. This is because seismic sources are usually associated with a capacity to produce some maximum magnitude M_{max} and for engineering purposes earthquakes of very small magnitudes that do not cause damage to structures are not of interest (Abrahamson, 2006). The corresponding probability density function using the minimum and maximum values is expressed below in its bounded form and is displayed in Figure 5-1:

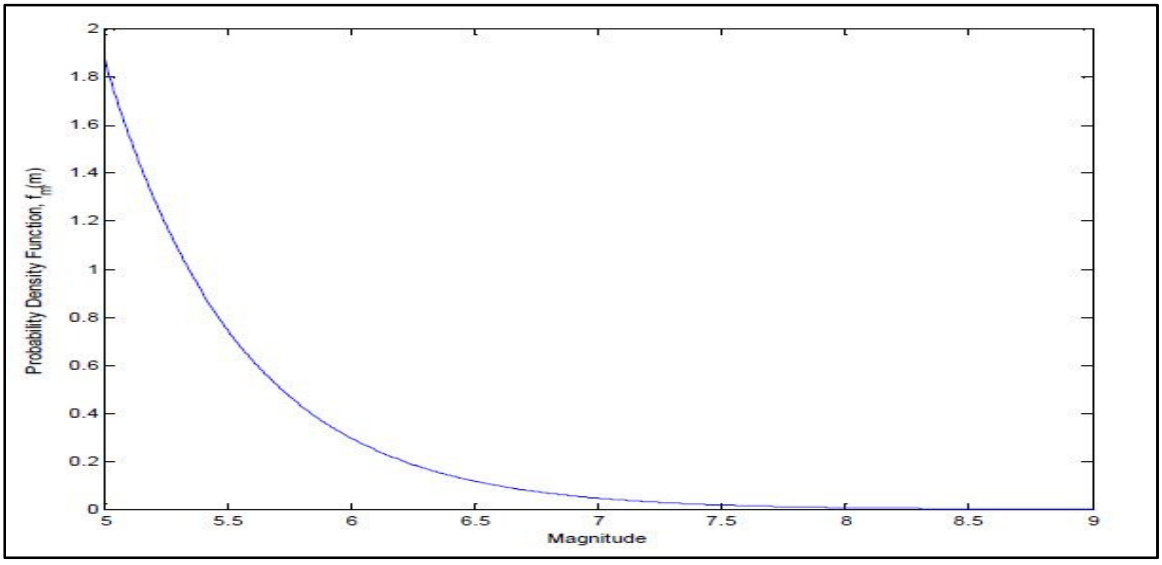

Figure 5. 1 Magnitude probability distribution function of truncated exponential model

5.4.2 Recurrence Relation and *b*-value for the Study Area

5.4.2.1 Recurrence Relation

The ability to predetermine aspects of individual earthquakes remains questionable at best. Most of our knowledge of earthquake seismology is based on observational and empirical methods. A fundamental problem arising from our reliance on empirical techniques is the amount of data available. To undertake any reliable study, data must be consistent, especially in seismology, where raw seismograms must undergo a significant amount of processing to produce solutions

for hypocenters and source types and orientations. Unfortunately, homogenous earthquake catalogues, where consistent processing has been used, span a period of time significantly less than recurrence times for large earthquakes. As it is these large earthquakes that cause the most damage and present the most risk to human life, it is desirable to be able to try to constrain how often they occur. Having a better understanding of recurrence times for large earthquakes will allow long-term seismic hazard to be assessed more accurately, reducing the risk to human life and infrastructure.

The frequency magnitude earthquake distribution, FMD, known in the eastern world as Ishimoto (Iida, 1939) relation and in the west as the (Gutenberg and Richter 1954) relation, defines the distribution of earthquakes with respect to magnitude and represents one of the reliable empirical relations to characterize seismicity which is a fundamental input in seismic hazard analysis and also to obtain the amplitude of stress used for tectonic investigation of the region (Ayele and Kulhanek, 1997). The earthquake recurrence is expressed by the equation of the form:

$$\log N = a - bM \qquad 5.10$$

Where, N is the cumulative number of earthquake with magnitude greater or equal to M in a given region and *a* and *b* are positive real constants. The slope *b* in the equation referred to as b-value or b-coefficient characterizes the seismicity and is a measure of the relative abundance of large to small earthquakes for a given region in a specified time interval. Since potential damage at a site is dominated by the occurrence of larger earthquakes, b-value has great importance in seismic hazard analysis.

5.4.2.2 b-Value

Moreover, it is a tectonic parameter considered as an index of the stress condition in the crust of the earth under a particular local region (Gouin, 1976). In addition, the slope *b* is associated with depth of occurrence, tectonics, stress-drop and source dimension of the earthquake. It is also an indication of the rate at which earthquakes of a given magnitude have occurred and will most probably continue to occur in the future (Kebede and Asfaw, 1996). The b-value depends up on the time and area (place) considered. It is usually close to one over long period and large regions and shows statistically significant variations for shorter time windows and limited geographical areas. Large values of *b* are those above one and small *b* has values below one. Furthermore, the

b-values are bound to exhibit substantial variation with a change either in the reference magnitude, or in the range of the magnitude categories, or in the length of the sampling period, or in the size of the area element or of the total region under study (Ayele and Kulhanek, 1997).

Henceforth, there are several possible explanations for different b-values, which are summarized as follows: A large value for *b* in an area indicates that small earthquakes occur frequently, and a small value for *b* indicates small earthquakes are not so frequent and large earthquakes are more likely to occur. The b-value is also found to decrease with depth and increase in magma supply; that is, small values for *b* are usually characteristics of regions with deep earthquake foci. Experiments also indicate that high stress level results in low value for *b,* and low stress results in high values of *b* in the seismogenic region of interest. And high b-value is associated with small source dimension and normal faulting. Also low b-values are associated with large source dimension and reverse faulting.

If systematic errors from earthquake location, earthquake detection, and magnitude determination can be minimized, variation in b-value can indicate tectonic and rheological conditions near the earthquake source. The decrease in b-value is interpreted in the form of stress increase and vice versa before an approaching seismic event, as a replication of the degree of material heterogeneity or as a decrease of thermal gradients. In addition, the inverse correlation between the amount of stress accumulated in the hypocentral area and b-value is obviously of particular interest in the prediction of major earthquakes i.e. fluctuation of *b*-value with duration of months and years are known to precede large shocks (Ayele and Kulhanek, 1997).

To evaluate b-values, the magnitude available for each earthquake has to first be examined and converted to a single unified magnitude using appropriate relation, and then the largest of the obtained magnitude value is used in the evaluation of b-value. The b-value can be calculated by least-squares regression, but the presence of even a few large earthquakes influence the resulting b-value significantly. As an alternative, the maximum likelihood method has been used to estimate b-value when the number of infrequent large earthquakes changes. There are cases, however, such as estimating the probability of the largest magnitude of earthquakes, where the least-square method is more suitable. But both methods have their own merit and drawbacks. Because the least-square method assumes a normal distribution of the events about the mean and the maximum likelihood method assumes various distributions, it follows that the curve slopes

should be identical only in the case of normal distribution; they exhibit substantial differences in other cases. By the method of maximum likelihood, the b-value is estimated using the relation (Aki, 1965)

$$b = \frac{\log e}{M - M_o} = \frac{0.434}{M - M_o} \qquad 5.11$$

Where, M is the mean magnitude of all events greater than magnitude M_0.

Among works of the analysis of the b-value in the region, the one by Gouin (1979), Ayele and Kulhanek (1997) and Kebede and Kulhanek (1994) worth mentioning. Ayele and Kulhanek(1997) in their investigation of the spatial and temporal variation of seismicity ,the b-value in the Horn of Africa is estimated for the period 1960-1993 using the maximum likelihood approach. They sampled a minimum of 20 events with magnitude equal to or greater than 4.5 with a sliding circular space window of radius 2°. The size of this window is chosen arbitrarily as a compromise between resolution and enough statistical sampling. The centre of this window is shifted by 0.5 either in latitude of longitude at a time. Their estimate of b-values for the whole region varies from 0.55± 0.12 to 1.31± 0.29 and shown in Figure 5.2. There are no b-value estimates for grid points that have less than 20 events for each sampling. That is why there is no representative estimate of b-value for that MER region. In this study the b-value of 0.50, 0.75 and 0.71 were obtained from the previous research works for the three seismic zones considered to generate earthquakes that affect the study area. But from the present study the b-value of 0.67, 1.03 and 1.11 were obtained using GEM catalogue for the three seismic zones: MER, Afar and Escarpment that are considered to generate earthquakes that affect the study area.

Due to the limited number of grid points for contouring or surface plotting, the b-value is represented by symbols as displayed in the figure. The b-value estimate for the whole region varies from 0.55±0.12 to 1.31±0.29.

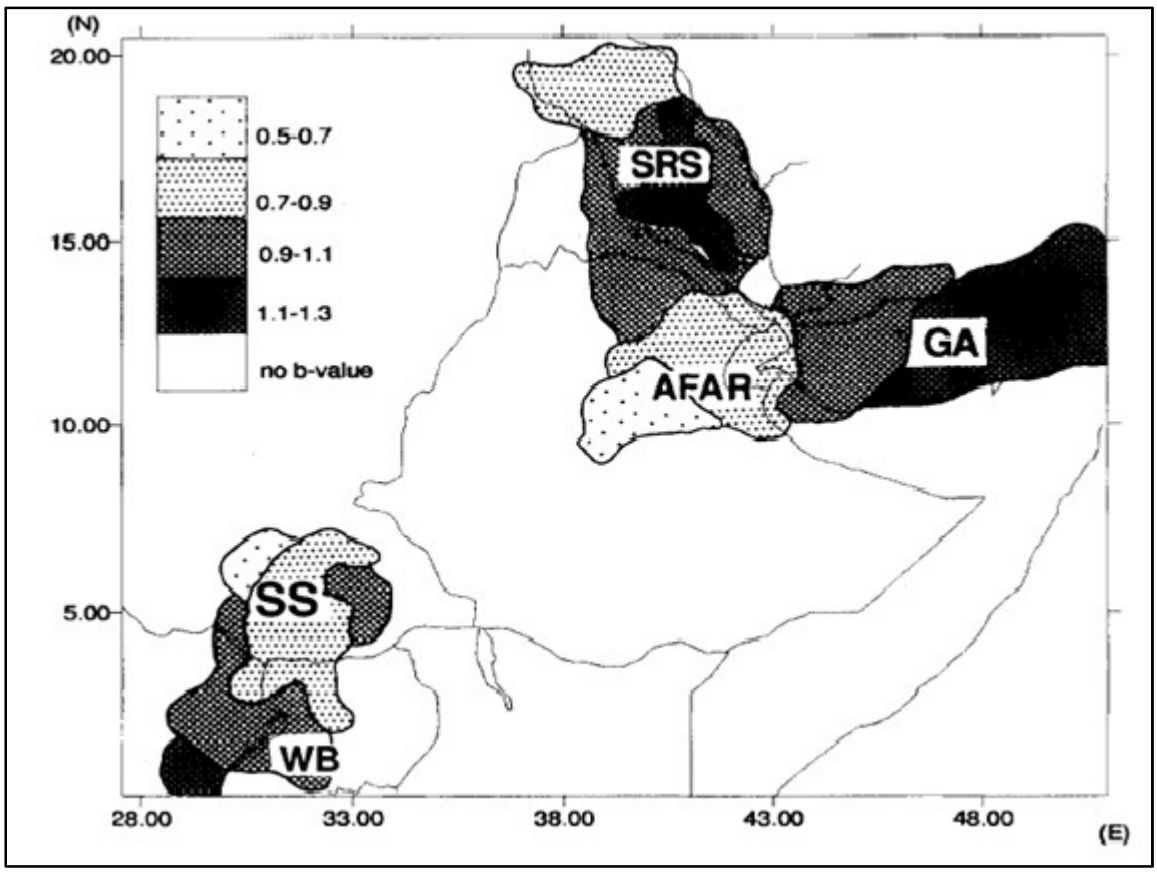

Figure 5. 2 Spatial variation of b-value for the time period 1960-1993.

The figures below show well-behaved linear relationships of LogN and Magnitude greater than M for the three sources. The usage of N varies from N-cummulative, the number of shocks of magnitude M or greater, to N the number of shocks per magnitude class. In either case the slope, b, derived from a plot of logN-cum and log N versus M will be the same. This is the famous b-value. Where N may be specified in two ways: 1) as the total number of shocks in a specified magnitude interval, as the cumulative number of earthquakes of magnitude M or greater and 2) the cumulative number of shocks exceeding magnitude M. Further, N may or may not be normalized per unit time and/or unit area but here N is normalized per unit time of 100 years. The values and significance of the constants b and a obviously depend upon the specified sampling and also the particular magnitude scale being used. Whether one plots the number of earthquakes by magnitude interval ($M \pm \Delta M/2$), by cumulative number $\geq M_1$ or by cumulative number > M, the slope b of a log-normal plot should in theory be identical.

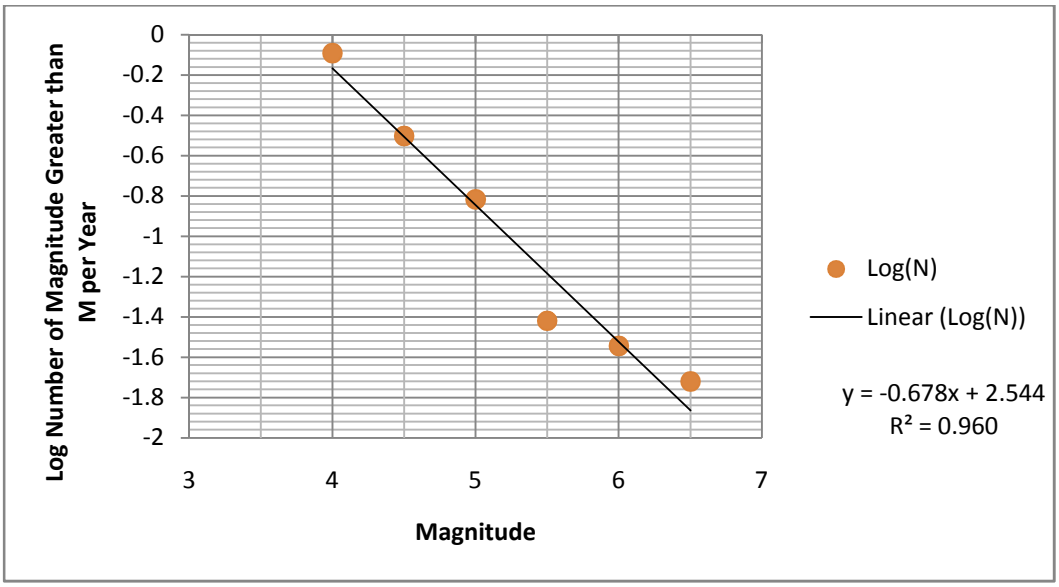

Figure 5. 3 Gutenberg-Richter b-Lines for MER (source1), Constructed based on instrumental records of last 100 years .

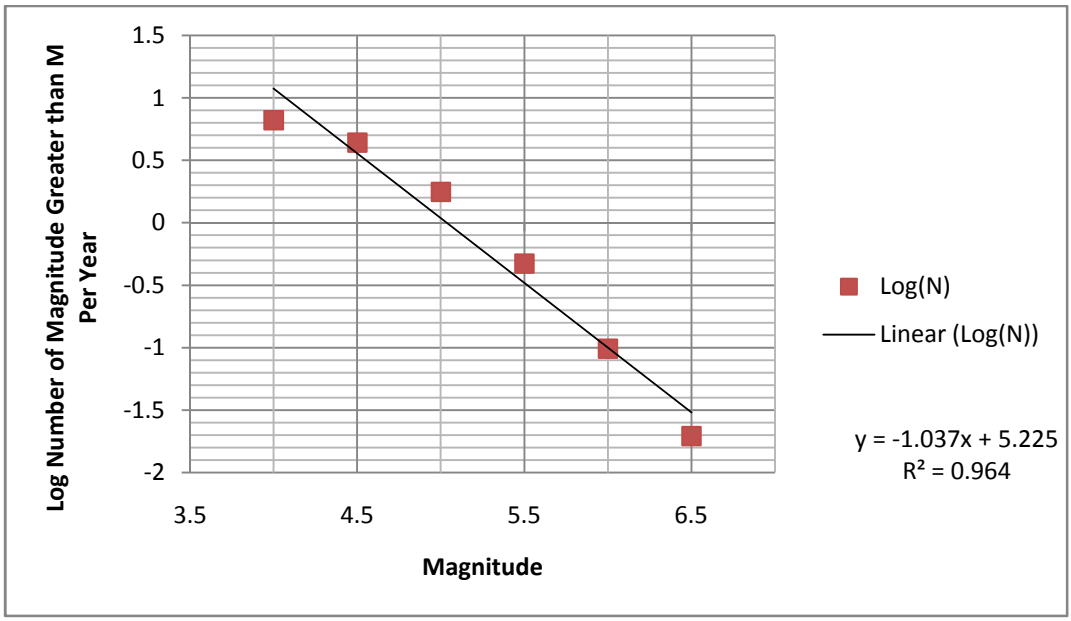

Figure 5. 4 Gutenberg-Richter b-Lines for Afar (source2), Constructed based on instrumental records of last 100 years.

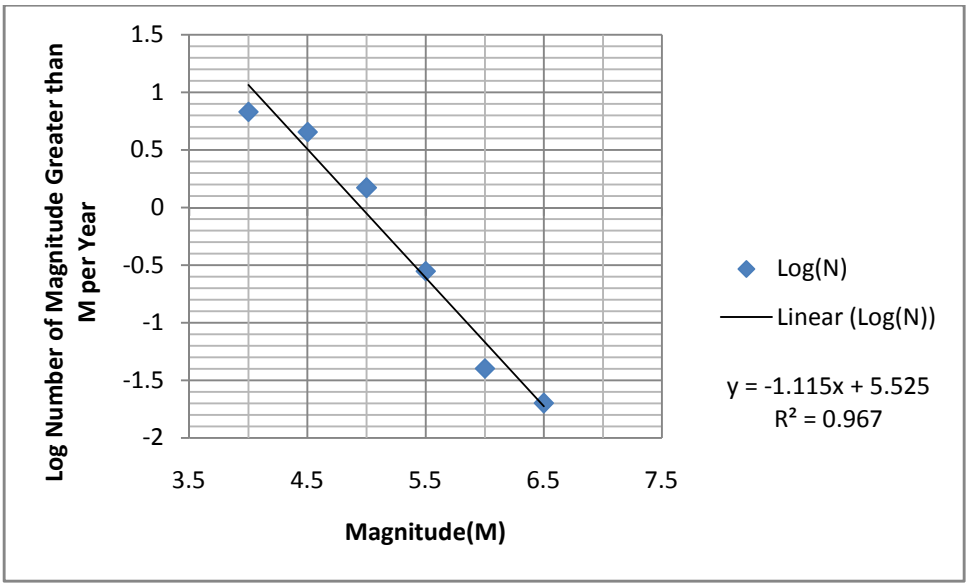

Figure 5. 5 Gutenberg-Richter b-Lines for Escarpment (source3), Constructed based on instrumental records of last 100 years.

From the b-line (Fig.5.3 - 5.5) a b-value of 0.678, 1.035 and 1.115 were found for the three source zones respectively. The b-value for Afar and the Escarpment source zones shows relatively large value, this indicate that small earthquakes of magnitude less than 4 occurs frequently in the area. But a relatively small b-value (0.678) for the MER source zone were found, this indicates small earthquakes of magnitude less than 4 are not frequent and large earthquakes of magnitude greater than 4 are more likely to occur in the area. It is known that large size earthquake of magnitude 6.8 occurred in this zone in 1906 at an epicentral distance of about 120 km south of Addis Ababa. This was the largest earthquake ever that was recorded in Ethiopia (Mammo, 2005).

5.4.3 Magnitude Distribution of the Study Area

Randomness in the relative number of large, moderate and small magnitude earthquakes that will occur on a given source can be defined through a probability density function. Magnitude limits in evaluating the seismic hazard of the area source1 (MER).

$m_o = 4$ $M_{max} = 6.8$

Magnitude probability density function from equation (5.10) is given by:

$$f(M) = c \cdot \beta \cdot e^{-\beta(M - m_o)} \quad 5.12$$

Where: $c = \frac{1}{1 - e^{-\beta(m_{\max} - m_o)}}$

$$LnN = \alpha - \beta M \qquad 5.13$$

$\beta = 1.56$ and $\alpha = 5.86$

$$c = \frac{1}{1 - e^{-1.56(6.8-4)}} = 1.013$$

$$f(M) = 1.013 \cdot 1.56 \cdot e^{-1.56(M-4)} \qquad 5.14$$

The magnitude range is divided into subintervals with increments of 0.5 M.

Table 5. 2 Magnitude probability density function calculation for the source zones.

Magnitude Probability Density Function			
β	1.56	2.389	2.569
M_{max}	6.8	6.22	6.56
M	f(M) source 1	f(M) source 2	f(M) Source 3
4.0	1.58	2.401	2.752
4.5	0.72	0.727	0.712
5.0	0.33	0.220	0.197
5.5	0.15	0.067	0.055
6.0	0.08	0.020	0.015
6.5	0.03	0.006	0.004
7.0	0.01	0.001	0.001

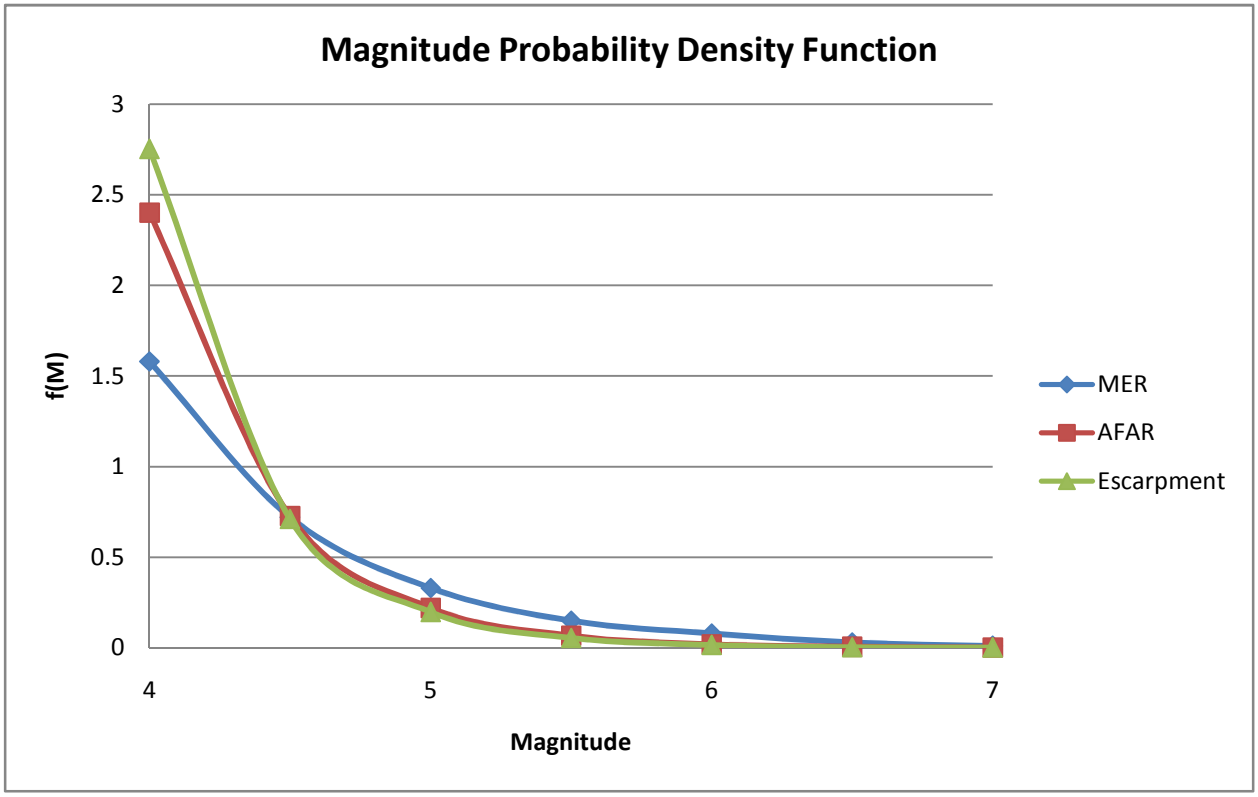

Figure 5. 6 Magnitude Probability Density Function diagram for the tree sources zones.

As can be seen in Figure 5.6, the earthquake magnitudes are exponentially distributed. This implies that the mean recurrence rate for small magnitude earthquakes is greater than that of large magnitude earthquakes for Escarpment seismic source than MER and Afar seismic source zones.

CHAPTER SIX

6 Estimating Ground Motion

Estimates of ground motion are used in the design of structures in one of two ways, either implicitly through the use of building codes or explicitly through the site-specific design of structures (Boore, 2003). Although recently there have been significant efforts to instrument seismically active regions to gather more ground motion recordings, there are still not a sufficient amount of data to allow for direct empirical estimation of design ground motions. As a result, considerable work has been dedicated to develop relations to estimate ground motion parameters critical for the design of structures based on seismic source characteristics (e.g. magnitude, distance).

6.1 Attenuation Relationships

The description of the ground motion attenuation is generally performed using empirical ground-motion models that describe the distribution of expected ground motion parameters measures as a function of a few independent parameters, such as magnitude, source-to-site distance and site classification. The variability of these predictions is usually referred to as aleatory variability and represented by the standard deviation (or standard error, σ) of the logarithmic residuals. The starting point to generate such relationships is the assembling of a database of a sufficient number of records that can be then regressed in order to estimate the ground motion parameters of interest. The relationships that link a particular ground motion measure with the quantities that control it are called ground motion predictive equations (GMPEs). Magnitude and source-to-site distance are two factors that conspicuously affect the shaking at a site. The amount of energy released during a seismic event is related to its magnitude:

An attenuation expression provides a functional relationship between earthquake properties (e.g., peak ground acceleration) or response quantities (e.g., spectral response values) and various parameters such as magnitude, soil conditions, site-to-source distance, etc. Although many response quantities are useful, traditionally peak acceleration is most commonly used in engineering applications. Specifically, attenuation is defined as the loss of energy of a seismic

wave as it travels through the earth, which is not caused by geometric spreading, but depends on the characteristics of the transmitting media (Telford et al, 1990).

The attenuation of seismic waves is a function of a number of variables which generally can be categorized as: source mechanism, travel path, and local conditions. For example, source mechanism encompasses factors such as stress and strain conditions, rupture dimensions, and source depth. Inclusive in travel path are such factors as geometric spreading, reflection, refraction, absorption, and geologic structure. Subsurface conditions, topographic variations, and soil-structure interaction all constitute local conditions.

Two factors that often are represented in attenuation expressions are geometric spreading and absorption. The inclusion of geometric spreading and absorption in many relationships is possible because these phenomena are relatively well understood. The concept of geometric spreading can be easily illustrated when related to the conservation of energy. Spherical wave-fronts occupy more area as they progress from a seismic source.

Absorption is more complex than geometric spreading. In general, absorption results from friction in the medium and scattering of the waves which can cause destructive interference. An often used expression that relates absorption to frequency and rock properties is $Q = Q_o f^n$, where Q is called the quality factor, f is frequency, and Qo and n are constants dependent on rock properties. Large values of Q correspond to low absorption (and attenuation), and vice-versa. Observations have shown that seismic waves are attenuated less in the overlying mantle in the eastern united States (US) as opposed to the folded and fractured mountainous topography of the western US (Reiter, 1990). In extending the above sunlight analogy, the earth is spared from many harmful cosmic rays that are absorbed in its atmosphere.

6.1.1 Types of Attenuation Relationships

The actual functional form of an attenuation expression depends on the approach used to derive it or the theory on which it is based. In general, most expressions are variations of two types. While many names have been used to title these two categories, in this paper they are referred to as empirical and theoretical. As will be seen subsequently, these titles are somewhat ambiguous because many empirical type expressions contain theoretically based terms, and many theoretical type relationships incorporate empirically derived constants. The distinction between empirical

and theoretical expressions is as follows. Empirical type relationships are typically derived by applying regression analysis methods to observed and recorded earthquake data. On the other hand, theoretical expressions attempt to model directly the physics of earthquakes and related mechanisms, with constants being determined empirically. In some cases, the distinction as to whether an expression is empirical or theoretical is difficult to separate.

6.2 Overview of Empirical Ground Motion Equations

Characterizations of ground motions typically take the form of a probability distribution function of a particular ground motion parameter (such as peak acceleration or response spectra) which is defined by its statistical moments (e.g. median, standard deviation). These statistical moments are determined using equations known as attenuation relations, which are derived through regression analysis of empirical data and are based on magnitude, source-to-site distance, and other seismological parameters.

The general form of an attenuation relation can be expressed as:

$$Ln(Y) = c_o + c_2 m + c_3 m^{c_4} + c_5 \ln(r) + f(F) + f(HW) + f(S) + \varepsilon \qquad 6.1$$

Where Y = Ground motion amplitude parameter (e.g. PGA)

$c_0, c_1 \ldots c_5$ = Constants determined by regression analysis

m = Moment magnitude

r = Source to site distance

S = Factor accounting for local site conditions

F = Factor accounting for fault type (e.g. strike-slip, reverse)

HW = Factor accounting for hanging-wall effects

This general form relies on a number of assumptions that serve as the basis for most attenuation relations (Stewart et al, 2001).

1) Uncertainty in ground motions – Attenuation relations define not only the mean ground motion, Y, but additionally the uncertainty or variability, ε or σ_Y, in ground motion amplitudes. Typically, ground motion amplitudes are assumed to be lognormally distributed and thus the mean and uncertainty are represented as $Ln(Y)$ and σ_{LnY} respectively. This assumption however, has been shown to break down for near-source ground motions and therefore other distributions of uncertainty should be considered.

2) Magnitude dependence **-** Several magnitude scales such as moment magnitude are derived using the logarithm of peak ground motion parameters. Therefore *Ln(Y)* is assumed to be proportional to the magnitude, *m* of the event. This assumption however, has been shown to break down for high frequency ground motion at large magnitudes due to saturation.

3) Radiation damping **-** The energy released by a seismic source during an earthquake is radiated out through traveling body waves. As they travel away from the source, the wave amplitudes reduce at a rate of *1/r* (where *r* is the source-to-site distance), a phenomenon known as radiation damping. The source-to-site distance, a key parameter is defining the attenuation of ground motions, is a somewhat ambiguous term with several existing definitions. It is therefore critical to clearly understand which distance parameter is appropriate for the specific model used. Some examples of common definitions for *r* are shown in the figure 6.1 below.

4) Factors influencing attenuation (f(F),f(HW),f(S)) **-** Attenuation of ground motions can be significantly affected by several factors related to source and site characteristics.

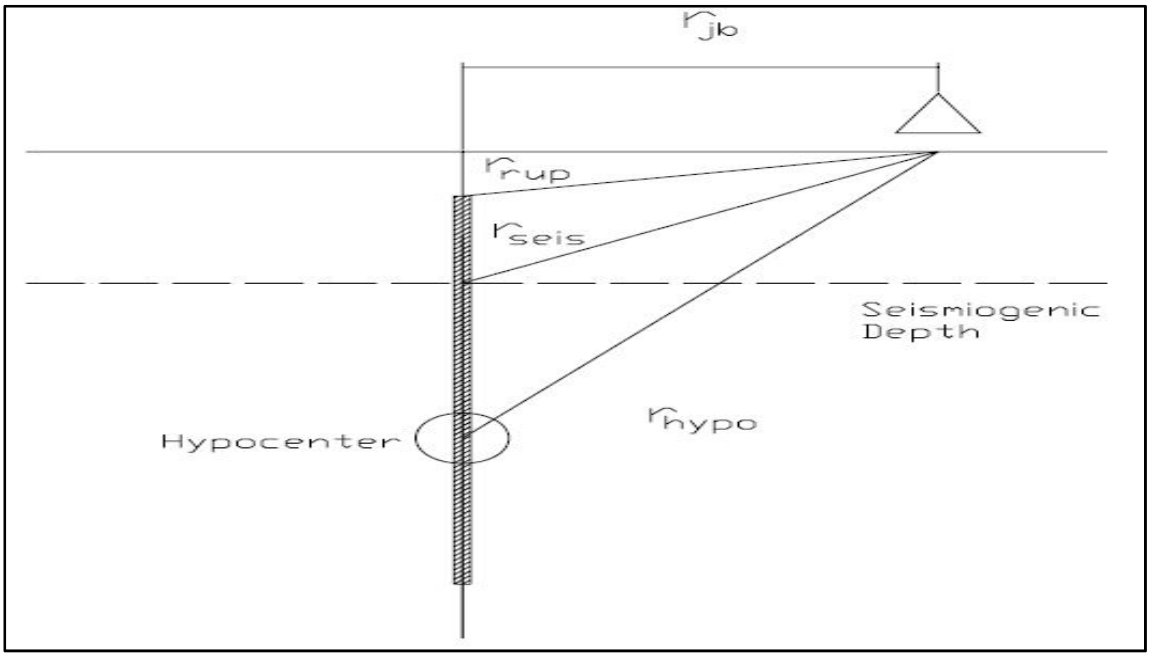

a

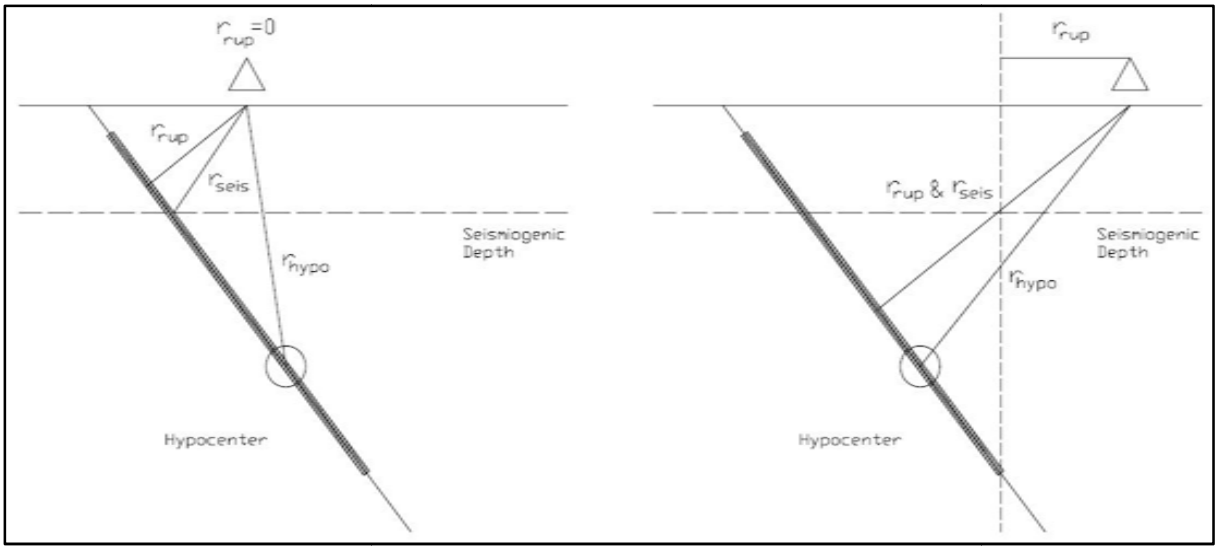

b

Figure 6. 1 Source-to-site distance measures for ground motion attenuation models for (a)Vertical faults and (b) Dipping faults.

6.3 Selection of the Attenuation Relationships for the study area

For this study, two attenuation relationships have been basically selected. These are the relationships proposed by (Abrahamson and Silva 1997) and (Campbell and Bozorgnia 2003). In the following sections, the reasons of their selections and their characteristic features will be clarified, somewhere together with their comparisons with the other ground motion relationships.

Gouin(1979) in his study, until such a time as local attenuation curves became available and as a first approximation, has adopted the strong ground motion attenuation relation that shown on Figure 6.2 for the western USA, where the Rocky Mountains can be approximated to the tectonically disturbed rift regions. This is partly supported by the fact that in both California and in the region under study substantial parts of the surface areas are plate boundaries, and also the hypo central depths of earthquakes, which influence strong ground motion significantly, are similar as both regions are characterized by the occurrence of shallow focus earthquakes. Of the few observations made in the rift none contradicts this choice (Gouin 1979).

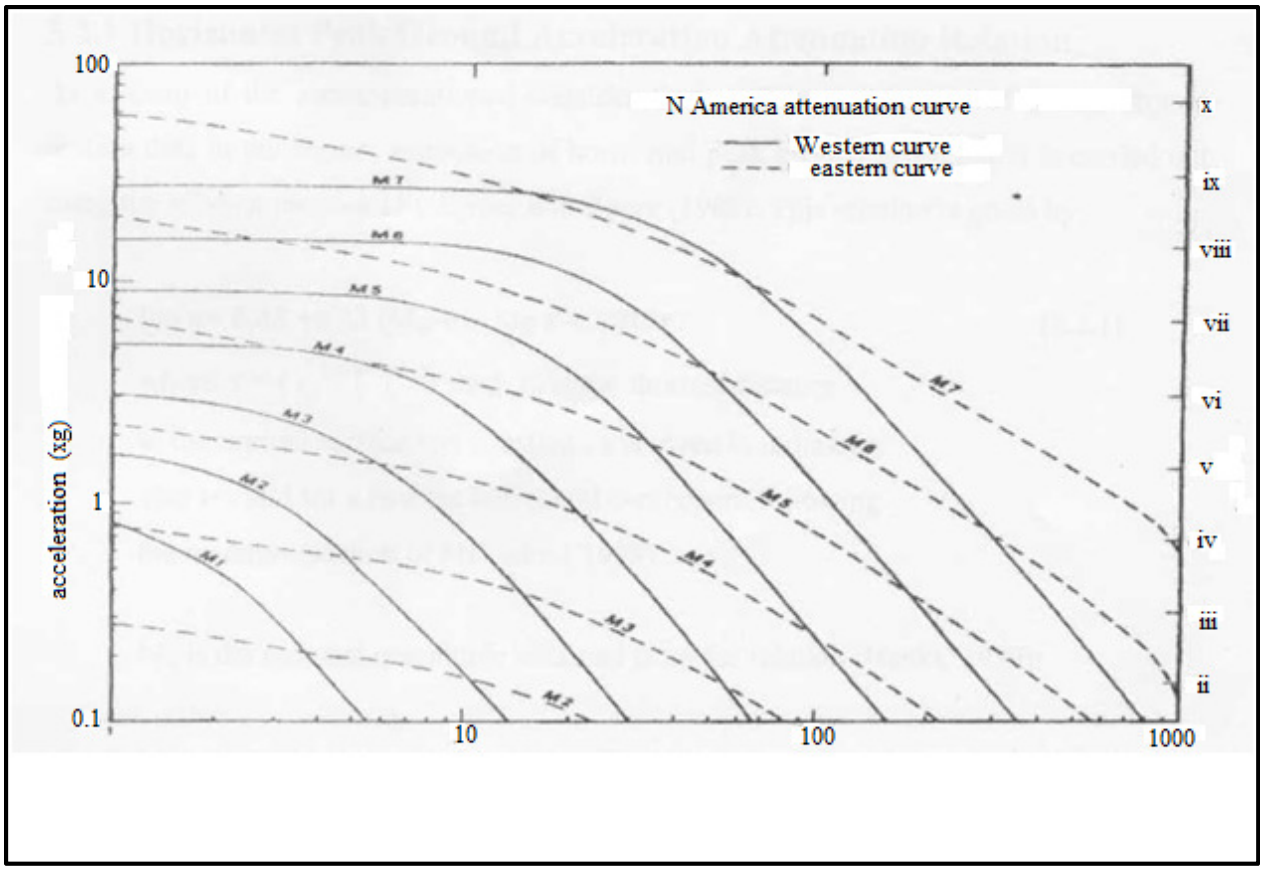

Figure 6. 2 The attenuation curves of America (after Gouin, 1979).

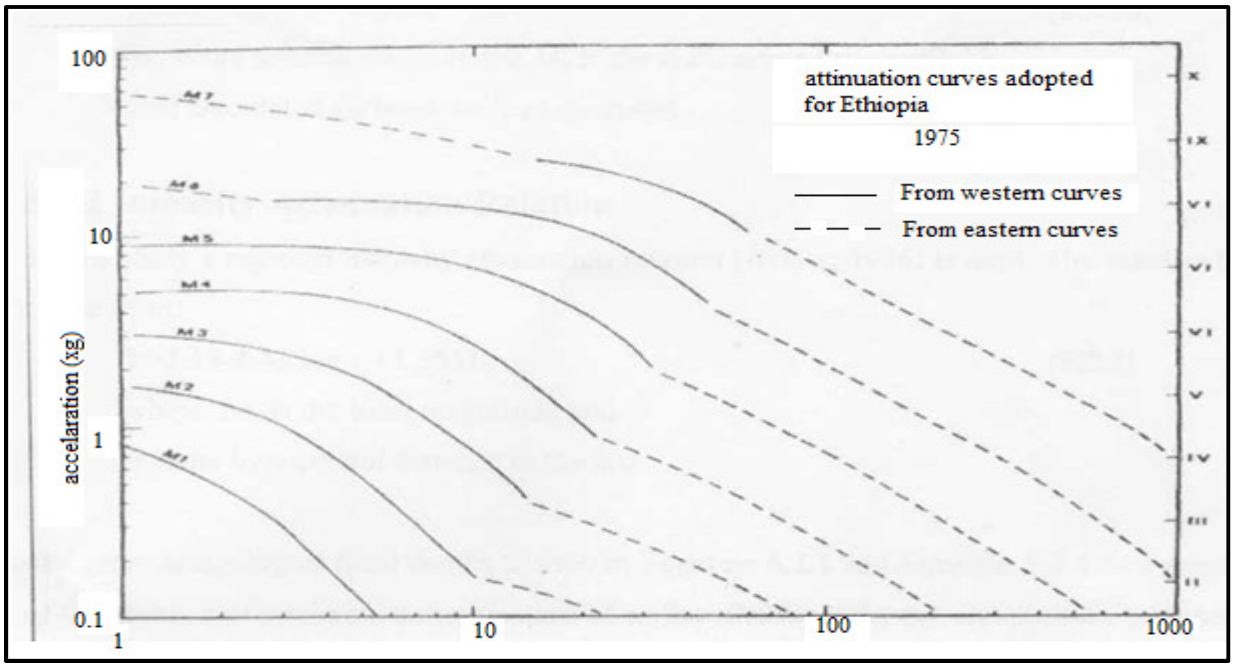

Figure 6. 3 The adopted attenuation curves for Ethiopia (after Gouin, 1979).

6.4 NGA model (Attenuation Relationships) derived by Campbell and Bozorgnia (2008)

The empirical ground motion model (also referred to as an attenuation relation or ground motion prediction equation) derived by (Campbell and Bozornia 2008) is new ground motion model supersedes the existing ground motion models for peak ground velocity (PGV) (Campbell, 1997) and peak ground acceleration (PGA) and 5% damped pseudo-absolute response spectral acceleration (PSA) (Campbell and Bozorgnia, 2003). This NGA model represents a major advancement in ground motion prediction made possible by the extensive update of the PEER strong motion database and the supporting studies on 1-D ground motion simulation, 1-D site response, and 3-D basin response sponsored by the NGA project.

6.4.1 Database

The database used for this model is a subset of the updated PEER strong motion database (Chiou et al., 2008). The general criteria that we used to select this subset was intended to meet our requirements that (1) the earthquake be located within the shallow continental lithosphere (i.e., the Earth's crust) in a region considered to be tectonically active, (2) that the recording be located at or near ground level and exhibit no known embedment or topographic effects, (3) that the earthquake have enough recordings to reliably represent the mean horizontal ground motion (especially for small-magnitude events), and (4) that the earthquake or the recording be considered reliable according to criteria set forth in (Campbell and Bozorgnia 2007). Application of the above criteria resulted in the selection of 1561 recordings from 64 earthquakes with moment magnitudes (M) ranging from 4.3–7.9 and rupture distances (R_{RUP}) ranging from 0.1–199 km. The distribution of the recordings with respect to magnitude and distance is shown in Fig. 6.4.

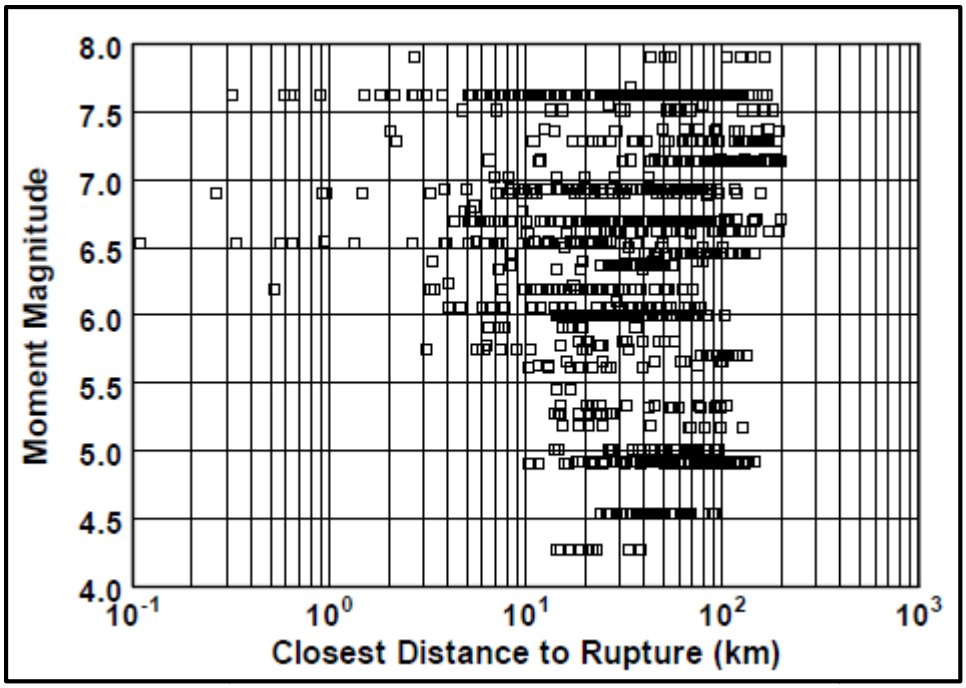

Figure 6. 4 Database used in the analysis.

6.4.2 Ground Motion Model

The functional forms used to define NGA model were selected according to (1) their sound seismological basis; (2) their unbiased residuals; (3) their ability to be extrapolated to values of magnitude, distance, and other explanatory variables that are important for use in engineering and seismology; and (4) their simplicity, although this latter consideration was not an overriding factor. The third criterion was the most difficult to achieve because the data did not always allow the functional forms of some explanatory variables to be developed empirically. In such cases, theoretical constraints were used to define the functional forms based on supporting studies sponsored by the NGA project (Power et al., 2008).

During the model development phase of the study, regression analyses were performed in two stages for a limited set of oscillator periods (T) using a two-stage nonlinear regression procedure. In Stage 1, the mathematical terms involving individual recordings (the intra-event terms) were fit by the method of nonlinear least squares using all of the recordings. In Stage 2, the mathematical terms common to all recordings of a specific earthquake (the inter-event terms) were fit by the method of weighted least squares using the event terms from Stage 1 as the "data". Each event term was assigned a weight that was inversely proportional to its calculated

variance from Stage 1. This two-stage analysis allowed us to decouple the intra-event and inter-event terms, which stabilized the regression analysis and allowed us to independently evaluate and model magnitude scaling effects at large magnitudes. Once the functional forms for all of the mathematical terms were established, a series of iterative random-effects regression analyses were performed for the entire range of periods in order to derive a smoothed set of model coefficients and to calculate the final values of the inter-event and intra-event standard deviations.

6.4.2.1 Definition of Ground Motion Components

The ground motion component used in NGA model is not the traditional geometric mean of the two "as-recorded" horizontal components that has been used in past studies. The principle drawback of the old geometric mean is its dependence on the orientation of the sensors as installed in the field. The new geometric mean, referred to as "GMRotI50" by (Boore et al. 2006), is independent of both sensor orientation and oscillator period and, as a result, represents a more robust horizontal ground motion component. It was found to have a value that is on average within a few percent of the old geometric mean. In some engineering applications it is necessary to calculate the median and aleatory uncertainty of the arbitrary horizontal component (Baker and Cornell, 2006). The median estimate of this component is equivalent to the median estimate of the traditional geometric mean. However, its variance must be increased by the variance of the component-to-component variability between the two horizontal components of the recording. The relationship between the new geometric mean and other horizontal ground motion components, such as the maximum arbitrary (as-recorded) horizontal component, the maximum rotated horizontal component, and the strike-normal component can be found in (Campbell and Bozorgnia 2007, 2008) and references therein.

6.4.2.2 Median Ground Motion Model

The median estimate of ground motion can be calculated from the general equation

$$\ln Y_{ij} = f_{mag} + f_{dis} + f_{flt} + f_{hng} + f_{site} + f_{sed} \qquad 6.2$$

Where,

$$f_{mag} = \begin{cases} c_o + c_1 M; & M \le 5.5 \\ c_o + c_1 M + c_2 (M - 5.5); & 5.5 < M \le 6.5 \\ c_o + c_1 M + c_2 (M - 5.5) + c_3 (M - 6.5); & M > 6.5 \end{cases} \quad 6.3$$

$$f_{dis} = (c_4 + c_5 M) \ln \sqrt{R_{RUP}^2 + c_6^2}) \quad 6.4$$

$$f_{flt} = c_7 F_{RV} f_{flt,Z} + c_8 F_{NM} \quad 6.5$$

$$f_{flt,Z} = \begin{cases} Z_{TOR}; & Z_{TOR} < 1 \\ 1; & Z_{TOR} \ge 1 \end{cases} \quad 6.6$$

$$f_{hng} = c_9 f_{hng,R} f_{hng,M} f_{hng,Z} f_{hng,\delta} \quad 6.7$$

$$f_{hng,R} = \begin{cases} 1; & R_{JB} = 0 \\ \left[\max(R_{RUP}, \sqrt{R_{JB}^2 + 1}) - R_{JB}\right] \Big/ \max(R_{RUP}, \sqrt{R_{JB}^2 + 1}); & R_{JB} > 0, Z_{TOR} < 1 \\ (R_{RUP} - R_{JB}) \Big/ R_{RUP}; & R_{JB} > o, Z_{TOR} \ge 1 \end{cases} \quad 6.8$$

$$f_{hng,M} = \begin{cases} 0; & M \le 6.0 \\ 2(M - 6.0); & 6.0 < M < 6.5 \\ 1; & M \ge 6.5 \end{cases} \quad 6.9$$

$$f_{hng,Z} = \begin{cases} 0; & Z_{TOR} \ge 20 \\ (20 - Z_{TOR}) \Big/ 20; & 0 \le Z_{TOR} < 20 \end{cases} \quad 6.10$$

$$f_{hng,\delta} = \begin{cases} 1; & \delta \le 70 \\ (90 - \delta) \Big/ 20; & \delta > 70 \end{cases} \quad 6.11$$

$$f_{site} = \begin{cases} c_{10}\ln\left(\frac{V_{s30}}{k_1}\right) + k_2\left\{\ln\left[A_{1100} + c\left(\frac{V_{s30}}{k_1}\right)^n\right] - \ln\left[A_{1100} + c\right]\right\}; & V_{s30} < k_1 \\ (c_{10} + k_2 n)\ln\left(\frac{V_{s30}}{k_1}\right); & k_1 \le V_{s30} < 1100 \\ (c_{10} + k_2 n)\ln\left(\frac{1100}{k_1}\right); & V_{s30} \ge 1100 \end{cases} \quad 6.12$$

$$f_{sed} = \begin{cases} c_{11}(Z_{2.5} - 1); & Z_{2.5} < 1 \\ 0; & 1 \le Z_{2.5} \le 3 \\ c_{12}k_3 e^{-0.75}\left[1 - e^{-0.25(Z_{2.5}-3)}\right]; & Z_{2.5} > 3 \end{cases} \quad 6.13$$

In the above equations,

Y_{ij} is the median estimate of the geometric mean horizontal component (GMRotI50) of PGA (g), PGV (cm/s), PGD (cm) or PSA (g) for site *j* of event *i*;

M is moment magnitude;

R_{RUP} is the closest distance to the coseismic rupture plane (km);

R_{JB} is the closest distance to the surface projection of the coseismic rupture plane (km);

F_{RV} is an indicator variable representing reverse and reverse-oblique faulting,

where F_{RV} = 1 for 30° < **λ** < 150°, F_{RV} = 0 otherwise, and **λ** is the rake defined as the average angle of slip measured in the plane of rupture between the strike direction and the slip vector;

F_{NM} is an indicator variable representing normal and normal-oblique faulting, where $\boldsymbol{F_{NM}}$ = 1 for –150° < λ < –30° and *FNM* = 0 otherwise;

Z_{TOR} is the depth to the top of the coseismic rupture plane (km);

δ is the dip of the rupture plane (°);

V_{S30} is the time-averaged shear-wave velocity in the top 30 m of the site profile (m/s);

A_{1100} is the median estimate of PGA on a reference rock outcrop with V_{S30} = 1100 m/s (g); and

$Z_{2.5}$ is the depth to the 2.5 km/s shear-wave velocity horizon, typically referred to as basin or sediment depth (km).

$\boldsymbol{c_i}$ empirical coefficients and *c*, *n* and $\boldsymbol{k_i}$ are theoretical coefficients. When PSA < PGA and $T \le$ 0.25 s, PSA should be set equal to PGA to be consistent with the definition of pseudo-absolute acceleration.

The new NGA ground motion prediction equations to be appropriate for estimating PGA, PGV, PGD and linear elastic response spectra (T = 0.01–10 s) for shallow continental earthquakes occurring in western North America and other regimes of similar active tectonics such as southern Europe (Campbell and Bozorgnia, 2006; Stafford et al., 2008). The model is considered most reliable when evaluated for (1) M > 4.0; (2) M < 8.5 for strike-slip faulting, M < 8.0 for reverse faulting, and M < 7.5 for normal faulting; (3) R_{RUP} = 0–200 km; (4) V_{S30} = 150–1500 m/s or alternatively NEHRP site classes B (V_{S30} = 1070 m/s), C (V_{S30} = 525 m/s), D (V_{S30} = 255 m/s) and E (V_{S30} = 150 m/s); (4) $Z_{2.5}$ = 0–10 km; (5) Z_{TOR} = 0–15 km; and (6) δ = 15– 90°. As an example, the predicted attenuation and magnitude scaling characteristics of PGA and response spectra (M = 7.0 and R_{RUP} = 10 km, respectively) for rock with $VS30$ = 760 m/s, a sediment depth of 2.5 km, and strike-slip faulting are displayed in Figs. 6.5.

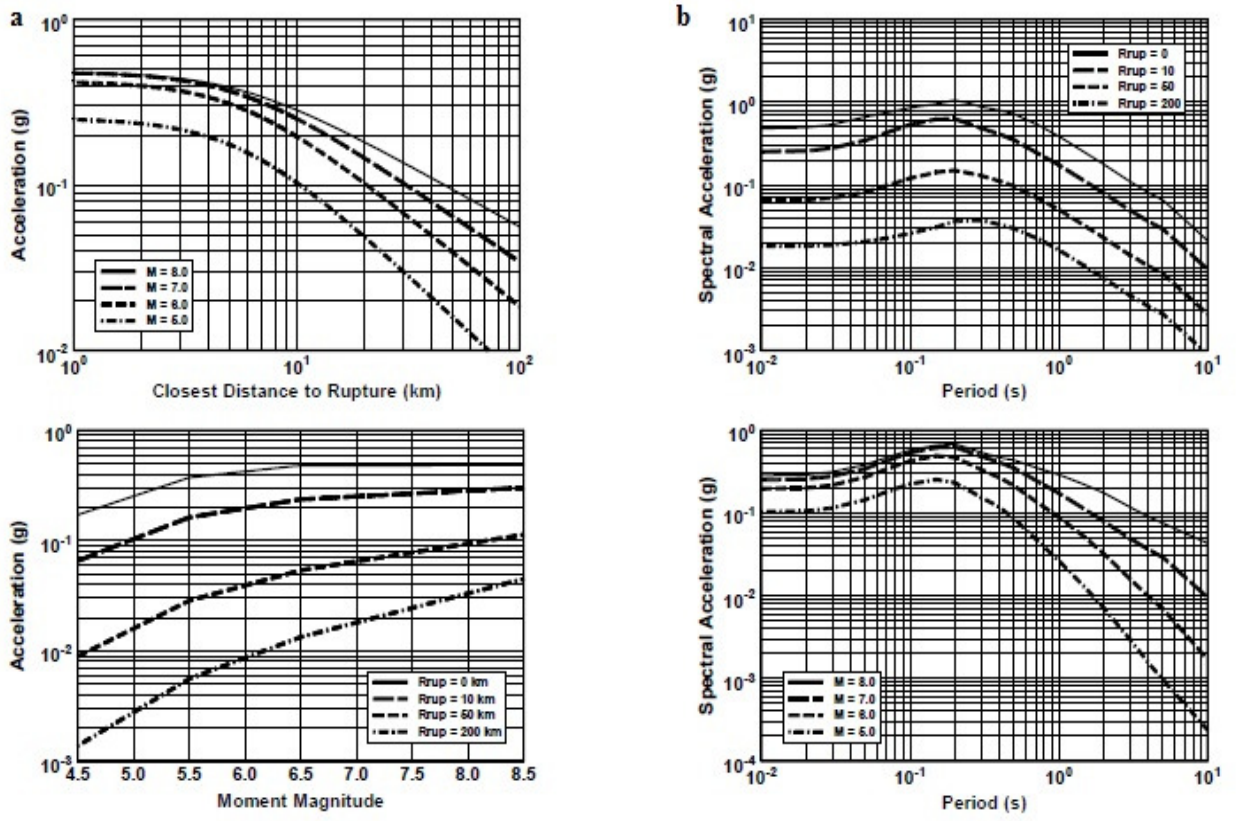

Figure 6. 5 (a) Predicted estimates of PGA and (b) Predicted estimates of PSA.

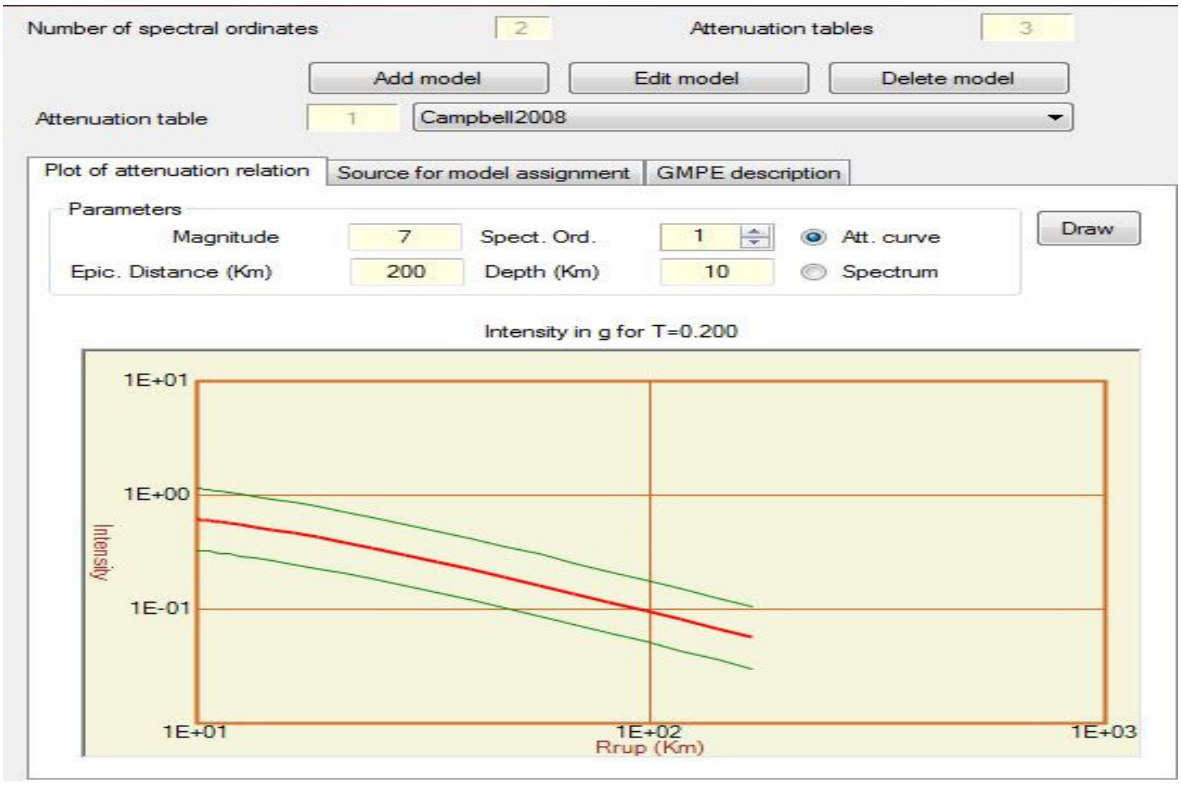

Figure 6. 6 Plot of attenuation relation by (Campbell and Bozorgnia 2008) using CRISIS2012 computer program.

Table 6. 1 Description ground motion prediction equation by (Campbell and Bozorgnia 2008).

GMPE description	
Brief description	NGA model by Campbell & Bozorgnia(2008)
Original units	G
Dimension	Acceleration
Spectral period range	0 to 10
Valid distance range	0 to 200
Valid magnitude range	4 to 8.5
Type of distance metric	Rrup
Residuals distribution	LogNormal
Tectonic region	Active_Shalow_Crustal

6.5 Local Site Condition

Effects of local site conditions can be represented in many forms, ranging from a simple constant to more complex functions that attempt to characterize non-linearity in ground response. While some models use a simple soil/rock soil classification (Abrahamson & Silva, 1997; Sadigh et al, 1997) others use more quantitative methods of classification, such as the 30m shear wave velocity. In general, the standard error in attenuation relations are assumed to be unaffected by site conditions. In this study attenuation relation or NGA model by (Campbell and Bozorgnia 2008) was used. This model was incorporated in the CRISIS2012 program; it allows the calculation of shear wave velocity at the top 30m that indicates the local site condition.

6.5.1 Surface wave properties

Seismic waves can be categorized by whether they travel through a medium (body waves) or along the medium's surface (surface waves). Body waves propagate by a series of compressions and dilatations of the material or by shearing the material back and forth. The first type of body wave is variously known as a dilatational, longitudinal, irrotational, compressional, or P-wave, the latter name being due to the fact that this type is usually the first (primary) event on an earthquake seismogram. The P-wave forces particles of the medium to move back and forth parallel to the direction of propagation. The second type is referred to as the shear, transverse, rotational, or S-wave (because it is usually the second event observed on an earthquake seismogram). Under S-waves, the medium is displaced transversely to the direction of propagation (Fig.6.7). Moreover, because the rotation varies from point to point at any given instant, the medium is subjected to varying shearing stresses as the wave moves along. S-wave particle motion is often divided into two components: the motion within a vertical plane through the propagation vector (SV-wave), and the horizontal motion in the direction perpendicular the plane (SH-wave).

In an infinite homogeneous isotropic medium, only body waves exist (Aki and Richards, 2002). However, when the medium does not extend to infinity in all directions, surface waves (known in seismic exploration as ground roll) can be generated. The primary type of surface wave is the Rayleigh wave. This wave travels along the surface of the earth and involves an interference of the P-wave and SV-wave. The particle motion is confined to the vertical plane that includes the direction of propagation of the wave. The motion is counter clockwise (retrograde) at the surface,

changing to purely vertical motion at a depth of about one fifth of a wavelength, and becoming clockwise (prograde) at greater depths. The amplitude of the Rayleigh wave motion decreases exponentially with depth. Because of the existence of vertical medium-velocity gradients in the real world, the velocity of the Rayleigh wave varies with wavelength (called dispersion curves); longer period waves travel faster because they sense the faster material at greater depth. The second type of surface wave is the Love wave. Love waves are formed through the constructive interference of high order SH multiples. The particle motion is horizontal and in the direction of SH waves. The amplitude of this wave motion decreases exponentially with depth. They exhibit dispersion as well.

Geometrical spreading for surface waves is proportional to $r^{-0.5}$, in contrast to the body wave where the geometrical spreading is proportional to r^{-1}, where r is distance from the source (Anderson, 1991). Rayleigh waves often are dominant events in seismic records. The amplitude of surface waves decreases exponentially with depth. Most of the energy propagates in a shallow zone, roughly equal to one wavelength. Consequently, the wave propagation is influenced by the properties of this limited, near surface portion of the geological or geotechnical profile.

The propagation of surface waves in a vertically heterogeneous medium shows a dispersive behavior. Dispersion means that different frequencies have different phase velocities. In a homogeneous medium, the different wavelengths (Rayleigh wave only) “sample” different depths of the subsoil. Since the material is homogeneous, all the wavelengths have the same velocity. In other words, Rayleigh waves are non-dispersive and Love waves do not exist in a homogeneous medium. If the medium is not vertically homogeneous, for instance it is layered, with layers having different mechanical properties, the different wavelengths “sample” different depths to which different mechanical properties are associated. Each wavelength propagates at a phase velocity depending on the mechanical properties of the layers involved in the propagation. So the surface wave does not have a single velocity, but a phase velocity that is a function of frequency.

This relation between frequency and phase velocity is called a dispersion curve and depends on the geology underneath. At high frequency, the phase velocity is close to the S-wave velocity through the uppermost layer. At low frequency, the effect of deeper layers become important,

and the phase velocity tends asymptotically to the S-wave velocity of the deepest material, as if it extends infinitely in depth (the half space).

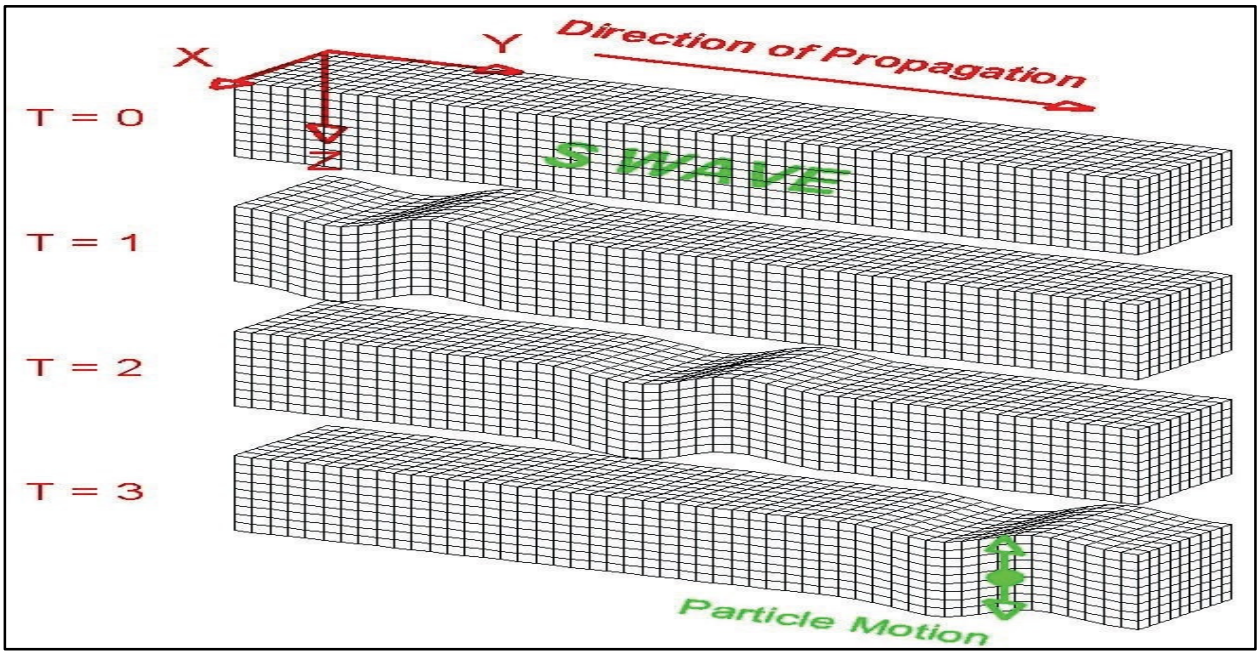

Figure 6. 7 S-wave motion.

The shape of dispersion curves is related to geologic profiles. Longer wavelengths penetrate deeper than shorter wavelengths for a given mode and are more sensitive to the elastic properties of the deeper layers. For a profile where S-wave velocity increases with depth, a normal dispersion curve (phase velocities decrease with frequency) will be observed (Fig.6.8). For a profile where S-wave velocity decreases with depth, a reverse dispersion curve (phase velocities increase with frequency) will be observed. In an irregular S-wave velocity profile, the phase velocities show a complex relation with frequency (Fig.6.8). In reality, the S-wave velocities increase with depth in most geological structures. Most of the observed dispersion curves are normal. A complex and a reverse shape of dispersion curves also observed in our surface wave surveys data taken in Debrezeit. This is due to the local deposition of black cotton soil eroded from small rims near Kuriftu lake. The observation of a reverse dispersion curve in the data might be caused by the limited frequency bandwidth of the surveys. The observed reverse curve actually is one part of the complex dispersion curves.

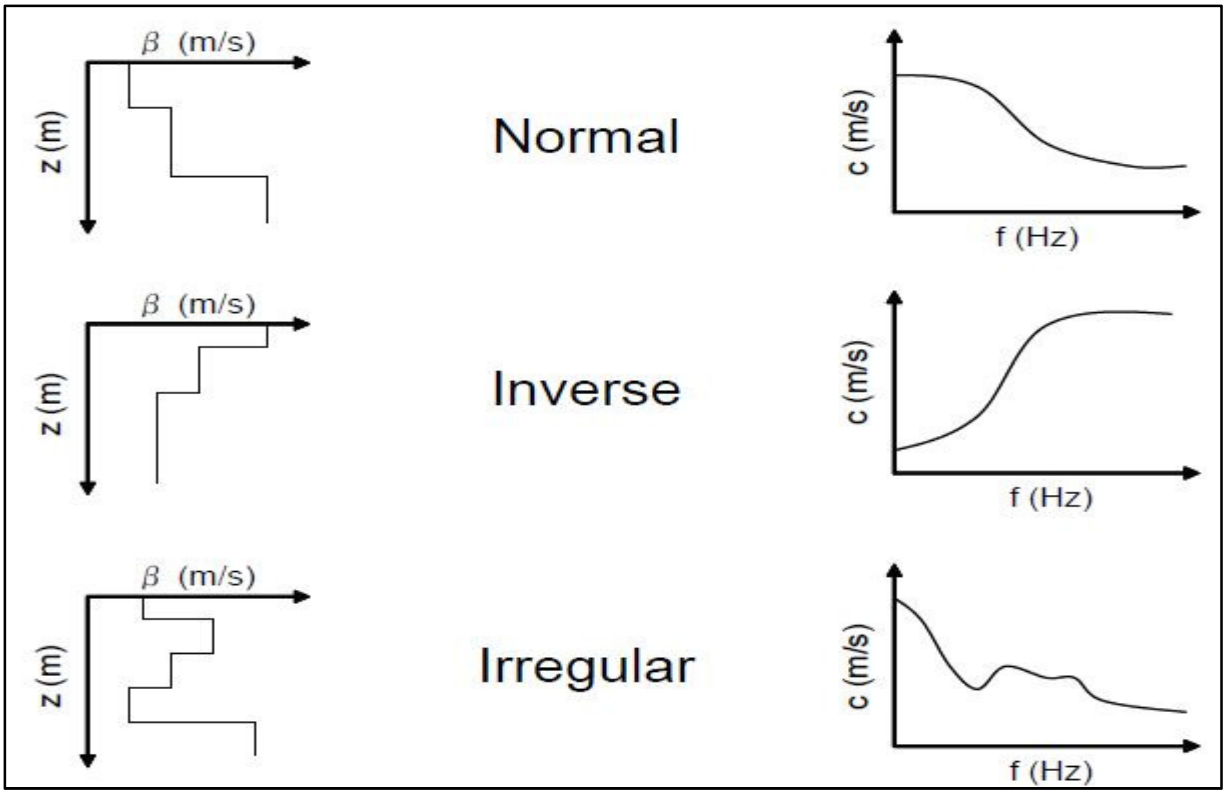

Figure 6. 8 Shows velocity model and dispersion curve (Phase velocities vs. frequencies).

A normal dispersion curve results from a profile where S-wave velocity increases with depth. For a profile where S-wave velocity decreases with depth a reverse dispersion curve will be observed over some range of frequency. For an irregular S-wave velocity profile, phase velocities show a complex relation with frequencies.

Like a vibrating string, the surface wave propagation in vertically heterogeneous media is actually a multi-modal phenomenon. For a given geology, at each frequency different wavelengths can exist. Hence different phase velocities are possible at each frequency, each corresponding to a mode of propagation. The different modes can exist simultaneously (Aki and Richards, 2002). The different modes, except the first one, exist only above their cut-off frequency, which is for each mode the lowest limit frequency at which the mode can exist. With a finite number of layers, in a finite frequency range, the number of modes is limited. At very low frequency, below the cut-off frequency of the first higher mode, only the fundamental mode exists. Modes are not just theory or mathematically possible solutions; they are often observed in experimental data, also in the frequency ranges of interest for engineering purposes. The energy

associated to the different modes depends on many factors, the geology at first, but also the depth and the kind of source.

The first mode is sometimes dominant over a wide frequency range, but in many common situations higher modes play important roles and are dominant in energy. So they cannot be neglected. The different modes have different phase velocities. Therefore, they are separated at distance from the source. At short distances modes superimpose on one another, and mode identification can be impossible. At the engineering scale, the modal superposition is important. The effective Rayleigh phase velocity deriving from the modal superposition is only an apparent velocity that depends on the observation layout, source orientation, and position.

6.6 Seismic Acquisition Techniques Used in shallow site Investigation

Many seismic methods have been used by seismologists to determine the velocity structure of the Earth at different scales (Lay and Wallace, 1995). They include the reflection seismic method used by exploration geophysicists, and the use of body-wave arrival times, surface-wave dispersion, and free-oscillation periods of the Earth. Those methods are now being successfully adopted in the determination of shallow S- wave structure to help in the specification of design ground motions for engineering purposes (Horike, 1985, 1988; Nazarian and Stokoe, 1985; Stephenson et al., 2005). According to Boore (2006), the seismic methods used in shallow site investigations are categorized according to invasiveness. The noninvasive methods are further organized according to number of stations used. The multiple station groups is subdivided into those methods that use active sources, those that use passive sources, and those that combine active and passive sources.

6.6.1 Multi Channel Analyses of Surface Waves (MASW) Method

The MASW method is based on the fact that the S-wave velocity is the dominant influence on Rayleigh wave velocities for a layered earth model, which assures us that inverting phase velocities will give us an S-wave velocity profile (one-dimensional S-wave velocity function, Vs against depth) at the centre of a receiver spread. Because data are acquired in the standard CDP acquisition format similar to conventional petroleum exploration data acquisition, phase velocities of ground roll can be extracted from each shot gather so that numerous 1D S-wave

profiles along a survey line can generated. A two-dimensional vertical section of S-wave velocity is finally generated by any contour drawing software.

The amplitude of earthquake ground motion can be increased or decreased by both the properties and configuration of the near surface material through which seismic waves propagates. Those properties which most affect the level of ground motion are impedance and absorption. As (Aki and Richard 1980) point out, impedance is the resistance to particle (rock or soil) motion. As waves propagate upward to the surface of the earth through different layers of rocks, they generally encounter a decrease in acoustic impedance, and therefore resistance to wave motion decreases. To preserve energy the amplitude of the wave increases, and hence amplification occurs (Mammo, 2005).

The simultaneous recording of 12 or more receivers at short (1-2m) to long (50-100m) distances from an impulsive or vibratory source gives statistical redundancy to measurements of phase velocities. Multichannel data displays in a time variable frequency format also allow identification and elimination of non fundamental mode Rayleigh waves and other coherent noise during the analysis process. The field setup, acquisition process and analysis procedure are explained below in detail.

6.6.2 Field Investigation at Kuriftu site

MASW survey in linear array was conducted in Debrezeit at one location by 24 geophones for estimating 2D Velocity profiles. Figure 6.9 shows the base map of the field survey done by linear array for nine spread. In this survey spacing between the geophones is 10 meters. All the geophones are connected to the seismograph and the source is applied at the offset of -30m and with 60m increment from the first source to end shot. A trigger cable is used to initialize the recording by connecting directly with sledge hammer and the seismograph. The generated Rayleigh wave data are recorded at all shot points on an average of 10 to 15 stacks.

6.6.2.1 Data Acquisition

The 24 channel signal enhancement seismograph is used for acquisition of the seismic data. Geophones of 28 Hz are used and they are connected to the seismograph with connecting cables as shown in Fig. 6.10. The field procedure used to acquire the seismic data was an inline spread in which the source and 24 28-Hz vertical geophones were placed in a straight line. The energy

source was activated at 7 different places along the spread. To generate shear wave the plate was struck vertically in the direction perpendicular to the spread.

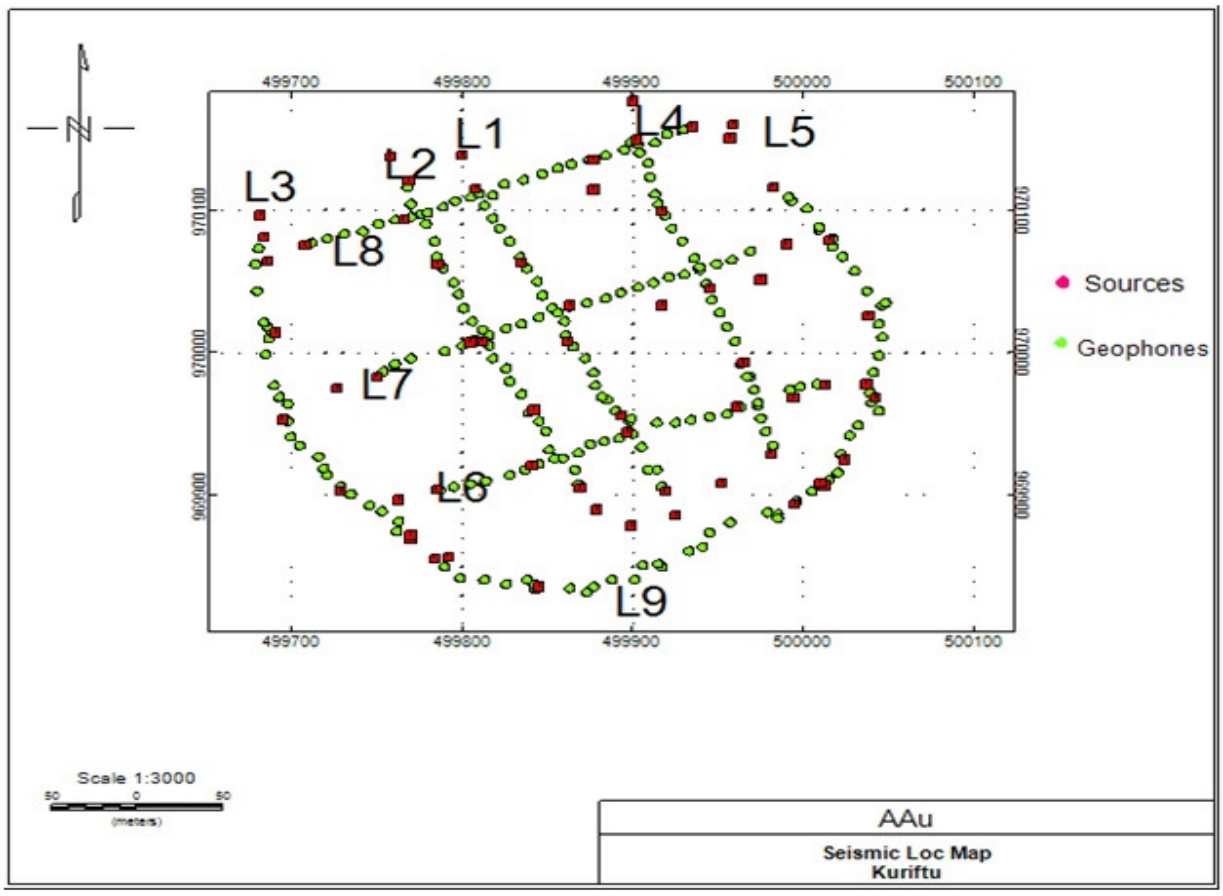

Figure 6. 9 Base map of the study site (Profile L1 to L9).The red symbols are shot(recording) points and the greens are geophones.

A sledge hammer of 12 kg weight manually impacted on 150cm^2 Iron plate is used for creating the energy. Fixed receiver configuration is used and the source is placed between each one forth the spread length and at both ends of the spread line. Around 20 shots are created at each test location (source location) for the present study. Data for each shot is digitally recorded and saved in the equipment McSEIS-SX 24 Seismogram.

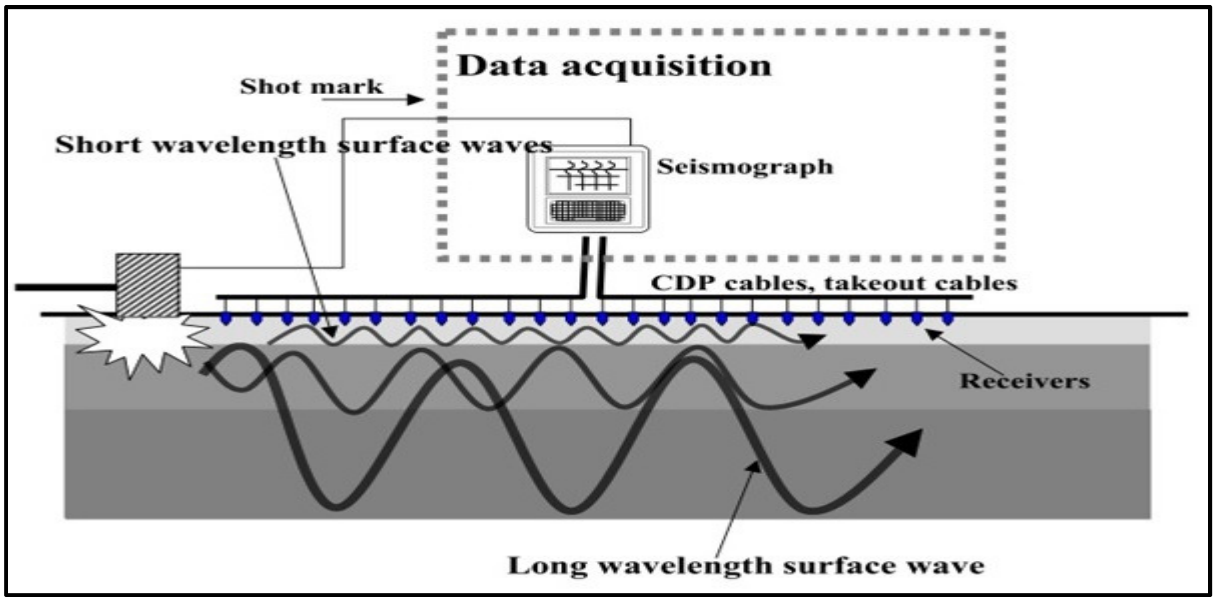

Figure 6. 10 Schematic diagram of data acquisition process.

The following are the recording parameters (Table 6.3) during the acquisition process.

Table 6. 2 Seismic data recording parameters

Recording system:	McSEIS-SX 24
Sampling Interval:	200 μs
Memory:	2kb
Recording	
Format:	SEG-2
Pre trigger:	OFF
Stack mode:	Summation
Geophones:	24 geophones of 28 Hz frequency
Geophones array:	Linear with geophone spacing of 10m
Source:	12kg sledge hammer on 150cm^2 metal plate
Source array:	Source is shifted with 60m interval
Offset distance:	30m

6.6.2.2 Data Analysis and Presentation

SeisImager/SW software has three more software's i.e., Pickwin, WaveEq and GeoPlot. Figure 6.11 gives the flowchart with the detailed steps involved in the analysis of surface wave data for getting two dimensional shear wave velocity models.

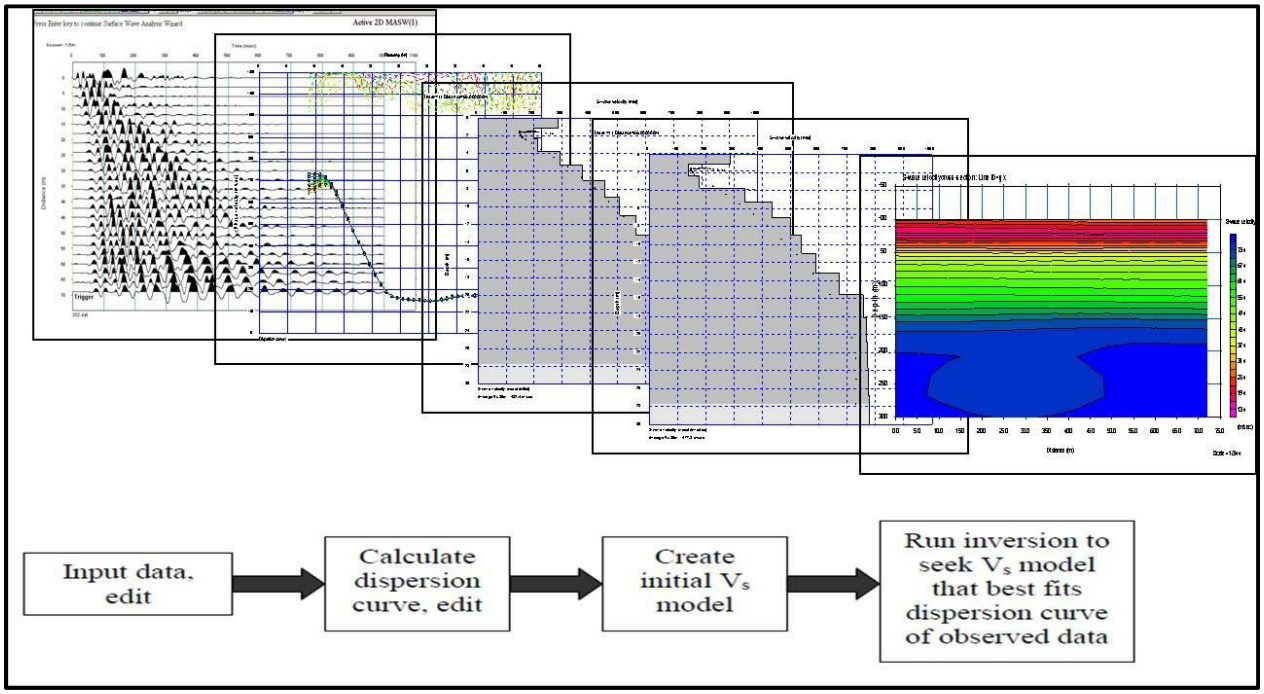

Figure 6. 11 General steps of the 1D/2D Multichannel Analysis of Surface Waves (MASW) (Geometrics, 2006).

An initial velocity model should be defined such that Vs at a depth Z_f is 1.09 times the measured phase velocity C_f at the frequency where wavelength λ_f satisfies the relationship

$$\mathbf{Z_f = a\ \lambda_f} \qquad 6.14$$

Where **a** is a coefficient that changes with frequency slightly and is based on extensive modeling. Finally 2D velocity model can be generated in Geoplot. According to NEHRP guidelines, Vs_{30} for a layered structure is determined for site classification.

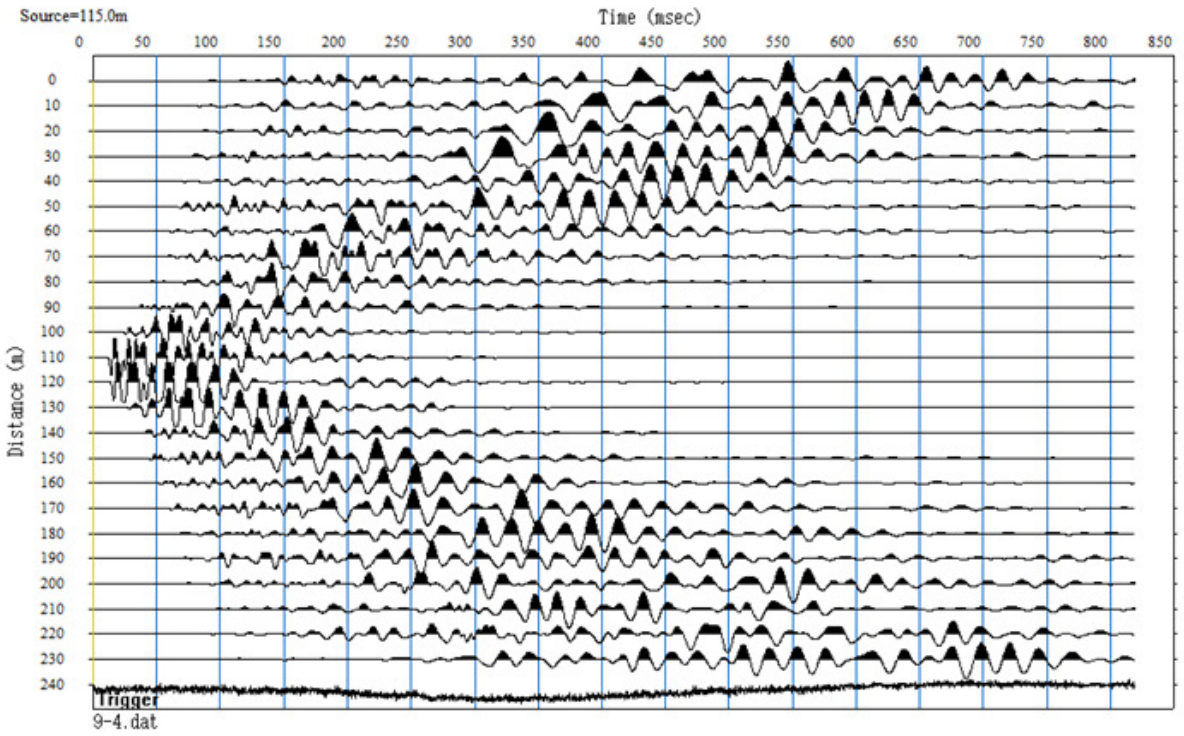

Figure 6. 12 Multichannel Records of the wave form at Kuriftu KaleHiwot church with Source at Mid Point of the Survey Length for spread 9.

The first step in the analysis is making the file list in which all waveform files and source receiver configuration are mentioned and then cross correlation CMP gather is calculated. Dispersion curves are calculated by converting it into frequency domain and then checked. Generation of a dispersion curve is one of the most critical steps for generating an accurate shear wave velocity profile. Dispersion curves are generally displayed as phase velocity versus frequency. This relation can be established by calculating the phase velocity from the linear slope of each component of the swept frequency record. Figure 6.13 and figure 6.14 shows the phase velocity curves of profile 9 and profile 5. The 2D shear wave velocity profiles are calculated using non linear least square method using the dispersion data.

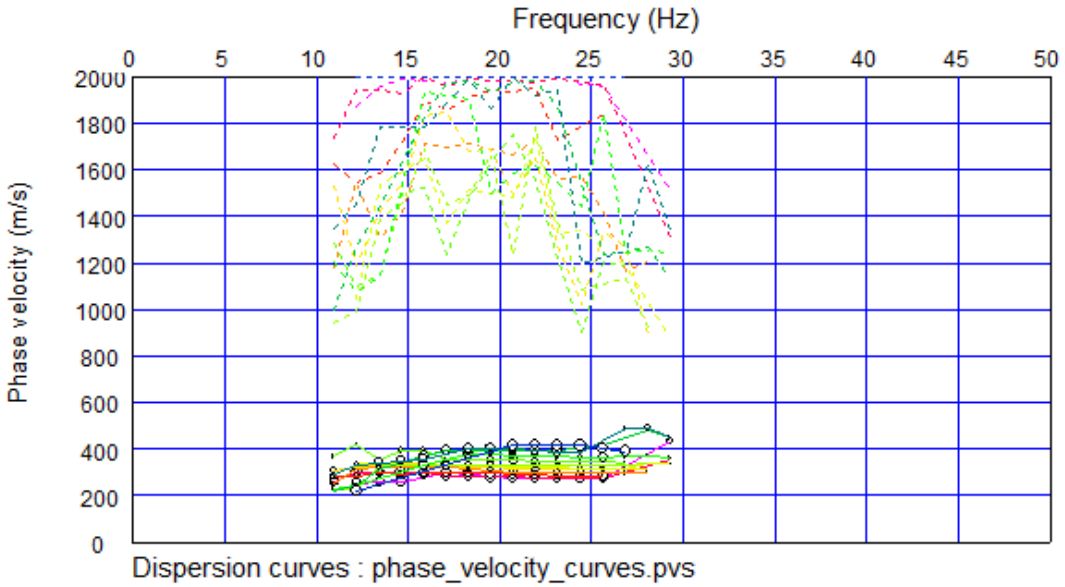

Figure 6. 13 Dispersion Curves for profile 9.

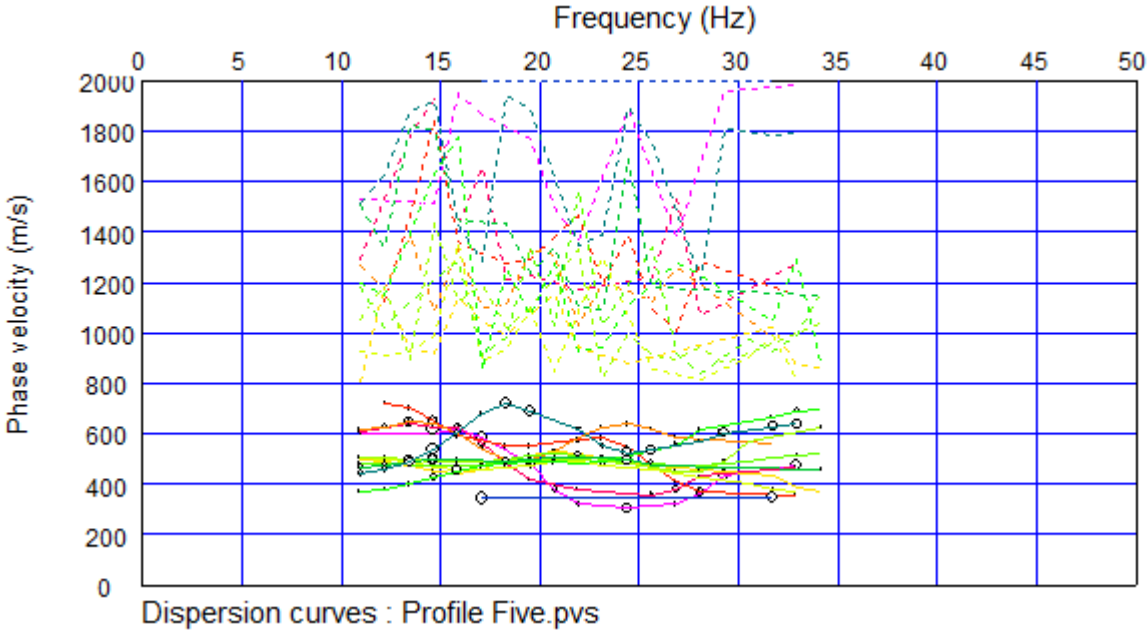

Figure 6. 14 Dispersion Curves for profile 5.

A total of more than 63 shots of surface wave data were acquired along nine lines, five lines in the north-west direction and four in the north-east direction inside Kuriftu Kale Hiwot Church. Surface wave profiling using the MASW linear array method will provide a non destructive,

quick and accurate shallow subsurface image of the shear wave velocities. Here the shear wave velocity section for the site with varying soil thickness is shown below. Figure 6.15 and 6.16 gives the 2D S-wave velocity section of profile 6, 7 and 8 and profile 1, 4 and 9 respectively. The average thickness of top soil in the Debrezeit area varies from 0 to 14m.

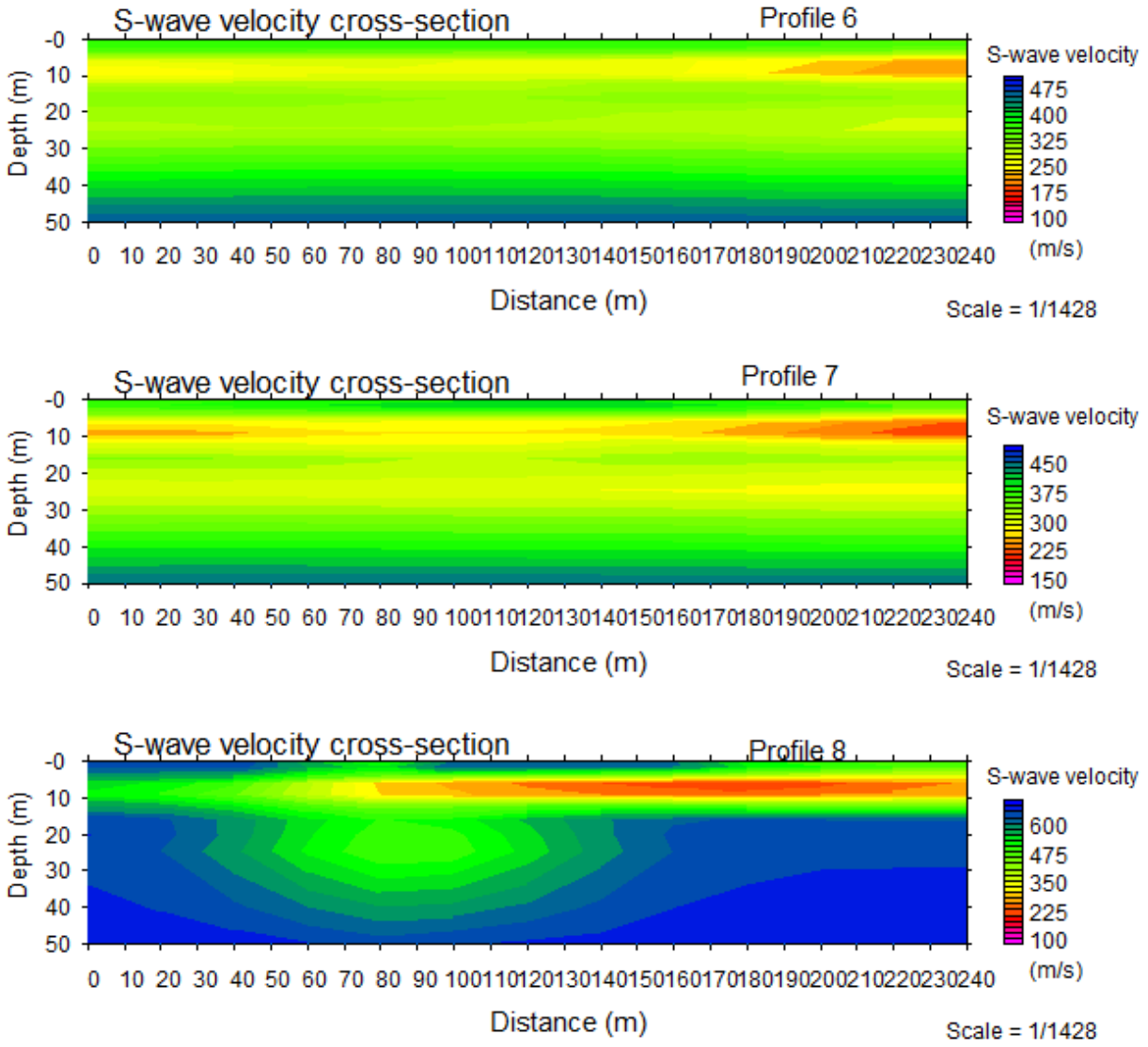

Figure 6. 15 Shows S-wave cross-section of Profile 6, Profile 7 and Profile 8.

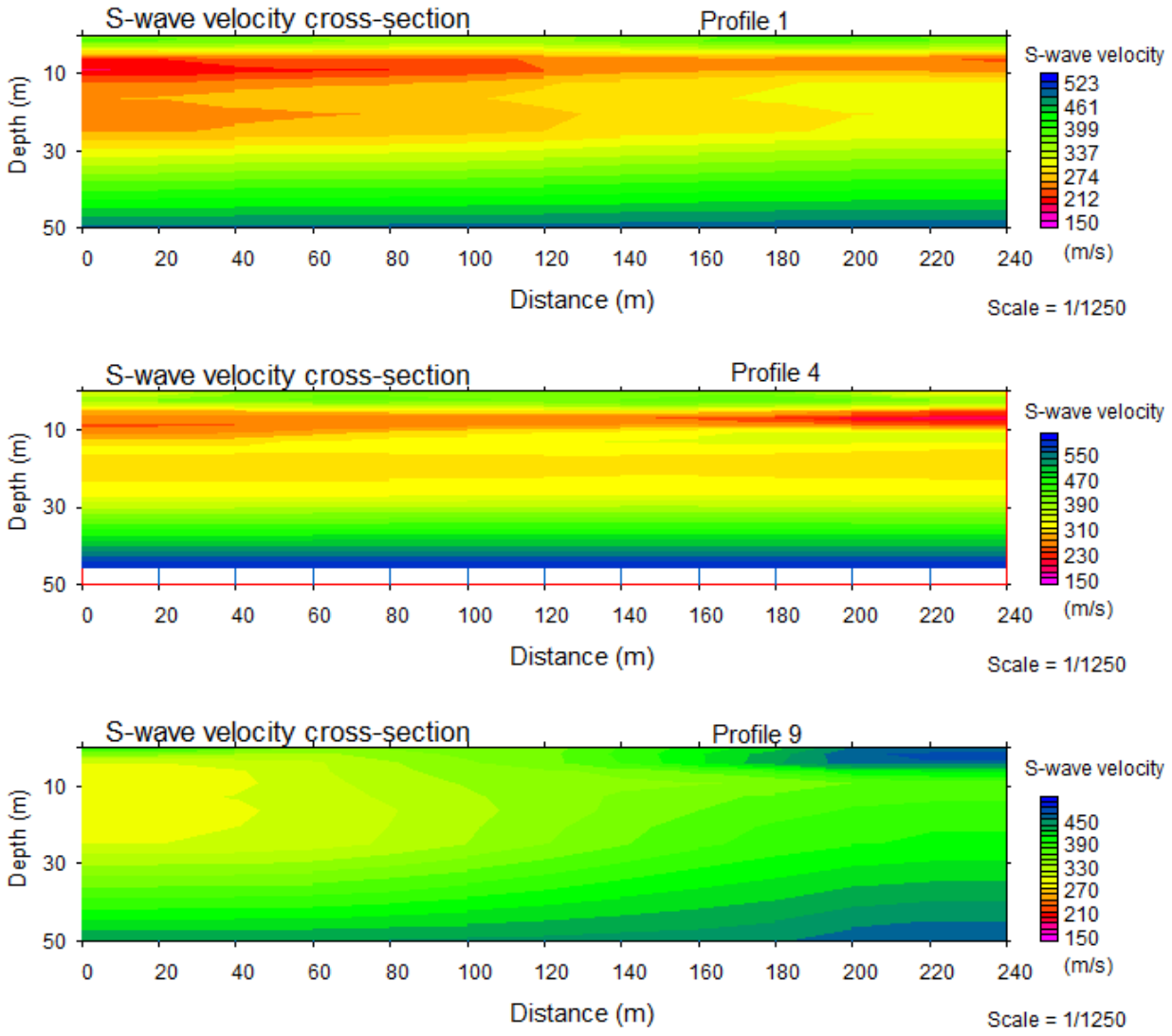

Figure 6.16 1Shows S-wave cross-section of Profile 1, Profile 4 and Profile 9.

At Kuriftu site the mean Vs30 value of 360m/s were found this can be classified as soil class C according to NEHRP criteria. From NEHRP recommendation, the soils with the lower shear wave velocity values, or the NEHRP soil class letter farther from A (Appendix X), will experience more earthquake ground shaking than bedrocks due to the wave-amplifying properties of the soil. This means that most part of city will more or less experience soil amplification from earthquake ground motion.

CHAPTER SEVEN

7 Hazard Curve Calculation

7.1 Introduction

Once ground motion estimates have been computed and characterized by distribution functions, the final seismic hazard can be determined. This final step determines how often a specified level of ground motion will be exceeded at the site of interest. This specified level can be the peak ground acceleration or any ground motion parameter (e.g. duration, displacement). Taking the form of an annual rate of exceedance or a return period, the resulting hazard consists of hazard contributions from each independently defined source.

By using the total probability theorem, the probability of exceeding a certain level of ground motion x at a given site can be written as:

$$p = P(Y \geq y) = \iiint P(y \geq y | m, r, \varepsilon) f_M(m) f_R(r) f_\varepsilon(\varepsilon) dm dr d\varepsilon \qquad 7.1$$

Where, m is the earthquake magnitude, r the source-to-site distance and $\mathcal{E}$ the number of standard deviations of the ground motion model to be considered in the integration. $f_M(m)$, $f_R(r)$ and $f_\varepsilon(\mathcal{E})$ denote the probability density functions of the magnitude, of the distance and of the error of attenuation equation respectively.

Equation (7.1) provides the probability of exceedance a certain level of ground motion at a site due to a given source. Under the hypothesis of a Poisson earthquake recurrence model, the "critical" events are the seismic events that cause $Y > y$. By multiplying this probability by the rate of occurrence of such, the annual rate (υ_y) at which the level y can be exceeded is found (with the assumption of the independence between the time of occurrence and magnitude of the earthquakes):

$$\upsilon_y = \upsilon P(Y > y) \qquad 7.2$$

Summing over all the I possible sources, the annual rate of exceeding a level y is:

$$\upsilon_{tot} = \sum_{i=1}^{I} \upsilon_{yi} = \sum \upsilon_i P_i(Y > y) \qquad 7.3$$

Finally, using the Poissonian assumption, the probability of exceeding any ground motion level in the next T years [$P(Y > y; T)$] is:

$$P_{Poiss} = 1 - e^{-\upsilon_{tot} T} \quad 7.4$$

and the return period is its reciprocal:

$$RP(y) = \frac{1}{P(Y > y, T)} \quad 7.5$$

Equation (7.4), normally referred to as "hazard curve", gives the annual probability of exceedance of different values of a selected ground motion parameter. The PSHA procedure computes the mean annual rate of exceedance based on the aggregate risk from potential earthquakes and sources. It may be useful sometimes to estimate the most likely earthquake magnitude and the most likely source-to-site distance in order, for example, to select existing ground motion records for response analyses. This process is called disaggregation and gives as result the most likely ($M;R$) case for a certain site and return period.

7.2 Hazard Curve Computation using CRISIS2012 Computer program

CRISIS2012 provides a user-friendly environment to compute seismic hazard. The hazard is computed using a probabilistic model that considers the earthquake rates of occurrence, ground motion attenuation characteristics and geographical distribution of earthquakes. Earthquake occurrence is assumed to follow a Poisson process, and two types of occurrence model are accepted: truncated Gutenberg-Richter distribution and characteristic earthquake model, as formulated by (Jara and Rosenblueth 1988). Also, the code accommodates uncertainty in the seismicity model parameters (b-value and maximum magnitude). The sources can be described as area sources, faults and point sources. Moreover the code provides some built-in Ground Motion Prediction Equations (GMPE), as well as the possibility of defining new models through tables. The results are given in terms of exceedance curves, uniform hazard spectra and disaggregation plots (CRISIS2012 manual).

In order to compute seismic hazard, the territory under study is first divided into seismic sources according to geotectonic considerations; in most cases, it is assumed that, within a seismic source, an independent earthquake-occurrence process is taking place. For each seismic source, earthquake occurrence probabilities are estimated by means of statistical analysis of earthquake catalogs.

In the more general case, earthquake occurrence probabilities must stipulate the probability of having *s* events (*s*=0, 1, …, *Ns*) of magnitude M_i in the following T_j years at a given source *k*. We will denote these probabilities as $P_k(s,M_i,T_j)$; they completely characterize the seismicity of source *k*.

Seismic hazard produced by an earthquake of magnitude M_i at a single point source, say the k-th, and for the next T_j years, can be computed as:

$$\Pr\left(A \geq a \mid M_i, T_j, k\right) = 1 - \sum_{s=0}^{Ns} P_k\left(s, M_i, T_j\right)\left[1 - P_r\left(A \geq a \mid M_i, R_k\right)\right]^s \qquad 7.6$$

Where $\Pr(A \geq a \mid M_i, R_k)$ is the probability that intensity *a* is exceeded given that an earthquake of magnitude *Mi* took place at source *k*, that is separated from the site of interest by a distance *Rk*. Please note that this probability depend only on magnitude and source-to-site distance, and it is normally computed giving a probabilistic interpretation to intensities predicted by ground motion prediction models or attenuation relations. We also note that implicitly in equation (7.6) is the assumption that exceedances of intensity values at source *k* given that an earthquake of magnitude M_i occurred are independent from each other. This is the reason why the non-exceedance probability of *a* given that *s* events of magnitude M_i took place at source *k* can be computed as $[1 - \Pr(A \geq a \mid M_i, R_k)]^s$.

Seismic hazard contained in equation 7.6 is more easily expressed in terms of non-exceedance probabilities:

$$\Pr\left(A \leq a \middle| M_i, T_j, k\right) = \sum_{s=0}^{Ns} P_k\left(s, M_i, T_j\right)\left[\Pr\left(A \leq a \middle| M_i, R_k\right)\right]^s \qquad 7.7$$

Equation 7.7 gives the non-exceedance probability of intensity value *a* given that only earthquakes of magnitude M_i took place. The non-exceedance probability of *a* associated to the occurrence of earthquakes of all magnitudes at source *k* in the next T_j years can be computed as:

$$\Pr\left(A \leq a \middle| T_j, k\right) = \prod_{i=1}^{Nm} \Pr\left(A \leq a \middle| M_i, T_j, k\right) \qquad 7.8$$

Where *Nm* is the number of magnitude bins into which the earthquake occurrence process has been discretized. Again, we have used the independence hypothesis among earthquakes of all magnitudes.

But seismic sources are usually points, lines, areas or volumes, so a spatial integration process must be carried out to account for all possible focal locations. We will assume that the spatial integration process leads to *N* sources. So finally, assuming that earthquake occurrences at different sources are independent from each other, we obtain that the non-exceedance probability of intensity *a* in the next *Tj* years due to earthquakes of all magnitudes located at all sources, can be computed with

$$\Pr\left(A \le a \middle| T_j\right) = \prod_{k=1}^{N} \Pr\left(A \le a \middle| T_j, k\right) \tag{7.9}$$

$$\Pr\left(A \le a \middle| T_j\right) = \prod_{k=1}^{N} \prod_{i=1}^{Nm} \Pr\left(A \le a \middle| M_i, T_j, k\right) \tag{7.10}$$

$$\Pr\left(A \le a \middle| T_j\right) = \prod_{k=1}^{N} \prod_{i=1}^{Nm} \sum_{s=0}^{Ns} P_k\left(s, M_i, T_j\right)\left[\Pr\left(A \le a \middle| M_i, R_k\right)\right]^s \tag{7.11}$$

Finally,

$$\Pr\left(A > a \middle| T_j\right) = 1 - \prod_{k=1}^{N} \prod_{i=1}^{Nm} \sum_{s=1}^{Ns} P_k\left(s, M_i, T_j\right)\left[\Pr\left(A \le a \middle| M_i, R_k\right)\right]^s \tag{7.12}$$

Equation 7.12 is the one used by CRISIS to compute seismic hazard for situations in which the sources are spatially distributed (k =1,…,N), there are earthquakes of various magnitudes (M_i , i=1,…Nm) and the earthquake occurrence probabilities in known time frames *Tj* at source *k* are given by $P_k(s,Mi,Tj)$, that is, the probability of having *s* events of magnitude M_i in the next *Tj* years at source *k*.

The equations presented here are, in general, applicable to non-Poisson occurrence process. But they are also applicable to the Poisson process. Let us see what results we obtain if we assume that the occurrence process is Poissonian.

Let us assume that at all sources a Poisson occurrence process is taking place for earthquakes of all magnitudes. Under this assumption, $P_k(s,M_i,T_j)$ takes the form of, precisely, a Poisson probability distribution:

$$P_k\left(s, M_i, T_j\right) = \frac{\left[\Delta\lambda_k\left(M_i\right)T_j\right]^s \exp\left[-\Delta\lambda_k\left(M_i\right)T_j\right]}{s!}, s \geq 0 \qquad 7.13$$

Where, $Dl_k(M_i)$ is the number of earthquakes of magnitude *Mi* that, per unit time, take place at source *k*. In other words, this quantity is the conventional exceedance rate of earthquakes in the range of magnitudes represented by *Mi*, that is,

$$\Delta\lambda_k\left(M_i\right) = \lambda_k\left(M_i - \Delta M/2\right) - \lambda_k\left(M_i + \Delta M/2\right) \qquad 7.14$$

Replacing equation 7.13 in equation 7.8 we obtain:

$$\Pr\left(A \leq a \middle| M_i, T_j, k\right) = \sum_{s=0}^{\infty} \frac{\left[\Delta\lambda_k\left(M_i\right)T_j\right]^s \exp\left[-\Delta\lambda_k\left(M_i\right)T_j\right]}{s!}\left[\Pr\left(A \leq a \middle| M_i, R_k\right)\right]^s \qquad 7.15$$

Note that now the sum extends to infinity since, in the Poisson process, the possible range of values of s is 0 to infinity. The sum in equation 7.15 has analytical solution:

$$\Pr\left(A \leq a \middle| M_i, T_j, k\right) = \exp\left\{-\Delta\lambda_k\left(M_i\right)T_j\left[1 - \Pr\left(A \leq a \middle| M_i, R_k\right)\right]\right\} \qquad 7.16$$

$$\Pr\left(A \leq a \middle| M_i, T_j, k\right) = \exp\left\{-\Delta\lambda_k\left(M_i\right)T_j \Pr\left(A \geq a \middle| M_i, R_k\right)\right\} \qquad 7.17$$

Hence,from equation 7.12 we get that

$$\Pr\left(A > a \middle| T_j\right) = 1 - \prod_{k=1}^{N}\prod_{i=1}^{Nm} \exp\left\{-\Delta\lambda_k\left(M_i\right)T_j \Pr\left(A \geq a \middle| M_i, R_k\right)\right\} \qquad 7.18$$

$$\Pr\left(A > a \middle| T_j\right) = 1 - \exp\left\{-\sum_{k=1}^{N}\sum_{i=1}^{Nm} \Delta\lambda_k\left(M_i\right)T_j \Pr\left(A \geq a \middle| M_i, R_k\right)\right\} \qquad 7.19$$

But, under the Poisson assumption for the earthquake occurrences, the process of intensity exceedances is also a Poisson process, for which the exceedance probability of intensity *a* during the next *Tj* years would be given by:

$$\Pr\left(A > a \middle| T_j\right) = 1 - \exp\left\{-\upsilon(a) T_j\right\} \qquad 7.20$$

where n(*a*) is the exceedance rate of intensity *a*. Comparing equations 7.19 and 7.20 we obtain that

$$\upsilon(a) = \sum_{k=1}^{N} \sum_{i=1}^{Nm} \Delta\lambda_k(M_i) \Pr\left(A \geq a \middle| M_i, R_k\right) \qquad 7.21$$

Note that n(*a*), the well-known Poissonian intensity exceedance rate, does not depend anymore on *Tj*. In the limit, the inner sum of equation 7.21 can readily be recognized as the integral with respect to magnitude that is present in the conventional Esteva-Cornell approach to compute Poissonian seismic hazard. The outer sum in equation 7.21 is simply the aggregation of intensity exceedance rates due to all sources. In other words,

$$\upsilon(a) = \sum_{k=1}^{N} \sum_{i=1}^{Nm} \frac{\Delta\lambda_k(M_i)}{\Delta M} \Pr\left(A \geq a \middle| M_i, R_k\right) \Delta M \qquad 7.22$$

$$\upsilon(a) = \sum_{k=1}^{N} \int_M -\frac{d\lambda_k(M)}{dM} \Pr\left(A \geq a \middle| M, R_k\right) dM \qquad 7.23$$

Note that, due to the definition we used for $Dl_k(M_i)$ in equation 7.14, its sign changed when we converted it to its differential form. We have then shown that equation 7.12, derived for the general non-Poissonian case, is also valid for the Poissonian case, leading to the well-known Esteva-Cornell expression to compute seismic hazard.

7.3 Disaggregation Analysis

The hazard curves represent the combined effect of all earthquake magnitudes and distances on the probability of exceeding a certain level of ground motion at a site. From such curves, however, it is difficult to understand the controlling earthquake scenarios. A common practice is to break down the hazard into its contributions from different magnitude and distance bins, in order to highlight which event is governing the hazard (given a ground motion level). This

process is called "disaggregation". Although it has not been used in this thesis, the disaggregation is herein described for sake of completeness.

$$p = P(Y > y) = \sum_{j=1}^{N_M} \sum_{K=1}^{N_R} P\left(y > y \middle| M = m_j, R = r_k\right) f_M(m_j) f_R(r_k) \Delta m \Delta r \qquad 7.24$$

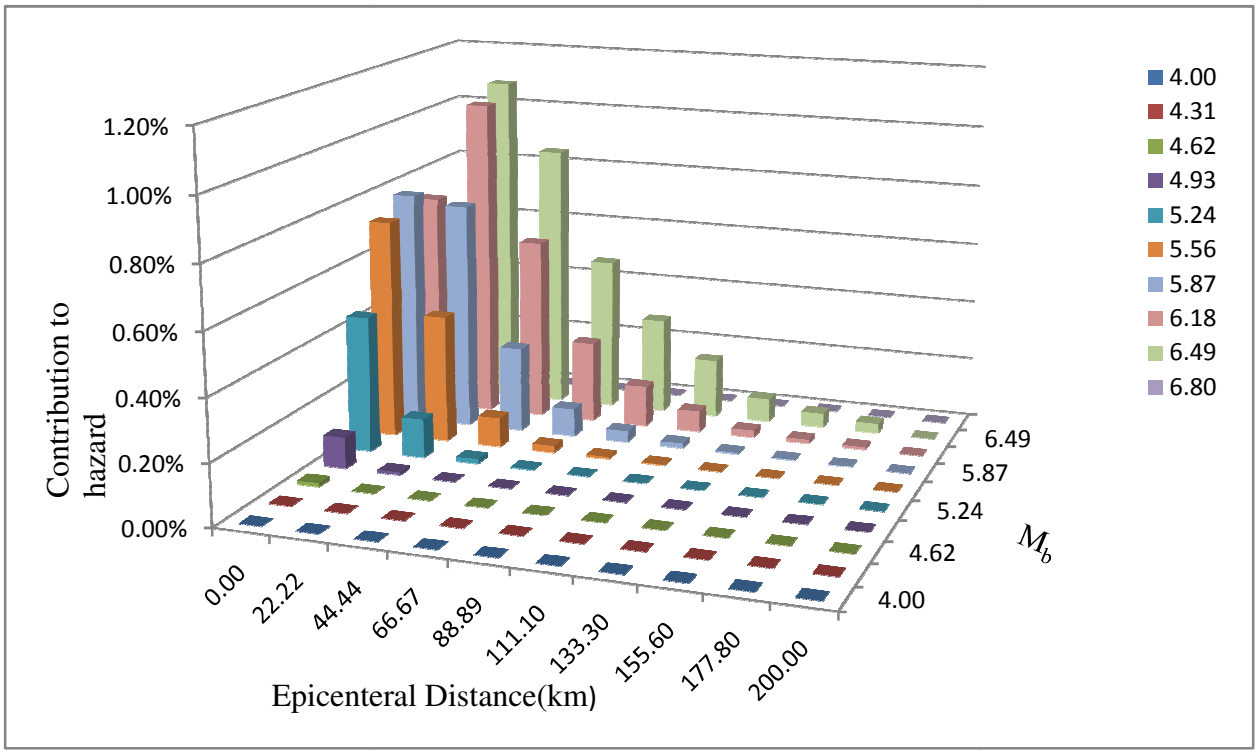

Figure 7. 1 Disaggregation analyses for Debrezeit area at three source zones.

Often, the output of a disaggregation analysis is not easy to interpret. Fig.7.1 Shows example of disaggregation analysis for Debrezeit city for different magnitude and epicenteral distance. The value in each cell is the probability that the intensity level of 0.045g is exceeded in 50 year if only earthquakes with magnitudes and distance within the cell's range are accounted for. The computations are carried out using seismotectonic model and ground motion prediction equation and the hazard is calculated for rock sites with site effect and *RP* = 475 years and at T=2sec. It is also worth noting that disaggregation results depend largely on the considered spectrum ordinate and return period. The contribution of the large magnitudes increases both with increasing return

periods and structural periods, since the larger the magnitude the higher is the energy at low frequencies.

7.4 Hazard Curve Evaluation for Debrezeit area

The rate of recurrence indicates the rate at which earthquake induce ground motions have occurred and probably will continue for sometimes in a given site. In practice, rates of recurrence can be expressed either; by giving the recurrence periods corresponding to a fixed set of amplitude or, by giving the maximum amplitudes corresponding to a fixed set of period. Knowledge of return period of the occurrence of destructive earthquake or ground motion is fundamental to the understanding of seismic hazard. Return period of a ground motion at a bed rock level at the grid site is computed based on equation 7.1 for various levels of PGA and intensity respectively and the result is presented in table 7.3:

The return period RP, and probability of exceedence PE are related as:

$$PE = \frac{1}{RP} \tag{7.25}$$

For the period concerned the time-independent poissonian probability distribution is often used to calculate the exceedance probability in certain years can be expressed:

$$P_i\left(PGA > a_i\right) = 1 - \exp\left(-r_i T\right) \tag{7.26}$$

7.5 Uniform hazard spectra

A common method of illustrating the seismic hazard results is through the "uniform hazard" (UH) spectra. First, the hazard at a suite of spectral periods is independently computed using response spectral attenuation relations in this case NGA model by (Campell and Bozognia 2008). Then, for a selected return period of 475 years, the ground motion for each spectral period is picked from the hazard curves. These ground motion values are then plotted at their respective spectral periods to generate the uniform hazard spectrum (Fig. 2.15 graphically shows this procedure). The term uniform is justified by the fact that all of its ordinates have the same probability of exceedance. However, since the ground motions are computed independently, the UH spectrum does not represent the spectrum of any single earthquake scenario. It is a common understanding that at low periods the hazard is mainly controlled by moderate magnitude

earthquakes at close distances to the site, while at longer periods the controlling events tend to become more and have larger magnitudes.

Table 7. 1 Exceedance probability for selected spectral periods.

Ground Motion(g)	Exceedance Probability T=0.010	T=0.050	T=0.100	T=0.200	T=0.500	T=1.000	T=1.500	T=2.000
0.01000	0.99961	0.99992	1.00000	1.00000	0.99994	0.97459	0.85968	0.67299
0.01668	0.98877	0.99671	0.99978	0.99998	0.99760	0.88270	0.65795	0.43331
0.02783	0.90080	0.95727	0.99373	0.99899	0.96888	0.67814	0.40654	0.22539
0.04642	0.64854	0.79034	0.93997	0.98113	0.83741	0.41357	0.20072	0.09649
0.07743	0.33617	0.49497	0.75605	0.87410	0.57075	0.19899	0.08167	0.03522
0.12916	0.12838	0.22823	0.46640	0.61764	0.29275	0.07848	0.02852	0.01118
0.21544	0.03779	0.07999	0.21576	0.32280	0.11765	0.02649	0.00872	0.00302
0.35938	0.00855	0.02171	0.07649	0.12715	0.03932	0.00777	0.00227	0.00065
0.59948	0.00140	0.00445	0.02097	0.03910	0.01124	0.00191	0.00047	0.00010
1.00000	0.00015	0.00065	0.00434	0.00939	0.00266	0.00036	0.00007	0.00001

Table 7. 2 UH Spectrum for selected spectral periods.

T(sec)	UH Spectrum
0.01	0.143
0.05	0.193
0.1	0.315
0.2	0.399
0.5	0.232
1	0.113
1.5	0.069
2	0.046

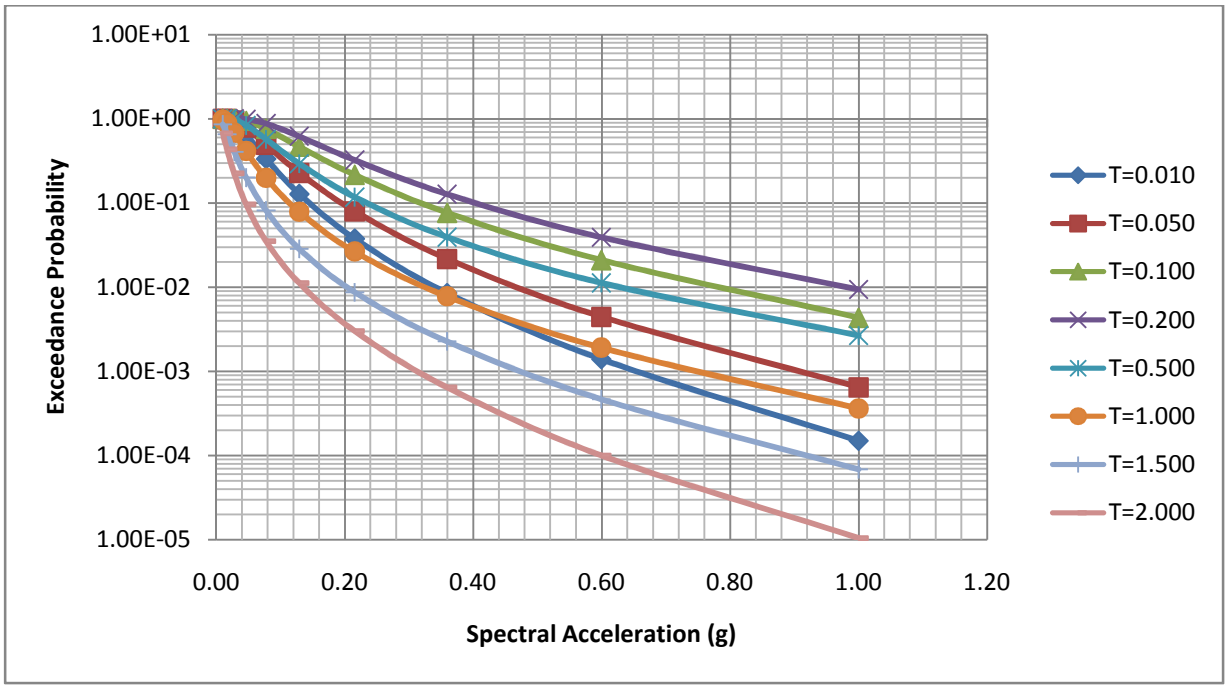

Figure 7. 2 Exceedance curves computed through a PSHA analysis at 8 vibration periods are displayed above, corresponds to an exceedance probability of 10% in the next 50 years and thus to a return period of 475 years.

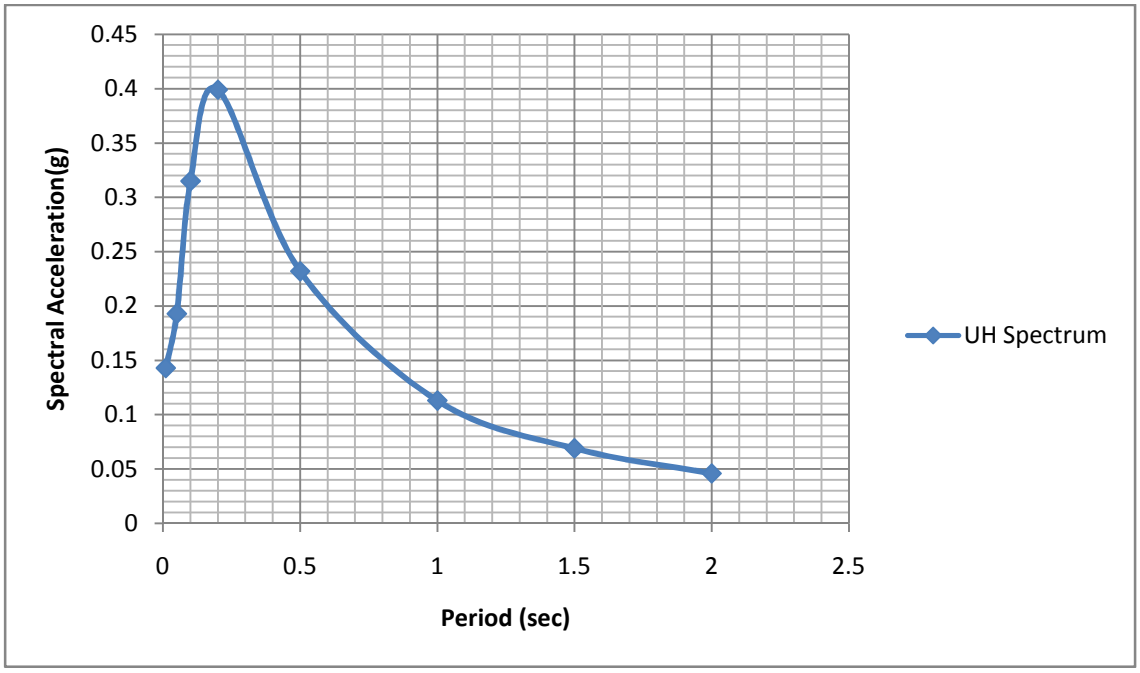

Figure 7. 3 Uniform Hazard Spectrum for 10% probability of exceedance in 50 years and RP=475 years.

Table 7. 3 Relation between intensity scales (MM), exceedance probability and return periods at different level of PGA at three selected location around Debrezeit area (site 1, site 2, site 3).

		site1		site2		site3	
PGA	I(MM)	EP	RP(Years)	EP	RP(Years)	EP	RP(Years)
0.02	IV	0.990	1	0.990	1	0.990	1
0.03	V	0.901	1	0.902	1	0.901	1
0.05	VI	0.634	2	0.635	2	0.635	2
0.08	VI	0.309	3	0.309	3	0.309	3
0.13	VIII	0.105	10	0.105	10	0.105	10
0.22	VIII	0.026	39	0.025	39	0.025	39
0.36	IX	0.0043	233	0.004	236	0.004	237
0.60	IX	0.00046	2182	0.00045	2234	0.00044	2256
1.00	X	0.00003	35172	0.00003	36715	0.00003	37400

Table 7. 4 Exceedance Probability in 50, 100, 250 and 500 years for PGA at 0.2 sec. at three locations around Debrezeit ((a) site1, (b) site 2 and (c) site 3) respectively.

(a)

	Exceedance probability			
Site:1	38.987	8.7970 kur7		
Ground Motion(g)	50 year	100 year	250 year	500 year
0.01	1.00E+00	1.00E+00	1.00E+00	1.00E+00
0.02	1.00E+00	1.00E+00	1.00E+00	1.00E+00
0.03	9.94E-01	1.00E+00	1.00E+00	1.00E+00
0.05	9.37E-01	9.96E-01	1.00E+00	1.00E+00
0.08	7.37E-01	9.31E-01	9.99E-01	1.00E+00
0.13	4.30E-01	6.75E-01	9.40E-01	9.96E-01
0.22	1.81E-01	3.30E-01	6.33E-01	8.65E-01
0.36	5.64E-02	1.10E-01	2.52E-01	4.40E-01
0.60	1.28E-02	2.55E-02	6.25E-02	1.21E-01
1.00	2.06E-03	4.11E-03	1.02E-02	2.04E-02

(b)

Exceedance probability				
Site:2	38.976	8.769	Kur4	
Ground Motion(g)	50 year	100 year	250 year	500 year
0.01	1.00E+00	1.00E+00	1.00E+00	1.00E+00
0.02	1.00E+00	1.00E+00	1.00E+00	1.00E+00
0.03	9.94E-01	1.00E+00	1.00E+00	1.00E+00
0.05	9.38E-01	9.96E-01	1.00E+00	1.00E+00
0.08	7.37E-01	9.31E-01	9.99E-01	1.00E+00
0.13	4.30E-01	6.75E-01	9.40E-01	9.96E-01
0.22	1.81E-01	3.30E-01	6.33E-01	8.65E-01
0.36	5.62E-02	1.09E-01	2.51E-01	4.39E-01
0.60	1.28E-02	2.53E-02	6.21E-02	1.20E-01
1.00	2.03E-03	4.06E-03	1.01E-02	2.02E-02

(c)

Exceedance probability				
Site:3	38.996	8.776	Kur5	
Ground Motion(g)	50 year	100 year	250 year	500 year
0.01	1.00E+00	1.00E+00	1.00E+00	1.00E+00
0.02	1.00E+00	1.00E+00	1.00E+00	1.00E+00
0.03	9.94E-01	1.00E+00	1.00E+00	1.00E+00
0.05	9.38E-01	9.96E-01	1.00E+00	1.00E+00
0.08	7.37E-01	9.31E-01	9.99E-01	1.00E+00
0.13	4.30E-01	6.75E-01	9.40E-01	9.96E-01
0.22	1.81E-01	3.30E-01	6.33E-01	8.65E-01
0.36	5.63E-02	1.09E-01	2.51E-01	4.40E-01
0.60	1.28E-02	2.54E-02	6.22E-02	1.21E-01
1.00	2.04E-03	4.08E-03	1.02E-02	2.02E-02

Table 7. 5 Exceedance Probability in 50, 100, 250 and 500 years for PGA at 0.1 sec. at three locations around Debrezeit ((d) site1, (e) site 2 and (f) site 3) repectively.

(d)

		Exceedance probability		
Site:1	38.987	8.797	Kur7	
Ground Motion(g)	50 year	100 year	250 year	500 year
0.01	1.00E+00	1.00E+00	1.00E+00	1.00E+00
0.02	1.00E+00	1.00E+00	1.00E+00	1.00E+00
0.03	9.94E-01	1.00E+00	1.00E+00	1.00E+00
0.05	9.37E-01	9.96E-01	1.00E+00	1.00E+00
0.08	7.37E-01	9.31E-01	9.99E-01	1.00E+00
0.13	4.30E-01	6.75E-01	9.40E-01	9.96E-01
0.22	1.81E-01	3.30E-01	6.33E-01	8.65E-01
0.36	5.64E-02	1.10E-01	2.52E-01	4.40E-01
0.60	1.28E-02	2.55E-02	6.25E-02	1.21E-01
1.00	2.06E-03	4.11E-03	1.02E-02	2.04E-02

(e)

		Exceedance probability		
Site:2	38.976	8.7690 Kur4	Kur4	
Ground Motion(g)	50 year	100 year	250 year	500 year
0.01	1.00E+00	1.00E+00	1.00E+00	1.00E+00
0.02	1.00E+00	1.00E+00	1.00E+00	1.00E+00
0.03	9.94E-01	1.00E+00	1.00E+00	1.00E+00
0.05	9.38E-01	9.96E-01	1.00E+00	1.00E+00
0.08	7.37E-01	9.31E-01	9.99E-01	1.00E+00
0.13	4.30E-01	6.75E-01	9.40E-01	9.96E-01
0.22	1.81E-01	3.30E-01	6.33E-01	8.65E-01
0.36	5.62E-02	1.09E-01	2.51E-01	4.39E-01
0.60	1.28E-02	2.53E-02	6.21E-02	1.20E-01
1.00	2.03E-03	4.06E-03	1.01E-02	2.02E-02

(f)

		Exceedance probability		
Site:3	38.996	8.776	Kur5	
Ground Motion(g)	50 year	100 year	250 year	500 year
0.01	1.00E+00	1.00E+00	1.00E+00	1.00E+00
0.02	1.00E+00	1.00E+00	1.00E+00	1.00E+00
0.03	9.94E-01	1.00E+00	1.00E+00	1.00E+00
0.05	9.38E-01	9.96E-01	1.00E+00	1.00E+00
0.08	7.37E-01	9.31E-01	9.99E-01	1.00E+00
0.13	4.30E-01	6.75E-01	9.40E-01	9.96E-01
0.22	1.81E-01	3.30E-01	6.33E-01	8.65E-01
0.36	5.63E-02	1.09E-01	2.51E-01	4.40E-01
0.60	1.28E-02	2.54E-02	6.22E-02	1.21E-01
1.00	2.04E-03	4.08E-03	1.02E-02	2.02E-02

Table 7. 6 Exceedance Probability in 50, 100, 250 and 500 years for PGA at 0.05 sec. at three locations around Debrezeit ((g) site1, (h) site 2 and (i) site 3) respectively.

(g)

		Exceedance probability		
Site:1	38.987	8.797	Kur7	
Ground Motion(g)	50 year	100 year	250 year	500 year
0.01	1.00E+00	1.00E+00	1.00E+00	1.00E+00
0.02	9.97E-01	1.00E+00	1.00E+00	1.00E+00
0.03	9.57E-01	9.98E-01	1.00E+00	1.00E+00
0.05	7.76E-01	9.50E-01	9.99E-01	1.00E+00
0.08	4.61E-01	7.10E-01	9.55E-01	9.98E-01
0.13	1.94E-01	3.50E-01	6.60E-01	8.84E-01
0.22	5.90E-02	1.14E-01	2.62E-01	4.56E-01
0.36	1.30E-02	2.58E-02	6.33E-02	1.23E-01
0.60	1.98E-03	3.96E-03	9.87E-03	1.96E-02
1.00	1.95E-04	3.91E-04	9.77E-04	1.95E-03

(h)

Site:2	Exceedance probability 38.976	8.769	Kur4	
Ground Motion(g)	50 year	100 year	250 year	500 year
0.01	1.00E+00	1.00E+00	1.00E+00	1.00E+00
0.02	9.97E-01	1.00E+00	1.00E+00	1.00E+00
0.03	9.57E-01	9.98E-01	1.00E+00	1.00E+00
0.05	7.77E-01	9.50E-01	9.99E-01	1.00E+00
0.08	4.62E-01	7.10E-01	9.55E-01	9.98E-01
0.13	1.94E-01	3.50E-01	6.59E-01	8.84E-01
0.22	5.87E-02	1.14E-01	2.61E-01	4.54E-01
0.36	1.29E-02	2.55E-02	6.27E-02	1.21E-01
0.60	1.94E-03	3.88E-03	9.67E-03	1.92E-02
1.00	1.88E-04	3.76E-04	9.41E-04	1.88E-03

(i)

Site:3	Exceedance probability 38.996	8.776	Kur5	
Ground Motion(g)	50 year	100 year	250 year	500 year
0.01	1.00E+00	1.00E+00	1.00E+00	1.00E+00
0.02	9.97E-01	1.00E+00	1.00E+00	1.00E+00
0.03	9.57E-01	9.98E-01	1.00E+00	1.00E+00
0.05	7.77E-01	9.50E-01	9.99E-01	1.00E+00
0.08	4.62E-01	7.11E-01	9.55E-01	9.98E-01
0.13	1.94E-01	3.50E-01	6.60E-01	8.84E-01
0.22	5.88E-02	1.14E-01	2.61E-01	4.54E-01
0.36	1.29E-02	2.56E-02	6.28E-02	1.22E-01
0.60	1.95E-03	3.90E-03	9.72E-03	1.94E-02
1.00	1.90E-04	3.80E-04	9.51E-04	1.90E-03

Table 7. 7 Exceedance Probability in 50 years for PGA at 0.05 sec. for MER and Escarpment seismic source zones.

	Exceedance Probability	
Ground Motion (g)	MER source zone	Escarpment source zone
0.01	0.9994	4.30E-2
0.02	0.9880	1.02E-2
0.03	0.9136	1.82E-3
0.05	0.7091	2.19E-4
0.08	0.4270	1.57E-5
0.13	0.1957	6.25E-7
0.22	0.0683	1.32E-8
0.36	0.0177	1.4E-10
0.60	0.0033	7.9E-13
1.00	0.0004	2.0E-15

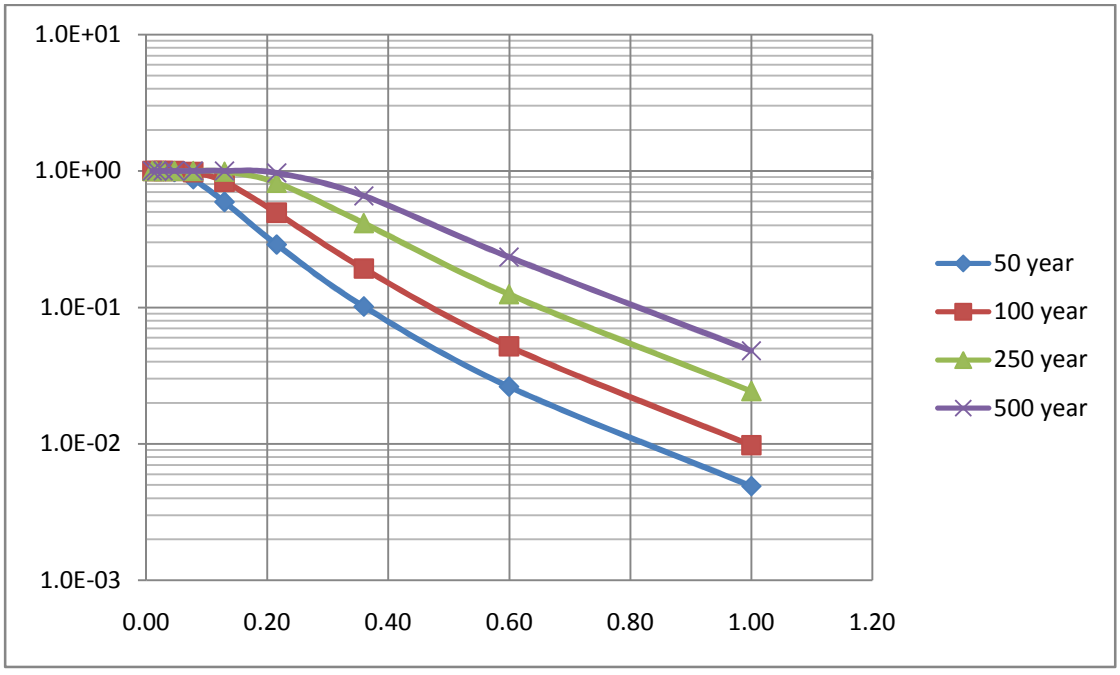

Figure 7. 4 Exceedance Probability in 50, 100, 250 and 500 years for PGA at 0.2 sec. at three locations around Debrezeit ((g) site1, (h) site 2 and (i) site 3) respectively.

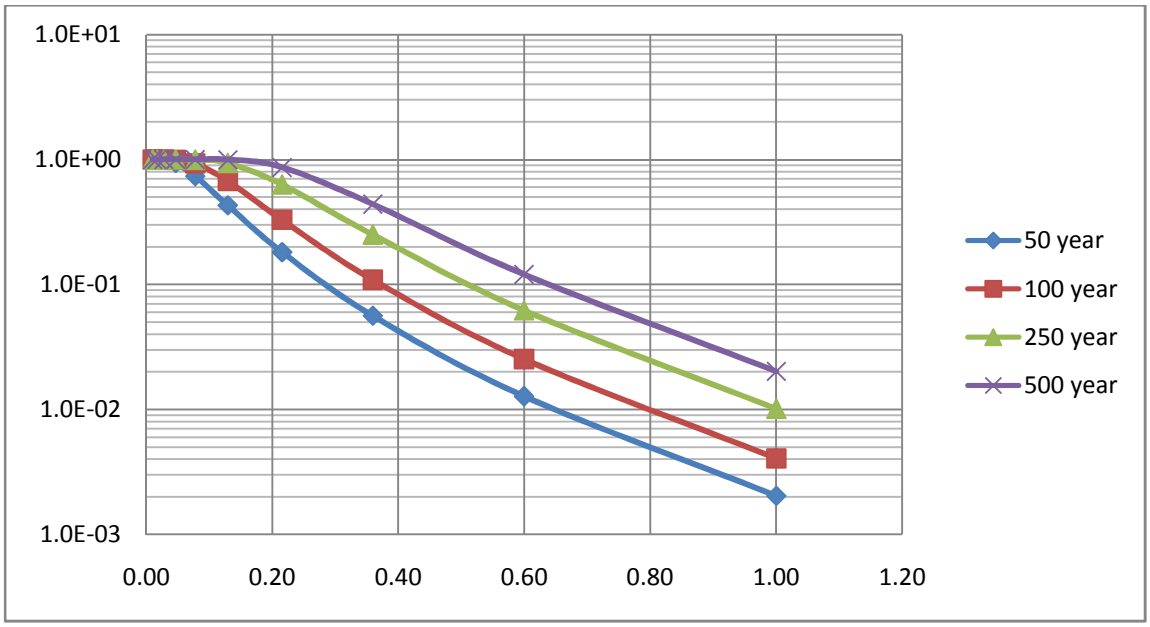

Figure 7. 5 Exceedance Probability in 50, 100, 250 and 500 years for PGA at 0.1 sec. at three locations around Debrezeit ((g) site1, (h) site 2 and (i) site 3) respectively.

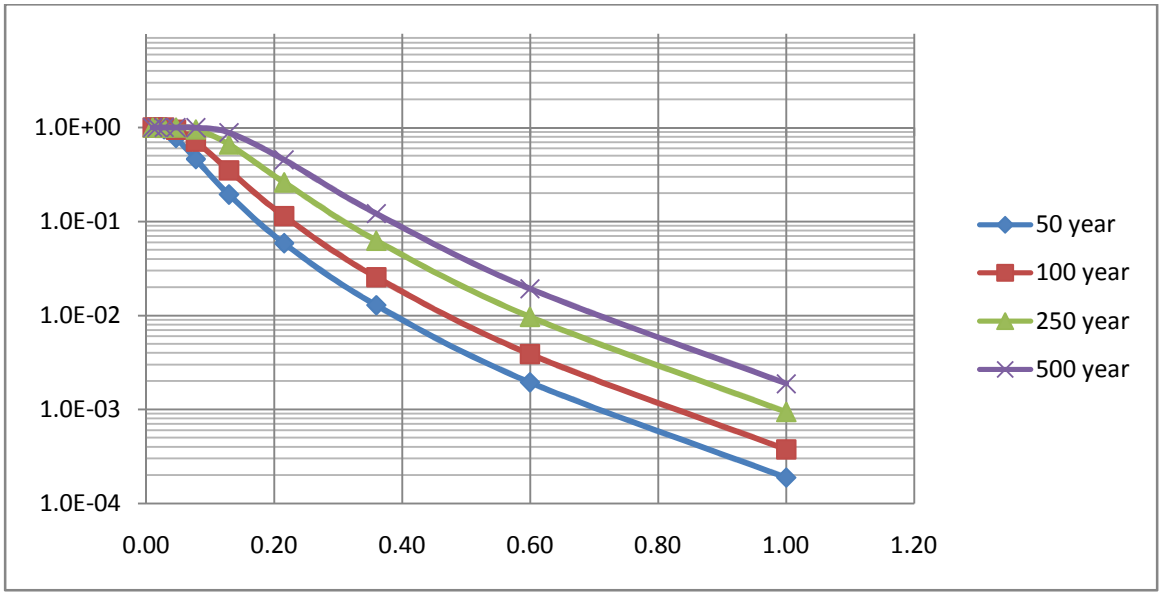

Figure 7. 6 Exceedance Probability in 50, 100, 250 and 500 years for PGA at 0.05 sec. at three locations around Debrezeit ((g) site1, (h) site 2 and (i) site 3) respectively.

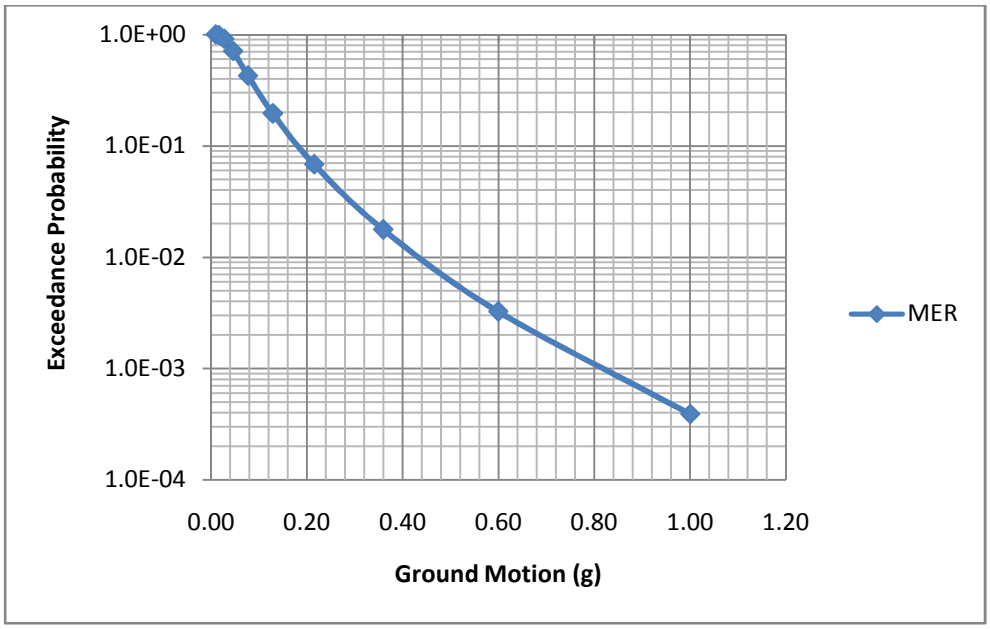

Figure 7. 7 Hazard curve in 50 years for PGA at 0.05 sec. for MER seismic source zones using NGA model by Campbell and Bozognia (2008).

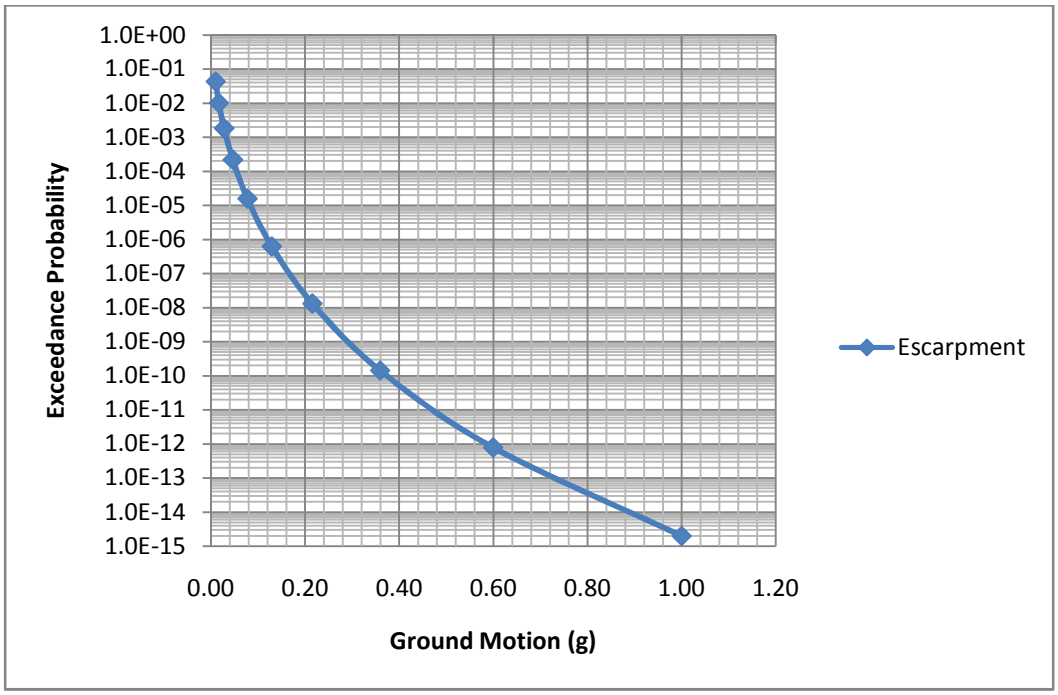

Figure 7. 8 Hazard curve in 50 years for PGA at 0.05 sec. for Escarpment seismic source zones using NGA model by (Campbell and Bozognia 2008).

7.6 Discussions

The primary output from a PSHA is a hazard curve showing the variation of a selected ground motion parameter, such as peak ground acceleration (PGA) or spectral acceleration (SA), against the probability of exceedance (or its reciprocal, return period). The probability of exceedance has been calculated for two seismogenic sources separately. For the purpose of the analysis a computer program CRISIS2012 has been used based on the methodology as detailed by Cornell (1968) and Kramer (1996). Figure 7.4 to 7.8 shows the variation of probability of exceedance with peak ground acceleration for three sites in Debrezeit at soil site and rock level and for the MER and Escarpment sources. This clearly highlights that the sources close to Debrezeit produce more hazard when compared to the source far away from Debrezeit. Even though PGA is used to characterize the ground motion, the spectral acceleration is generally used for design of engineering structures.

We have decided to estimate the ground motion parameters in 50 year time period, corresponding to the design lifetime for buildings and we have chosen 10% of exceedance that would lead to a return period of 475 years. We have incorporated the local site condition on the hazard computation therefore the results are valid for an ideal "bedrock" (Vs>800 m/s) and local site conditions (200<Vs30 <360). Furthermore during an earthquake the damage incurred by a structure is a function of its dynamic characteristics and the properties of the ground motion especially intensity duration and frequency content. The integration over all the grid points was carried out by running the CRISIS2012 computer package and the results are presented as follows below.

The 10% Exceedance probability in 50 years, for intensity 0.1g at a period of 0.2sec and 0.1sec are found to be 0.71 and 0.56 respectively. The exc. probability in 100 years will be 0.906 and 0.793 respectively for the area and at a period of 0.05sec the exc. Probability in 50 years became 0.29. Intensity(g) for exc. Probability of 0.02(2%) in 50 years at periods of 0.2sec, 0.1sec and 0.05sec are 0.652g,0.514g and 0.31g respectively.

Intensity(g) for exc. Probability of 0.02(2%) in 100 years at periods of 0.2sec, 0.1sec and 0.05sec are 0.802g, 0.641g and 0.384g respectively.

Intensity(g) for exc. Probability of 0.02(2%) in 250 years at periods of 0.2sec, 0.1sec and 0.05sec are 1g, 0.826g and 0.492g respectively.

Intensity(g) for exc. Probability of 0.05(5%) in 50 years at periods of 0.2sec, 0.1sec and 0.05sec are 0.47g, 0.37g and 0.23g respectively.

Intensity(g) for exc. Probability of 0.05(5%) in 100 years at periods of 0.2sec, 0.1sec and 0.05sec are 0.606g, 0.473g and 0.286g respectively.

Intensity(g) for exc. Probability of 0.05(5%) in 250 years at periods of 0.2sec, 0.1sec and 0.05sec are 0.798g, 0.638g and 0.383g respectively.

Intensity(g) for exc. Probability of 0.1(10%) in 50 years at periods of 0.2sec, 0.1sec and 0.05sec are 0.362g, 0.28g and 0.172g respectively.

Intensity(g) for exc. Probability of 0.1(10%) in 100 years at periods of 0.2sec, 0.1sec and 0.05sec are 0.464g, 0.371g and 0.225g respectively.

Intensity(g) for exc. Probability of 0.1(10%) in 250 years at periods of 0.2sec, 0.1sec and 0.05sec are 0.643g, 0.504g and 0.304g respectively.

Intensity(g) for exc. Probability of 0.1(10%) in 50 years at periods of 2sec, 1.5sec, 1sec and 0.5sec are 0.046g, 0.069g, 0.113g and 0.232g respectively.

PGA of 0.02890g, 0.02891g and 0.02893g are calculated for the three sites respectively at structural period of 0.1s corresponds to an exceedance probability of 99% in the next 50 year and the return period is 11 years.

A seismic hazard curve represents the values of annual rate of exceedance (or return period or probability of exceedance) within a certain design life against selected levels of ground-motion or response parameter (see Figure 7.1 to 7.8). The values of a hazard curve tell us whether a site or a region is of low, moderate or high seismic hazard and its slope may indicate if the larger earthquakes have relatively short or long recurrence intervals. It must be noted that the lower limit of acceleration perceptible to people is approximately 0.00lg and the level of acceleration taken as sufficient to produce damage to week construction is 0.lg. When the acceleration is between 0.lg and 0.2g most people will lose their balance and might even feel sick (Arnold and

Reitherman, 1982). Kebede and Asfaw (1996) has carried out the probabilistic seismic hazard analyzes to obtain hazard maps for Ethiopia and the neighboring countries using data of up to the time of their study. The hazard maps were produced for 0.01, 0.05 and 0.033 annual probabilities of exceedence and relatively low horizontal PGA values of 0.lg, 0.13g and 0.16g, respectively were found for the Ethiopian Rift system.

Gouin (1976) employed the extreme value method, Gumbel Type I, to produce the seismic zoning map for Ethiopia which was part of overall efforts to write a building code for the country. The hazard map was computed for 100 years return period with 0.9 probability of not being exceeded based on data up to 1974 and attenuation relation for western Northern America. The result he obtained for the Debrezeit was 0.05g inducing an intensity of VII in MM scale, (see appendix VI and VII). He has also predicated the Numerical values for amplitudes (earthquake intensities and ground acceleration) expected at important sites (capital cities, important towns, water reservoirs and dams) and hence the predicted value at Deberezeit for return periods of 50, 100, 200 and 300 years was 0.034g (corresponds to intensity in MM = VI), 0.066g (=VII), 0.127g (=VIII) and 0.19g (= VIII), respectively at a rock site.

The Ethiopians building code of standard (1995) that divides the country depending on local hazard in to four Seismic zone, assigns the effective peak ground acceleration (a_g) for reference return period of 100 years. On the basis of this categorization seismic zone 4 that covers the whole Main Ethiopian Rift system and possibly its margins has assigned the value of a_g= 0.03. The hazard level obtained in this study is higher than all the previous findings. The possible reason of the difference of the results of the previous studies and those mentioned above could be as a result of one or more of the following;

- The size of the area covered by earlier studies is wider and based on gross seismotectonic regionalization.
- The time interval considered in the previous works is only up to the time when the studies are conducted and hence, the recent events are not inclusive in it.
- It does not include site effect and there is also problem of appropriate attenuation model for the area.

CHAPTER EIGHT

8 Conclusion and Recommendations

8.1 Conclusion

The study area has varied topography and sites of alluvial formations. The area has an average top soil thickness of 0 to 14m and the average shear velocity at the top of 30m is found to be in the range of 200m/s to 360m/s. So, according to the NEHRP classification the site can be classified under soil class C. Problem of topography and local geology will further aggravate the situation of structures. Seismic hazards are much higher on unconsolidated soils and on major fault belts than on solid rock. The hazard level obtained from this study considers the area sources without considering fault sources but the amplification factor for the soil dynamic parameters are obtained by field investigation at one site. Because, in this study we found that the value of ground motion level is higher as compared to the ground motion value found in the previous study for the area. It is well known that secondary effects like collapse of structures are the main causes for the colossal loss of human lives in an earthquake. The collapse of non-dwelling structures such as dam, water tanks and chemical factories could also cause serious damages. For example location of large water tanks on hills down where the population is high is not a good choice. Town planners and designers in developing countries are facing the urgent task of providing shelter for growing urban population. On the other hand the requirement for seismic resistant structures imposes on the limited resource of these countries. When there is high problem of seismic risk such problems must be solved in an optimum way. The currently adopted trend towards high-rise buildings must ensure these structures are adequately protected from earthquakes.

8.2 Recommendations

Aware of the facts that:

The area is a region where economic development activities, very crucial to the nation, are extensively being undertaken and the high population density and production of the land justify investment on hazard mitigation, the following recommendations are given.

- The current Code of Buildings standards of the country should further be revised and be based on much more refined seismic micro-zoning.
- More accurate location of active fault zones that can generate destructive earthquakes in the area should be mapped to improve the definition of the areal source zones in the analyses of seismic hazard.
- With the detailed characterization of faults and geology of sites, site-specific seismic hazard analysis should be carried out for important structures.
- The better attenuation model of the country in general and the area of study in particular, that still adopted from other models with analogous crustal condition should be developed based on measurements of regional and local parameters and studies.
- The area must be divided into land use categories identifying residential quarters, general public utility services such as communications, water supplies, hospitals, schools and those buildings which when disturbed constitute a permanent public danger such as chemical plants, ammunition factories, etc
- There should be a trend of construction towards low rise buildings with reinforcement of the existing ones to resist earthquake damage.

References

Abrahamson, N.A. and J.J. Bommer (2005).Opinion Paper: Probability and Uncertainty in Seismic Hazard Analysis. Earthquake Spectra, **21**:1-5.

Abrahamson, N.A. and W.J. Silva. (1997). Empirical Response Spectral Attenuation Relations for Shallow Crustal Earthquakes. Seism. Res. Let., Vol. 68, No. 1.

Acton, G.D. and Stein,S., (1991). Block rotation and continental extension in Afar; a comparison to oceanic microplate systems. Tectonics, **10 (3)**:501-526.

Aki, K. (1972). Earthquake Mechanism. Tectonophysics,**13**, 423-446.

Aki, K., (1965). Maximum likelihood estimate of b in the formula logN=a-bM and its confidence limits. Bull, Earthq. Res. Inst, **43**: 237-239.

Atalay Ayele and Kulhanek, O., (1997). Spatial and Temporal variation of seismicity in the Horn of Africa 1960-1993. RASGJI 130, 805-810

Atalay Ayele, (1995). Earthquake Catalogue of the Horn of Africa for the period 1960-93, Seism. Dept., Uppsala Univ., Rept. 3.95, 1-32.

Atkinson, G.M. and D.M. Boore. (1997). Earthquake Ground Motion Prediction Equations for Eastern North America. Bull. Seism. Soc. Am., **93:** No.1, 314-331.

Barberi, F. and Varet, J., (1977). Volcanism of Afar small-scale tectonic implications. Bui. Geol. Soc. Amy **88**: 1251-1266

Bazzurro, P. and A.C. Cornell (1999). Disaggregation of Seismic Hazard. Bull. Seism. Soc. Am., **89:** No. 2, 501-520.

Berhe, S. M, (1986). Geologic and Geochronologic constraits on the evolution of the Red Sea-Gulf of Aden and Afar Depression. Journal of African Earth Science, **5:**101-117.

Boccalett, M., Tilahun Mammo, Bonini. M. and Abbebe, B., (1994). Seismotectonics of East African Rift System, evidence of active oblique rifting. Annales Tectonica, **8(2).**

Bolt, B.A. (1969). Duration of Strong Motion. Proc. of 4th Conf. EQ Eng., Santiago, Chile. pp. 1304-1315.

Bolt, B.A. and Abrahamson, N.A.(1982). New attenuation relations, peak and expected accelerations of strong ground motion. Bull Soc, Am, **72:** 2307 - 2321.

Bommer, J.J. and A. Martinez-Pereira (1999). The Effective Duration of Earthquake Strong Motion. J. Earthquake Eng. **3:** No. 2, 127-172.

Boore, D.M. and Joyner, W.B., (1991). Estimation of ground motion at deep-soil sites in eastern North America. Bull. Seismol. Soc .Am. **81:** (6), 2167-2185.

Boore, D.M., (1972). Note on the effect of topography on seismic SH waves. Bull.Seism.Soc. Am. **62:** 275-284.

Boore, D.M., and Joyner, W.B., (1997). Site amplifications for generic rock sites. Bull. Seism. Soc. Am. **87:** (2), 327-341.

Bullen K.E. and Bolt, B.A., (1985). An Introduction to the theory of seismology, 4th ed., Cambridge University press, Cambridge.

Campbell, K.W. and Bozorgnia, Y. (2007). Campbell-Bozorgnia NGA ground motion relations for the geometric mean horizontal component of peak and spectral ground motion parameters, PEER Report No. 2007/02, Pacific Earthquake Engineering Research Center, University of California, Berkeley, California, USA.

Campbell, K.W. and Bozorgnia, Y. (2008). NGA ground motion model for the geometric mean horizontal component of PGA, PGV, PGD and 5% damped linear elastic response spectra for periods ranging from 0.01 to 10 s. Earthquake Spectra, **24:** 139–171.

Cornell, C.A. (1968). Engineering Seismic Risk Analysis. Bull. Seism. Soc. Am.,**58:**1583-1606.

Cornell, C.A., and S. Winterstein (1988). Temporal and Magnitude Dependence in Earthquake Recurrence Models. Bull. Seism. Soc. Am., **78:** No. 4, 1522-1537.

Dixon, T. H., Stern, R. J. and Hussein, I. M., (1987). Control of Red sea rift geometry by Precambrian structures. Tectonics, **6:** 551-571.

Dolgoff, A. (1998). Physical Geology. City University of New York- New York city Technical College, Houghton Mifflin Company.

Duda, S.J., (1981). Earthquake Magnitude, Energy and Intensity. Institute of Geophysics, Hamburg University, Germany.

EM-DAT database, http://www.emdat.be/country_profile/index.html/ accessed on 6 May 2014.

ESCP- 1 (1983). Ministry of Works and Housing, Addis Ababa, Ethiopia, 1983.

Ethiopian Building Code of standard, (1995). Ministry of Works and Urban Development. Design of structures for earthquake resistance, ppl5, 108,110.

Ethiopian Central Statistical Agency, Ethiopian Census, first draft, 2007, Addis Ababa, Ethiopia. Summary and Statistical Report of the 2007 Population and Housing Census Results.

Fairhead, J. D. and Stuart, G. W., (1982). The seismicity of the East African rift system and comparison with other continental rifts. In: G. palmasson (edtor), continental and oceanic rifts. Geodynamics Ser., **8:** 41-61.

Fekadu Kebede (1996). Seismic Hazard Assessment for the Horn of Africa, Zede, Journal of Ethiopian Engineers and Architects, Addis Ababa, Ethiopia, 1996.

Fekadu Kebede(1997). Hazard Maps of Spectral Response Acceleration for Ethiopia, Proceedings of the Second Symposium of the Ethiopian Association of Seismology and Earthquake Engineering (EASEE), Addis Ababa, Ethiopia, April 4, 1997.

Fekadu Kebede, (1989). Seismotectonic studies of the East African rift system north of 12° to southern Red sea. Uppsala, Sweden, 5-75012.

Fekadu Kebede, and Kulhanek, O., (1989). Source parameters of selected earthquakes on the central and western margin of Afar. Tectonophysics, **170:** 243-357.

Fekadu Kebede, and Kulhanek, O., (1994). Spatial and temporal variations of values along the East African rift system and southern Red Sea, Planet Inter., **83:** 249-264.

Fekadu Kebede, and Lake Maryam Asfaw, (1996). Seismic Hazard Assessment for Ethiopia & the neighbouring countries. SINET: Ethiopia. J. Sci., **19(1):** 15-50.

Fekadu Kebede, Van Eck, T., (1997). Probabilistic seismic hazard assessment for the horn of Africa based on seismotectonic regionalization, Tectonophysics **270:** 221-237.

GEM-Catalogue, http://www.globalquakemodel.org/seismic-hazard/instrumental-catalogue/ accessed on 6 May 2014.

Gouin, P., (1976). Seismic Zoning in Ethiopia. Bull. Geophs . Obs. (Ethiopia), **17:** 1-46.

Gouin, Pierre, (1979). Earthquake History of Ethiopia and the Horn of Africa, International Development Research Center, Ottawa, Canada, IDRC- 118e, pp259.

Gutenberg, B. (1945). Amplitudes of P, PP, & S and Magnitudes of Shallow Earthquakes. Bull. Seism. Soc. Am., **35:** 57-69.

Gutenberg, B. (1945). Amplitudes of Surface Waves and Magnitudes of Shallow Earthquakes. Bull. Seism. Soc. Am., **35:** 3-12.

Gutenberg, B. and C.F. Richter (1956). Earthquake Magnitude, Intensity, Energy and Acceleration. Bull. Seism. Soc. Am., **46:** 105-145.

Hanks, T., (1979). b -values and square seismic source models implications for tectonic stress variations along active crustal fault zones and the estimation of high frequency strong ground motion J. Geophys. Res., **84:** 2235-2242.

Hanks, T.C. and H. Kanamori (1979). A Moment Magnitude Scale. J. Geophys. Res., **84:** 2345-2350.

Hempton, M.R., (1987). Constraints on Arabian plate motion and extensional history of the Red Sea, Tectonics, **6:** (6), 687 -705.

Henry, C. and S. Das (2001). Aftershock Zones of Large Shallow Earthquakes: Fault Dimensions, Aftershock Area Expansion and Scaling Relations. Geophys. J. Int., **147:** 272-293.

Hirn, A., Lepine, J.C. and Sapin, M., (1993). Triple Junction and ridge hotspots: earthquakes, faults, and volcanism in Afar, the Azores, and Iceland, J. Geophs. Res., **98:** (B7), 11995-12001.

Housner, G. W., and Jennings, P.C., (1982). Earthquake design criteria. Earthquake Engineering Research Institute of Technology. **140:** 324-357

Hunt, R.E., (1984). Geotechnical Engineering Investigation Manual. McGraw-Hill, New York.

IDNDR RADIUS Project, Addis Ababa Case Study, Final Report. Prepared by Addis Ababa RADIUS group, et al, September 1999.

Kanamori, H. and D.L. Anderson (1975). Theoretical Basis of Some Empirical Relations in Seismology. Bull. Seism. Soc. Am., **65:** No. 5, 1073-1095.

Kazmin, V., 1972a. Geology of Ethiopia, Geological Survey of Ethiopia.

Kiremidjian, A. and T. Anagnos (1984). Stochastic Time-Predictable Model for Earthquake Occurrences. Bull. Seism. Soc. Am., **74:** No.6, 2593-2611.

Kramer, S.L. (1996). Geotechnical Earthquake Engineering. New Jersey: Prentice Hill.

Lake Maryam Asfaw, (1981). The 28 July 1979 Earthquake in the southwest of Addis Abeba. SINET: Ethiop. J.Sc, **4:** 13-22.

Lake Maryam Asfaw, (1982). Site amplification in the Northern part of the East African Rift. Seism. Bull. Seism. Soc. Am., **72**: 327-329.

Lake Maryam Asfaw, (1990). Seismicity and Earthquake Risk in the Addis Ababa region. SINET, Ethiop. J. Sci. **13(1)**: 15-35.

Lake Maryam Asfaw, (1992). Seismic risk at site in the East African rift system. Tectonophysics, **209:** 301-309.

Lepine, L.C. and Hirn, A., (1992). Seismotectonics in the Republic of Djibout. Linking the Afar Depression and the Gulf of Aden, Tectonophysies, **209:** 65- 86.

Lomnitz, C., (1974). Global tectonics and earthquake risk. Geotectonics, Elsevier **5:** 370.

Maasha, N. and Molnar, P., (1972). Earthquake fault parameters and tectonics in Afica, J. Geophys. Res., **77 (29):** 5731-5743.

Mazzarini F., Tsegaye Abebe, Innocenti F., Manetti P., Pareschi M.T (1999). Geology of the Debrezeit area (Ethiopia). Acta Vulcanologica **11(1):** 131-142

McConnell, R. B., (1967). The East African rift system. Nature, **215:** 578-581.

McGuire, R.K. and Hanks, T.C., (1980). RMS accelerations and spectral amplitudes of strong ground motion during the San Fernando, California, earthquake, Bull. Seismol. Soc. Am., **70:** 1970-1919.

McGwire, R. (2004). Seismic Hazard and Risk Analysis. Earthquake Engineering Research Institute, MNO-10.

McGwire, R.K. (2001). Deterministic vs. Probabilistic Earthquake Hazards and Risks. Solid Dynamics and EQ Eng., **21:** 377-384.

Mogi, K., (1967). Regional variations in magnitude-frequency relation of Earthquakes, Bull. Earthq. Res. Inst., **45:** 67-86.

Mohr, P. A., (1967). The Ethiopian rift system. Bull. Geophys. Obs. (Ethiopia), **11:**

Mohr, P. A., (1970a). Plate tectonics of the Red sea and East Africa. Nature, **228:**

Mohr, P. A., (1970b). The Afar triple junction and sea-floor spreading. J. Geophys. Res., **75:** 7340-7352.

Mohr, P.A., (1968). Annular faulting in Ethiopian rift system Bull.Geophy. Obs. **12:**

Ogata, Y. and Yamashina, K., (1986). Unbiased estimate for b-values of magnitude frequency, J. Phys. Earth, **34:** 187-194.

Peterson, M., et al (2005). Time Independent and Time Dependent Seismic Hazard for State of CA. CA Seismic Hazard Paper, November 7.

Plummer, C., McGeary, D. and Carlson, D., (2003). Physical Geology, ninth edition. McGraw-Hill, pp 376-406.

Polykov, S.V.,(1985). Earthquake resistant structures. Mir publisher, Moscow, pp.374.

Power, M., Chiou, B., Abrahamson, N., Bozorgnia, Y., Shantz, T. and Roblee, C. (2008). An overview of the NGA project. Earthquake Spectra, **24:** 3–21.

Reid, H.F. (1911). The Elastic-Rebound Theory of Earthquakes. Berkley, CA. University of California Press.

Richter, C.F. (1935). An Instrumental Earthquake Magnitude Scale. Bull. Seism. Soc. Am., Rose School, Pavia, Italy, **25:** 1-32.

Rooney, T., Furman, T., Yirgu, G. & Ayelew, D., 2005. Structure of the ethiopian lithosphere: evidence from mantle Xenoliths, *Geochemica et Cosmochimica Acta*. **69,** 3889–3910,.

Sadigh, K., C.Y. Chang, J.A. Egan, F. Makdisi and R.R. Youngs (1997). Attenuation Relations for Shallow Crustal Earthquakes Based on California Strong Motion Data. Seism. Res. Letters. **68:** No. 1, 180-189.

Samuel Kinde Kassegne, "Proposed Considerations for Revision of EBCS-8:1995 for Conservative Seismic Zoning and Stringent Requirements for Torsionally Irregular Buildings", Published by EACE's Zede Research Journal, 2006.

Scholz, C.H., (1968). The frequency-magnitude relation of microfracturing in rock and its relation to earthquakes. Bull.seism. Soc. Am., **58:** 399-415.

Seifu Kebede (1999). Hydrology and hydrochemistry of Bishoftu crater lakes. Unpublished MSc Thesis Addis Ababa University, Ethiopia.

Shimazaki, K. and T. Nakata (1980). Time Predictable Recurrence for Larger Earthquakes. Geophys. Res. Letters **86:** 279-282.

Shudofsky, G.N., (1985). Source mechanisms and focal depths of East African earthquakes using Rayleigh wave inversion and body wave modeling, Geophys. Jr. Astr. Soc, **83:** 563-614.

Sigmundsson, F., (1992). Tectonic implications of the 1989 Afar earthquake sequence, Geophys. Res. Lett., **19:** 877-880.

Stewart, J.P., S. Chiou, J.D. Bray, R.W. Graves, P.G. Somerville, and N.A. Abrahamson, (2001). Ground Motion Evaluation Procedures for Performance Based Design. Peer Report 2001/09. Peer Center, College of Engineering, UC Berkley.

Sykes, L. R. and Landisman, M., (1964). The seismcity of East Africa, the Gulf of Aden and the Arabian and Red Seas. Bull. Seism. Soc. Am., **54:** 1969-1940.

Sykes, L. R., (1970). Focal mechanism solutions for earthquakes along the world rift system. Bull. Seism. Soc. Am., **60:** 1749-1752.

Tamiru Alemayehu and Antonio, V. (1995). Hydrogeology of Debre Zeit Area: Central Part of the Main Ethiopian Rift Valley, 2nd International Meeting for the Young Researchers in Applied Geology, pp.217-223.

Tamiru Alemayehu, (1992). Hydrogeology of Debre Zeit Area, MSc Thesis, Addis Ababa University.

Tapponnier, P., Armijo, R., Manighetti, I. and Courtillot, V., (1990). Bookshelf faulting and horizontal block rotations between overlapping rifts in southern Afar, Geophys. Res.Lett., **7:** 1-4.

Telford,W.M., Geldart, L.P. and Sheriff, R.E.,(1990). Applied Geophysics. Second edition. Cambridge University Press, Cambridge.

Tesfaye Chernet and Hart W.K (1999). Petrology and geochemistry of volcanism in the northern Main Ethiopian Rift-southern Afar transition region. Acta Vulcanologica **11**:21-42

Tesfaye Chernet, and Hart, W.K. (1999). Petrology and geochemistry of volcanism in the northern Main Ethiopian Rift – southern Afar transition region. Acta Vulcanologica, **11:** 21-41.

Tibebe Mengesaha. (2006). Geophysical Investigation for the Evaluation of Groundwater Resources at Ada`a Plain Near Debre Zeit. MSc thesis, Addis Ababa University.

Tilahun Mammo, (2005). Site specific ground motion simulation and seismic response analysis at the proposed bridge sites within the city of Addis Ababa. Elsevier, Engineering Geology **79:** 129-150.

Toro, G.R., N.A. Abrahamson and J.F. Schneider (1997). Model of Strong Ground Motions from Earthquakes in Central and Eastern North America: Best Estimates and Uncertainty. Seism. Res. Letters, **68:** No. 1, 41-57.

Tsegaye Abebe, F. Mazzarini, F. Innocenti, and P. Manetti (1998). The Yerer-Tullu Wellel volcanotectonic lineament: A transtensional structure in central Ethiopia and the associated magmatic activity, J. Afr. Earth Sci.

Tsegaye Abebe, Mazzarini F., Innocenti F., and Manetti P (1997). The Yerer-Tulu Wellel volcanotectonic lineament: a transtensional structure in central Ethiopia and associated magmatic activity. Jou. Afri. Earth sci. **26(1):**135-150.

Utsu.T., (1966). Statistical significance test of the difference in b-value between two earthquake groups, J. phys. Earth. **14:** 37-40.

Wells, D.L. and K.J. Coppersmith, (1994). New Empirical Relationships among Magnitude, Rupture Length, Width, Area & Surface Displacement. Bull. Seism. Soc. Am., **84:** 974-1002.

WoldeGabriel, G., Yemane, T., Suwa, G., White, T. & Asfaw, B., 1991. Age of volcanism and rifting in the Buri-Soyoma area, Amarco Horst, southern main Ethiopian Rift: geo- and biochronologic data, *J. Afr. Earth Sci.,* **13,** 437–447.

Wolfenden, E., Ebinger, C., Yirgu, G., Renne, P.&Kelley, S.P., 2005. Evolution of the southern Red Sea rift: birth of a magmatic margin, *Bull. Geol. Soc. Am.,* **117,** 846–864

Youngs, R.R. and K.J. Coppersmith (1985). Implications of Fault Slip Rates and Earthquake Recurrence Models to Probabilistic Seismic Hazard Estimates. Bull. Seism. Soc. Am., **75:** No.4, 939-964.

Appendices

Appendix I: Earthquake Catalog used for MER Seismic Source Zone (from ISC-GEM- Catalog).

Event ID	year	month	day	hour	minute	second	latitude	longitude	depth	magnitude	Sigma Magnitude
1	1906	8	25	11	54	0	7.62	40.22	10	6.51	0.2
2	1906	8	25	13	49	0	7.02	40.09	10	6.81	0.2
14	1960	7	14	18	39	35	7	37.5	10	6.32	0.2
26	1961	5	29	4	59	35	10	39	10	5.42	0.2
27	1961	5	29	10	52	1.2	10.4	39.4	10	5.42	0.2
28	1961	5	29	11	39	57	10.57	39.73	10	4.53	0.2
29	1961	5	29	11	59	9	10.5	39.5	10	4.53	0.2
30	1961	5	29	19	24	2	10.41	39.88	10	5.42	0.2
31	1961	5	29	19	26	5.5	10.4	40	10	5.42	0.2
32	1961	5	29	19	29	4.8	10.6	39.9	10	4.53	0.2
33	1961	5	29	19	40	28	10.41	39.86	10	4.53	0.2
34	1961	5	30	13	11	17	10.53	39.82	10	4.53	0.2
35	1961	6	1	21	7	21	10.7	39.64	10	4.53	0.2
36	1961	6	1	23	29	21.2	10.4	39.9	12	6.56	0.2
37	1961	6	1	23	56	52	10.6	39.59	10	4.53	0.2
38	1961	6	2	0	1	46	10.44	39.66	10	4.53	0.2
39	1961	6	2	0	8	57	10.37	39.96	10.9	4.53	0.2
40	1961	6	2	0	21	19	9.79	39.71	10	4.53	0.2
41	1961	6	2	0	57	55	9.84	39.86	10	4.53	0.2
42	1961	6	2	1	16	0.11	9.63	39.8	10	4.53	0.2
43	1961	6	2	1	16	7	9.4	40.2	10	4.53	0.2
44	1961	6	2	2	35	42	11.22	40.24	10	4.53	0.2
45	1961	6	2	3	19	39.5	9.89	39.65	10	4.53	0.2
46	1961	6	2	3	49	11	10.01	40.54	10	4.53	0.2
47	1961	6	2	4	51	14.8	10.3	39.8	10	6.47	0.2
48	1961	6	2	5	22	29	10.15	39.78	10	4.53	0.2
49	1961	6	2	5	44	53	10.22	39.92	10	5.82	0.2

50	1961	6	2	6	17	16	10.62	39.77	10	4.53	0.2
51	1961	6	2	7	2	52	10.15	39.89	10	5.76	0.2
52	1961	6	2	7	21	49.9	10.68	39.74	10	4.53	0.2
53	1961	6	2	22	19	34	10.38	39.98	10	4.53	0.2
54	1961	6	2	23	32	36	10.49	39.85	10	4.53	0.2
55	1961	6	3	2	5	34	10.24	39.81	10	4.53	0.2
56	1961	6	3	15	20	31	10.38	39.86	10	4.53	0.2
57	1961	6	3	15	23	15.8	9.8	39.6	10	5.8	0.2
58	1961	6	3	16	25	54	10.54	39.83	10	4.53	0.2
59	1961	6	4	0	41	43	10.29	39.72	10	4.53	0.2
60	1961	6	6	17	46	43	10.83	39.56	10	4.53	0.2
61	1961	6	7	15	11	6	10.54	39.74	10	4.53	0.2
64	1961	6	14	20	32	19	10	40	10	5.53	0.2
65	1961	6	19	4	34	0.12	10.39	39.91	10	4.53	0.2
67	1961	6	24	15	4	34	10.65	40.14	10	4.53	0.2
102	1964	7	3	19	18	32.7	11.05	39.7	10	5.2	0.2
104	1964	10	17	17	41	20	10.2	39.75	10	3.42	0.2
105	1964	10	17	18	3	3	10.2	39.75	10	3.42	0.2
106	1964	12	13	18	42	44	9.2	41.7	10	4.1	0.2
112	1965	4	14	7	53	0	11.3	39.6	10	4.35	0.2
118	1965	6	7	13	43	57.8	11.48	41.51	12	5.2	0.2
295	1968	1	23	19	18	14.04	8.69	37.41	10	5.2	0.2
313	1969	3	29	9	15	54	11.91	41.21	15	6.05	0.2
314	1969	3	29	11	4	52	11.92	41.36	15	5.75	0.2
316	1969	3	29	13	8	17	11.94	41.31	13	5.37	0.2
317	1969	3	29	18	30	49	11.87	41.4	9	4.86	0.2
322	1969	4	6	16	51	47	11.99	41.4	41	5.37	0.2
323	1969	4	7	6	23	55	11.92	41.4	8	4.94	0.2
324	1969	4	8	2	14	1	11.88	41.42	10	5.11	0.2
343	1971	7	11	20	52	0	9.6	39.6	10	4.55	0.2
345	1971	11	13	0	0	0	10	39.8	10	4	0.2
346	1971	11	13	15	47	44	11.03	39.71	9	5.37	0.2
348	1972	1	11	15	10	42.06	7	38	10	4.16	0.2
349	1972	1	11	15	11	0	7.2	37.7	10	4.16	0.2
359	1972	11	13	7	7	53.07	10	39.6	10	4.35	0.2
361	1973	3	8	5	14	55	7.7	38	10	4.23	0.2
381	1973	4	1	21	2	16	11.7	41.97	10	4.26	0.2
406	1974	2	25	16	5	18	10.2	39.8	13	4.94	0.2
420	1974	12	17	0	44	37	11.2	39.7	10	3.86	0.2
428	1975	8	23	21	35	21.2	10.52	39.75	13	5.2	0.2
429	1975	8	23	22	12	45	10.6	40	10	4.89	0.2

432	1976	1	10	16	10	0	10.48	38.93	10	4.16	0.2
452	1977	7	8	6	23	2.04	11.08	39.62	14	5.28	0.2
516	1979	7	28	19	22	0	8.85	38.7	10	3.79	0.2
579	1981	1	25	14	36	0	8.7	39.75	10	4.16	0.2
580	1981	1	27	0	14	0	8.7	39.75	10	4.38	0.2
581	1981	1	27	22	33	0	9	39.94	10	3.86	0.2
582	1981	1	27	22	42	0	9	39.94	10	4.01	0.2
583	1981	1	28	1	57	0	8.9	39.86	10	4.01	0.2
584	1981	1	29	3	58	0	8.9	39.86	10	4.38	0.2
585	1981	1	29	7	14	0	9	39.94	10	4.08	0.2
586	1981	1	29	14	3	0	8.7	39.75	10	4.01	0.2
587	1981	1	29	20	15	0	8.7	39.75	10	4.31	0.2
588	1981	1	30	4	20	0	9	39.94	10	4.23	0.2
589	1981	1	30	12	21	0	9	39.94	10	4.08	0.2
590	1981	1	30	16	57	0	8.7	39.75	10	4.08	0.2
591	1981	1	30	19	10	0	8.9	39.86	10	4.16	0.2
592	1981	1	30	22	26	0	9	39.94	10	4.31	0.2
593	1981	1	31	4	27	0	9	39.94	10	4.08	0.2
594	1981	1	31	15	38	0	8.9	39.86	10	4.31	0.2
595	1981	2	1	4	58	0	8.9	39.86	10	4.08	0.2
596	1981	2	1	9	56	0	8.9	39.86	10	4.01	0.2
597	1981	2	1	11	48	0	8.9	39.86	10	4.01	0.2
598	1981	2	2	12	1	0	8.7	39.75	10	4.08	0.2
599	1981	2	2	18	2	0	8.9	39.86	10	4.08	0.2
600	1981	2	3	15	20	0	9.1	40	10	4.23	0.2
602	1981	2	7	5	38	0	9	39.94	10	4.16	0.2
603	1981	2	7	22	34	0	9.1	40	10	4.31	0.2
604	1981	2	9	15	5	0	9	39.94	10	4.01	0.2
605	1981	2	11	16	37	0	8.7	39.75	10	4.23	0.2
606	1981	2	17	2	16	0	9.1	40	10	4.23	0.2
607	1981	2	18	20	5	0	9.1	40	10	4.01	0.2
608	1981	2	20	5	58	0	9	39.94	10	4.01	0.2
609	1981	2	20	9	55	0	9	39.94	10	3.94	0.2
610	1981	2	20	14	51	0	9.1	40	10	4.23	0.2
611	1981	2	20	18	30	0	8.9	39.86	10	4.38	0.2
612	1981	2	20	22	25	0	9	39.94	10	4.01	0.2
613	1981	2	22	4	53	0	9.1	40	10	4.01	0.2
614	1981	3	2	15	56	0	9.1	40	10	4.01	0.2
619	1981	11	26	23	42	0	7.95	38.7	10	4.23	0.2
620	1982	6	19	1	36	0	7.56	38.98	10	4.31	0.2
622	1982	7	21	2	56	0	9.75	39.5	10	4.17	0.2

624	1982	8	7	22	26	0	10.7	41.1	7	4.9	0.2
625	1982	8	15	6	51	0	10.5	41	10	4.23	0.2
626	1982	8	15	17	3	0	10.6	41	10	4.38	0.2
627	1982	8	15	17	13	0	9.9	40.65	10	4.01	0.2
628	1982	8	15	18	54	0	9.8	40.6	10	4.23	0.2
629	1982	8	16	7	35	0	10	40.7	10	3.86	0.2
657	1984	4	10	8	10	38.08	11.33	39.61	10	5.28	0.2
662	1984	8	24	9	3	0	8.95	39.95	10	4.83	0.2
666	1984	10	13	2	29	0	10.6	40	10	4.83	0.2
667	1984	10	23	21	19	0	10.1	37.05	6	4.86	0.2
675	1985	3	18	2	35	0	7.67	38.96	10	4.53	0.2
683	1985	8	2	20	39	0	7.65	38.93	10	4.61	0.2
684	1985	8	4	23	24	0	7.61	38.95	10	4.61	0.2
685	1985	8	14	20	37	44.04	8.28	38.5	13	5.11	0.2
687	1985	10	28	12	8	36.03	9.47	39.61	10	4.94	0.2
704	1987	9	15	0	0	26.09	11.3	41.6	10	4.46	0.2
742	1989	5	11	20	53	52	8.94	39.98	10	5.28	0.2
752	1989	8	20	11	16	56.06	11.77	41.96	12	5.88	0.2
753	1989	8	20	11	17	55.02	11.9	41.97	10	5.88	0.2
754	1989	8	20	11	46	28.01	11.88	41.82	10	6.13	0.2
755	1989	8	20	11	56	17	11.85	41.97	10	5.56	0.2
756	1989	8	20	12	13	36	11.4	41.7	10	4.03	0.2
758	1989	8	20	13	26	19.08	11.93	41.86	10	5.45	0.2
762	1989	8	20	18	25	13	11.8	41.81	10	4.89	0.2
763	1989	8	20	18	27	33.02	11.81	41.66	10	5.37	0.2
764	1989	8	20	18	39	48.08	11.95	41.87	10	5.62	0.2
765	1989	8	20	18	54	5.01	11.84	41.76	10	5.56	0.2
766	1989	8	20	19	25	56.06	11.89	41.82	12	6.13	0.2
768	1989	8	21	1	9	6.07	11.86	41.86	13	6.22	0.2
769	1989	8	21	1	34	5	11.6	41.9	10	5.11	0.2
770	1989	8	21	5	3	5.06	11.93	41.77	10	5.88	0.2
771	1989	8	21	5	5	46	11.92	41.74	10	5.45	0.2
772	1989	8	21	6	46	45	11.83	41.8	10	4.68	0.2
773	1989	8	21	7	7	38.05	11.76	41.69	10	5.37	0.2
776	1989	8	21	21	21	35	11.7	41.7	10	4.89	0.2
780	1989	11	6	8	23	50	11.9	41.94	10	4.16	0.2
789	1990	5	4	10	12	6	11.73	40.96	7	5.37	0.2
790	1990	5	16	17	17	23	11.9	41.8	10	4.89	0.2
852	1990	9	12	1	26	0	8.9	37.48	5	4.53	0.2
856	1990	11	2	4	51	0	8.07	38.53	5	4.53	0.2
879	1991	5	3	22	38	0	8.05	38.45	10	4.01	0.2

880	1991	5	3	23	25	0	8.05	38.45	5	4.16	0.2
886	1991	7	26	15	33	37.09	7.6	38.3	10	4.6	0.2
907	1992	12	22	10	36	33.07	11.98	41.77	10	4.77	0.2
913	1993	2	13	2	25	49.07	8.3	39.3	12	5.28	0.2
944	1993	3	16	22	59	45.08	11.62	41.98	16	5.79	0.2
982	1993	9	21	19	11	35.09	11.48	39.64	15	5.62	0.2
1012	1995	1	20	7	14	27.2	7.16	38.44	13	5.28	0.2
1075	1997	1	3	21	1	29.12	11.98	41.61	10	4.89	0.2
1113	1997	7	14	7	15	10.53	11.94	39.24	10	4.26	0.2
1137	2000	5	10	8	43	28.4	9.89	41.08	7	4.77	0.2
1138	2000	5	10	23	17	52.9	9.94	41.08	5	4.68	0.2
1139	2000	5	12	17	54	2.1	9.93	41.04	7	4.6	0.2
1140	2000	5	16	20	47	0.49	9.91	41.05	6	4.6	0.2
1172	2005	9	21	16	56	49.58	11.97	40.24	5	4.35	0.2
1177	2005	9	21	23	36	21.49	11.98	40.32	5	4.6	0.2
1267	2005	9	25	2	33	55.72	11.937	40.577	5	4.17	0.2
1273	2005	9	25	4	52	17.84	10.673	40.117	6.4	4.35	0.2
1300	2005	9	25	10	49	1.23	11.84	40.17	5	4.17	0.2
1325	2005	9	27	0	42	18.95	11.929	40.272	9.3	4.6	0.2
1367	2006	7	4	5	51	59.15	7.926	39.088	7.5	4.6	0.2
1410	2007	5	17	0	21	38.33	9.74	40.633	5	4.35	0.2
1413	2007	7	8	18	31	31.57	10.542	40.217	6	4.35	0.2
1414	2007	7	8	19	14	47.03	10.489	40.302	5	4.17	0.2
1465	2008	10	12	10	48	17.49	7.635	37.966	7	4.26	0.2
1466	2008	10	15	16	19	2.97	7.51	38.029	7	4	0.2
1496	2009	9	19	17	56	8.27	9.524	40.119	7	4.26	0.2
1540	2009	12	22	3	39	8.11	10.227	40.787	5	4.68	0.2
1739	2010	12	19	12	14	24.51	7.52	37.84	10	5.37	0.2
1854	2011	10	17	1	3	25.61	7.64	37.87	10	4.77	0.2

Note: Earthquake catalogue for Afar and Escarpment Seismic zones are not included here, but they are included in the analysis.

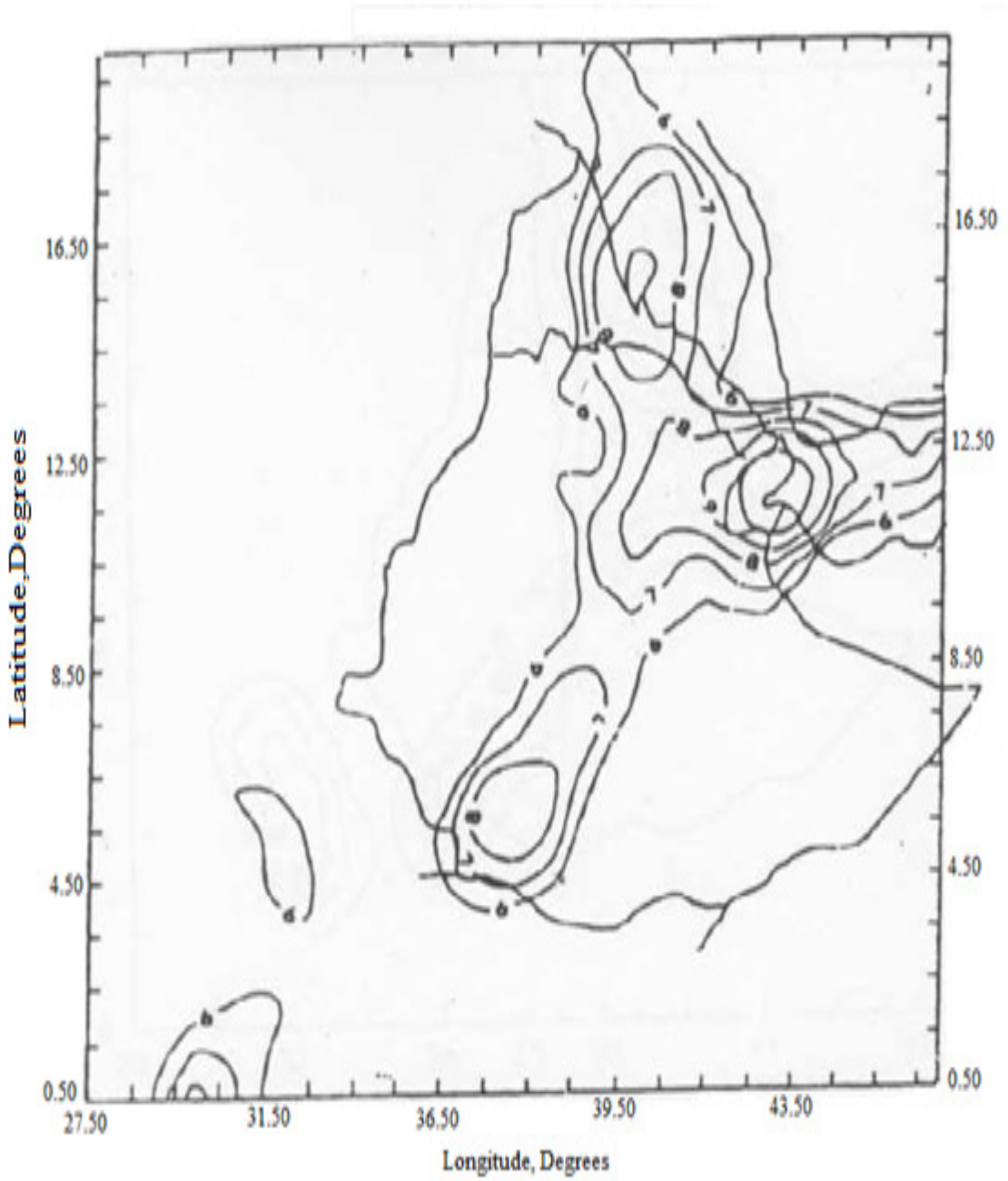

Appendix II: Seismic hazard intensity map of Ethiopia and the neighboring countries. The hazard is for 100 years return period with 90 % probability of not being exceeded.

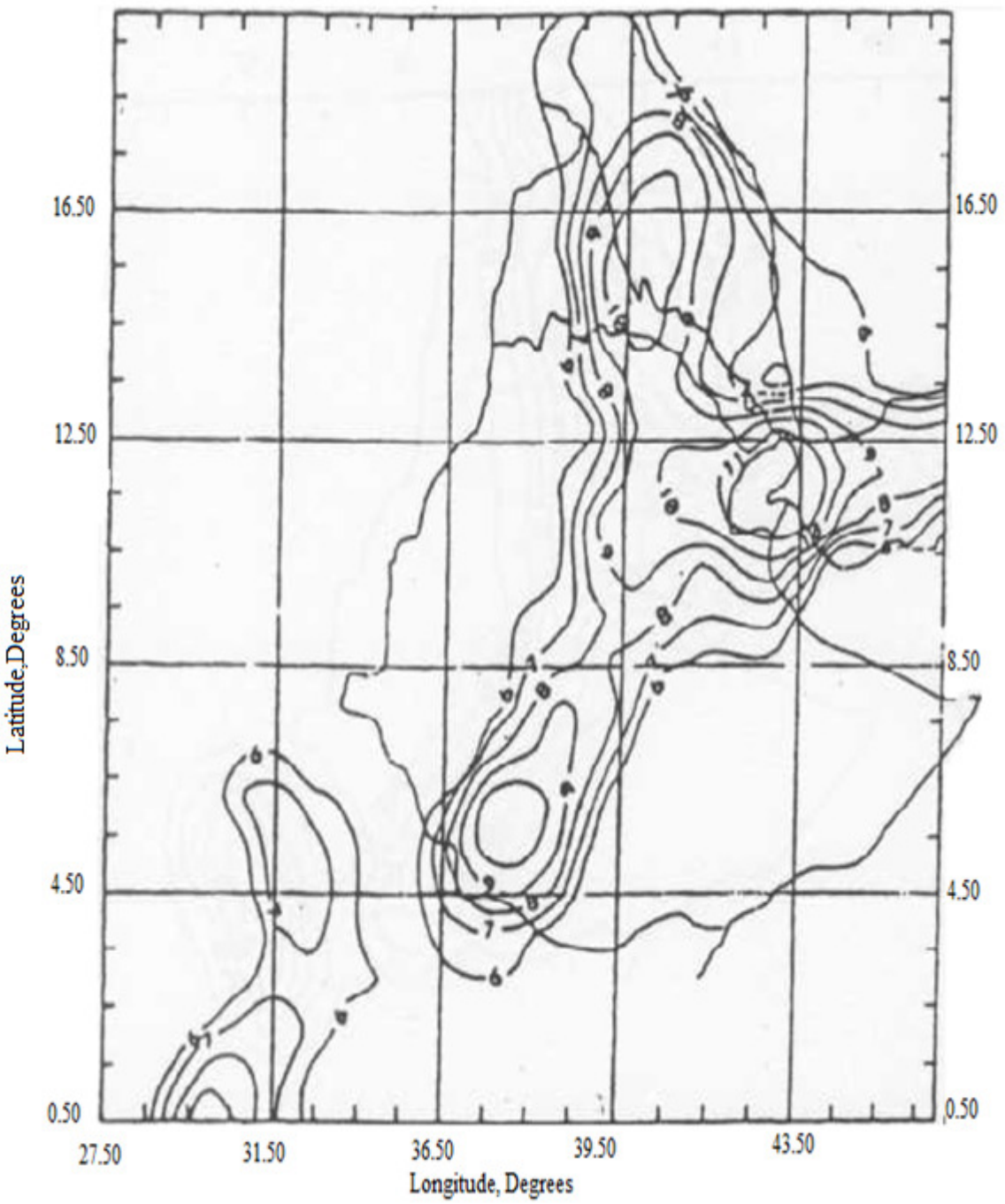

Appendix III: Seismic hazard intensity map of Ethiopia and the neighboring countries. The hazard is for 200 years return period with 90 % probability of not being exceeded.

Appendix IV: Seismic hazard map of Ethiopia and the neighboring countries. The hazard is for an annual probability of exceeded of 0.01.

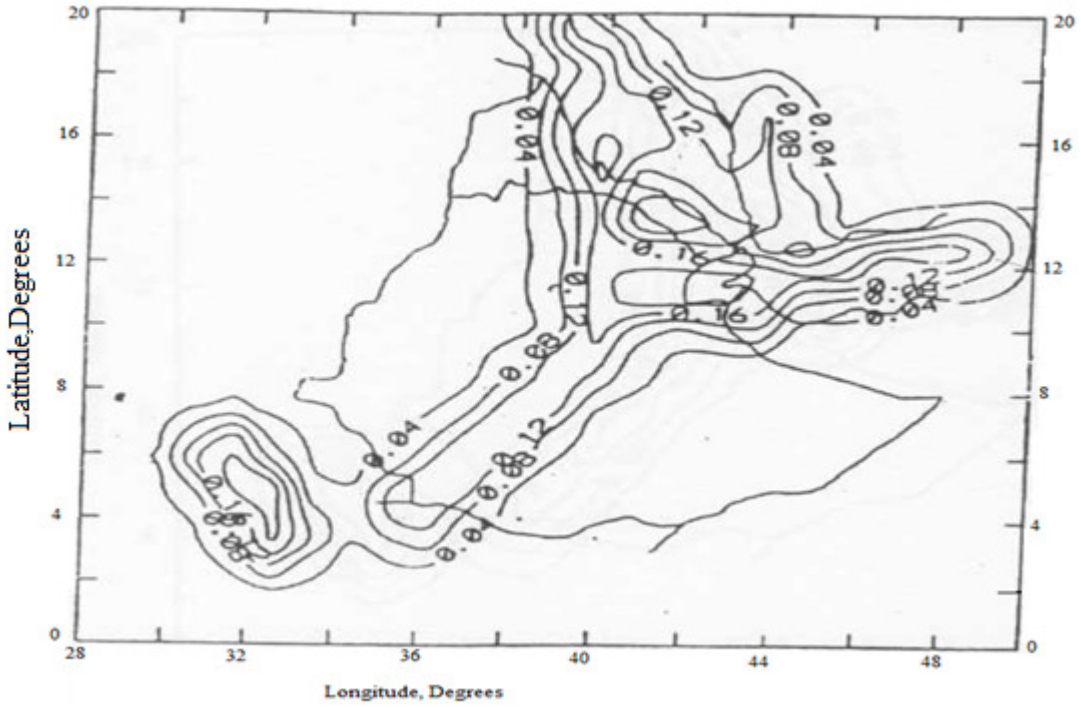

Appendix V: Seismic hazard map of Ethiopia and the neighboring countries. The hazard is for an annual probability of exceeded of 0.005.

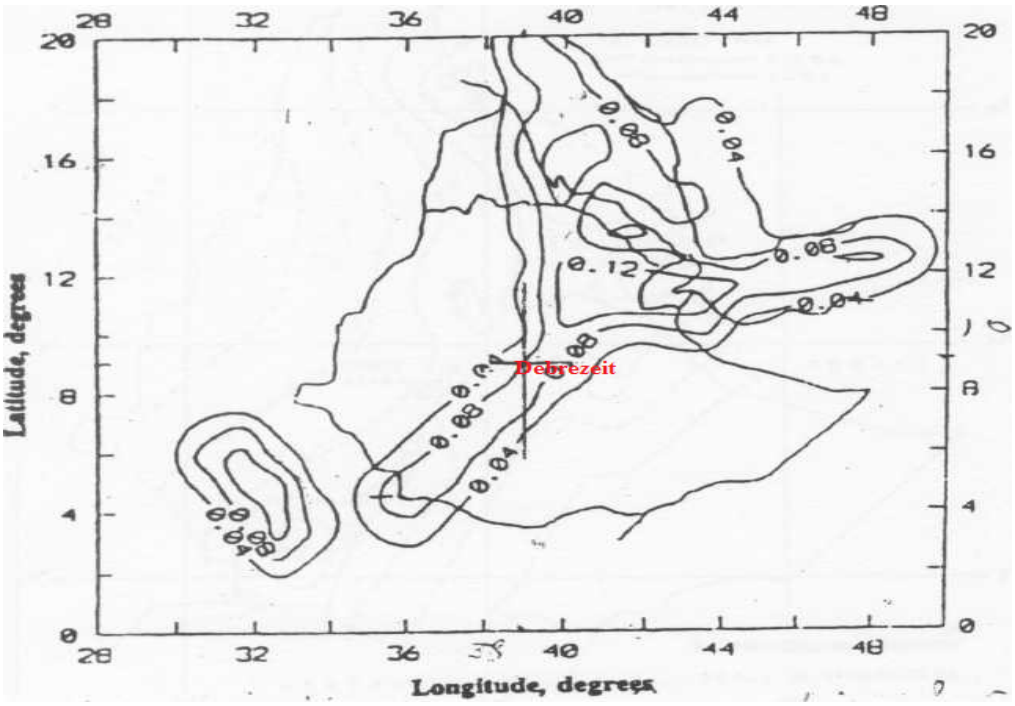

Appendix VI: Predicted earthquake intensities and ground accelerations for Capital cities and important towns.

Locations			**Estimated probability**							
Sites	**Coordinates**		**1/50 Years**		**1/100 Years**		**1/200 Years**		**1/300 Years**	
	N° E°		**I**	**A**	**I**	**A**	**I**	**A**	**I**	**A**
Addis Ababa	09.00°	38.77°	VI	3.6	VII	6.9	VIII	13.3	VIII	20
Adigrat	14.30	39.50	VII	5.1	VIII	10.0	VIII	19.3	IX	28
Aksum	14.13	38.92	VI	2.8	VII	4.9	VII	8.5	VIII	12
Arba Minch	06.00	37.70	VII	5.7	VIII	13.8	IX	33.4	X	56
Asayita	11.60	41.40	VII	7.6	VIII	16.7	IX	36.6	X	58
Asella	07.98	39.12	VI	2.8	VII	5.5	VIII	10.5	VIII	15
Asmara	15.33	39.00	VIII	12.7	IX	28.8	X	64.7	XI	104
Asseb	13.00	42.67	VI	3.1	VII	5.7	XI	10.3	VIII	15
Awasa	07.05	38.52	VII	5.2	VIII	12.2	IX	28.5	X	47
Awash Station	09.00	40.20	V	2.0	VI	3.4	VII	5.8	VII	8
Bako	05.80	36.50	VIII	11.4	IX	34.2	XI	103	XI	195
Bonga	07.30	36.20	VI	2.4	VII	4.7	VII	9.4	VIII	14
Debre Berhana	09.30	39.30	VI	2.9	VII	5.3	VIII	9.7	VIII	14
Debre Markos	10.35	37.75	V	1.7	VI	2.8	VII	4.7	VII	6
Debre Zeit	08.75	38.98	VI	3.4	VII	6.6	VIII	12.7	VIII	19
Dembi Dollo	08.60	34.80	V	1.2	VI	2.2	VI	4.0	VII	6
Dessie	11.10	39.50	VII	5.7	VIII	12.0	VII	5.3	IX	39
Gondar	12.60	37.50	V	1.5	VI	2.4	VIII	6.8	VII	5
Gore	05.15	35.57	V	1.6	VI	2.9	VIII	13.2	VII	8
Hagare Mariam	05.60	38.30	VI	2.8	VII	5.3	VIII	6.8	VIII	8
Harar	09.30	42.10	VI	3.5	VII	6.8	VIII	13.2	VIII	19
Jimma	07.65	36.82	VI	2.4	VII	4.8	VII	9.3	VIII	14
l.ekempt	09.10	36.55	V	1.6	VI	2.9	VII	5.2	VII	7
Massawa	15.60	39.50	IX	26.0	X	68	XI	176	XII >	300
Mekele	13.45	39.47	VII	4.6	VII	9.1	VIII	18.0	IX	27
Mizan Teferi	06.90	35.50	VI	2.4	VII	5.1	VIII	10.6	VIII	16
Moyale	03.53	39.02	V	1.3	VI	2.5	VII	4.8	VII	7
N azareth	08.63	39.28	VI	2.4	VI	4.4	VII	7.8	VIII	11
Serdo	11.98	41.20	VIII	9.9	IX	23.2	X	54.2	X	89
Tessenei	15.12	36.68	V	1.3	VI	2.2	VI	3.7	VII	5
Yabello	04.80	38.10	VI	2.4	VII	5.1	VIII	10.8	VIII	17
Y irga Alem	06.73	38.40	VI	3.9	VIII	8.7	VIII	19.0	IX	30

Appendix VII: Relation between Seismic Intensity, Maximum Ground Velocity and Maximum Ground Acceleration (according to Bolt, 1978).

Maximum Velocity(cm/s)	I (MM)	Maximum acceleration (g)
1-2	IV	0.015g - 0.02 g
2-5	V	0.03 g - 0.04 g
5-8	VI	0.06g – 0.07g
8-12	VII	0.10 g - 0.15 g
20-30	VIII	0.25 g-0.30 g
45-55	IX	0.50 g-0.55 g
>60	X	>0.6 g

Appendix VIII: Relation between Seismic Energy, Surface wave Magnitude M_s, Body wave Magnitude M_b, Maximum Intensity I_0, and Maximum Ground Acceleration. (according to Bath, 1973)

E (erg)	M_s	M_b	I_0	a_o (cm.s^{-2}) *
1020	5.4	5.9	VI-VII	40
1021	6.1	6.3	VH-VIII	100
1022	6.8	6.7	VIII-IX	200
1023	7.5	7.1	IX-X	400
1024	8.2	7.5	X-XI	1000
1025	8.9	7.9	XII	2000

* refers to Periods of ground motion ranging from 0.1 s to 0.5s

Appendix IX: Steps of 2D multi channel analysis of surface waves for profile one.

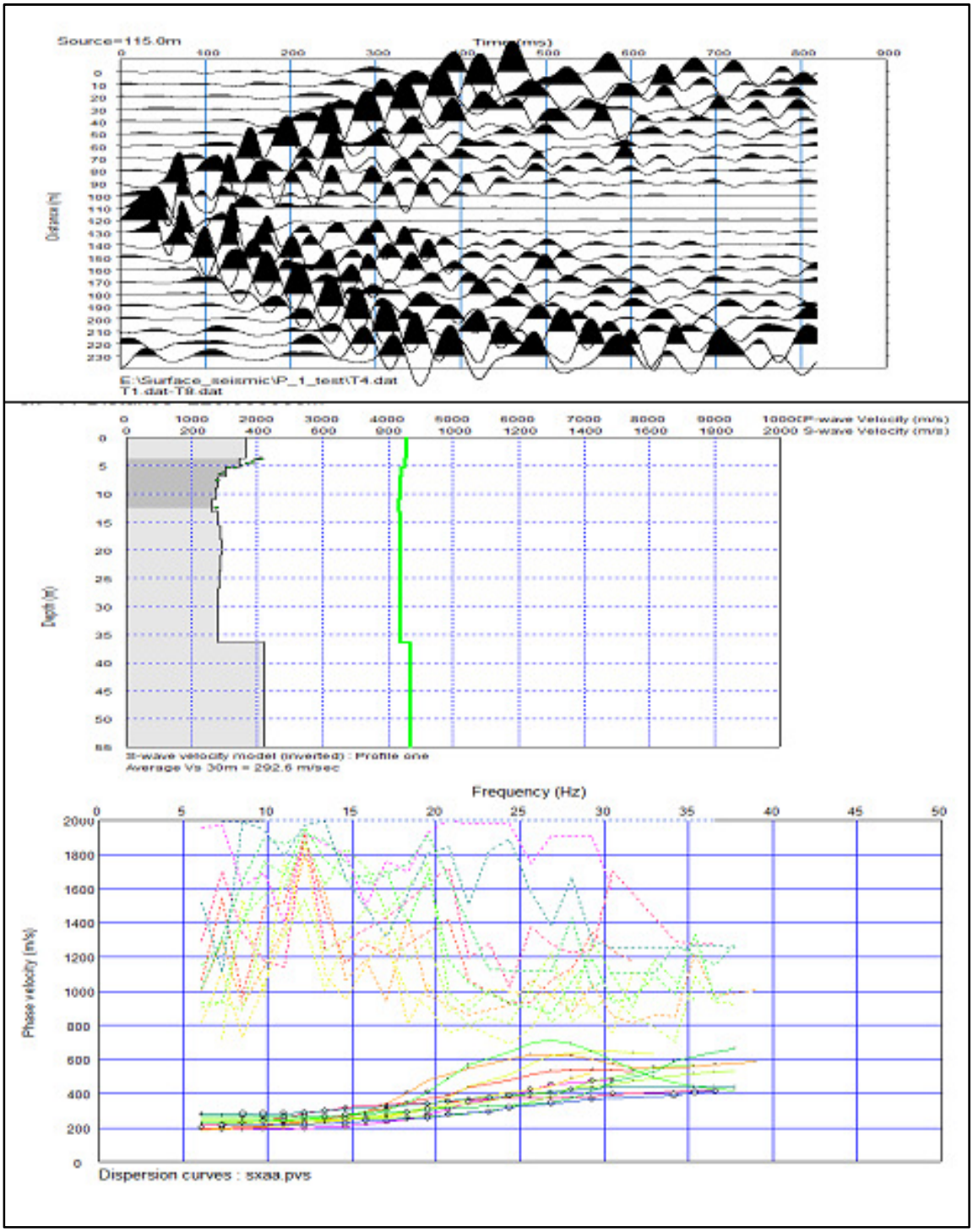

Appendix X: Soil profile type classification for seismic amplification.

Soil type NEHRP	**General description**	**Average shear wave velocity to 30 m (m/s)**
A	Hard rock	> 1500
B	Rock	760 < Vs ≤ 1500
C	Very dense soil and soft rock	360 < Vs ≤ 760
D	Stiff soil 15 ≤ N ≤ 50 or 50 kPa ≤ Su ≤ 100 kPa	180 ≤ Vs≤ 360
E	Soil or any profile with more than 3 m of soft clay defiled as soil with PI > 20, w ≥ 40%, and Su < 25 kPa.	≤ 180
F	Soils requiring site-specific evaluations	

N: SPT blow count, Su: Undrained shear strenghth
PI: Plasticity index, w: water content

Appendix XII: Global Vs30 map for the Debrezeit city and its surrounding from USGS Earthquake Hazard Program.

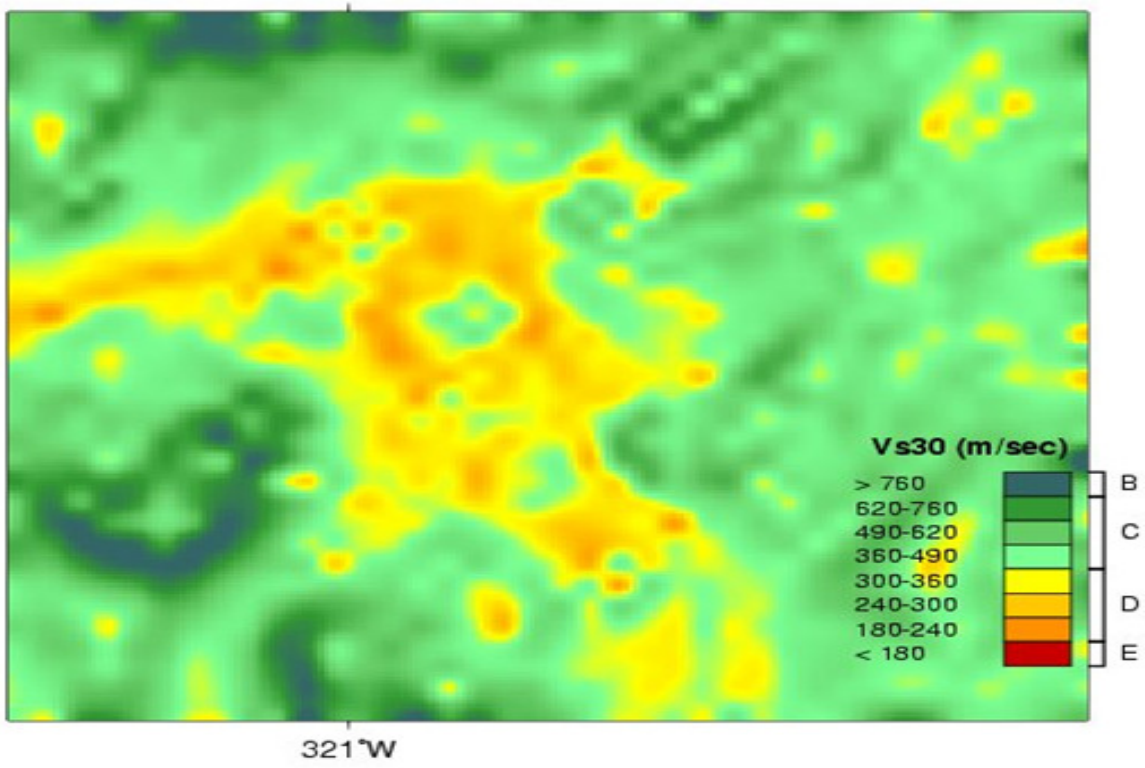

Declaration

I hereby declare that the thesis entitled "Seismic Hazard Analysis of Debrezeit Area" has been carried out by me under the supervision of Dr. Tilahun Mammo during the year 2013/14 as part of Master of Science program in Exploration Geophysics. I further declare that this work has not been submitted to any other University or institution for the award of any degree or diploma and all sources of material used for the thesis have been duly acknowledged.

Kasahun Dander

Signiture _____

Place and date of submission: School of Earth Sciences, Addis Ababa University

May, 2015